DOI: 10.1002/chem.201102827

N-Heterocyclic Tridentate Aromatic Ligands Bound to [Ln(hexafluoroacetylacetonate)$_3$] Units: Thermodynamic, Structural, and Luminescent Properties

Amir Zaïm,[a] Homayoun Nozary,[a] Laure Guénée,[b] Céline Besnard,[b] Jean-François Lemonnier,[a] Stéphane Petoud,*[c] and Claude Piguet*[a]

Abstract: Herein, we discuss how, why, and when cascade complexation reactions produce stable, mononuclear, luminescent ternary complexes, by considering the binding of hexafluoroacetylacetonate anions ($hfac^-$) and neutral, semi-rigid, tridentate 2,6-bis(benzimidazol-2-yl)pyridine ligands (**L*k***) to trivalent lanthanide atoms (Ln^{III}). The solid-state structures of [Ln(**L*k***)(hfac)$_3$] (Ln = La, Eu, Lu) showed that [Ln(hfac)$_3$] behaved as a neutral six-coordinate lanthanide carrier with remarkable properties: 1) the strong cohesion between the trivalent cation and the didentate hfac anions prevented salt dissociation; 2) the electron-withdrawing trifluoromethyl substituents limited charge-neutralization and favored cascade complexation with **L*k***; 3) nine-coordination was preserved for [Ln(**L*k***)(hfac)$_3$] for the complete lanthanide series, whilst a counterintuitive trend showed that the complexes formed with the smaller lanthanide elements were destabilized. Thermodynamic and NMR spectroscopic studies in solution confirmed that these characteristics were retained for solvated molecules, but the operation of concerted anion/ligand transfers with the larger cations induced subtle structural variations. Combined with the strong red photoluminescence of [Eu(**L*k***)(hfac)$_3$], the ternary system Ln^{III}/$hfac^-$/**L*k*** is a promising candidate for the planned metal-loading of preformed multi-tridentate polymers.

Keywords: lanthanides · ligand effects · nitrogen heterocycles · photophysical properties · thermodynamics

Introduction

Although neutral six-coordinate lanthanide beta-diketonates building blocks, [Ln(β-diketonate)$_3$], are famous for their exceptional luminescent properties,[1] some renewed interest has focused on their specific interactions with additional didentate or tridentate chelating receptors to produce engineered materials for metal–organic chemical-vapor deposition (MOCVD)[2,3] and for organic light-emitting diodes (OLEDs).[4] For instance, neutral [Eu(dibenzoylmethanide)$_3$] units were recently used for chelating to didentate 1,10-phenanthroline binding sites that were incorporated within photoluminescent conducting polymers,[5] whilst [Ln(hexafluoroacetylacetonate)$_3$], that is, [Ln(hfac)$_3$], were reacted with tridentate diglyme for the preparation of transparent films with non-linear optical responses (Scheme 1).[6]

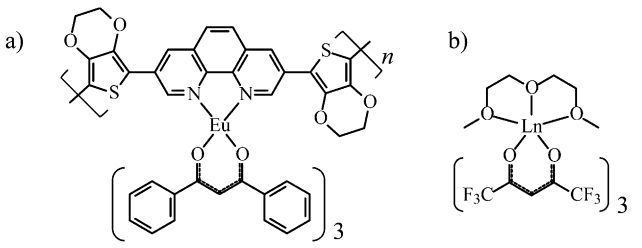

Scheme 1. a) Postulated molecular structure of the monomeric unit in a photoluminescent conducting europium-containing polymer;[5] b) chemical structure of [Ln(hfac)$_3$(diglyme)], which was designed as a precursor for volatile materials with tunable second-order nonlinear optical properties.[6]

Whilst countless reports have described the solid-state structures and the metal-centered luminescence of ternary [Ln(**L**)(β-diketonate)$_3$] complexes, where **L** is a didentate N-donor receptor typically derived from 2,2′-bipyridine or 1,10-phenanthroline,[2,7] much-less attention has been focused on analogous complexes that incorporate the extended tridentate 2,2′:6′,2″-terpyridine (terpy) derivatives.[8] Beyond 1) the C_1-symmetric molecular structure found in the crystals of nine-coordinate [Ln(terpy)(β-diketona-

[a] A. Zaïm, Dr. H. Nozary, Dr. J.-F. Lemonnier, Prof. Dr. C. Piguet
Department of Inorganic, Analytical,
and Applied Chemistry, University of Geneva
30 quai E. Ansermet, 1211 Geneva 4 (Switzerland)
E-mail: Claude.Piguet@unige.ch

[b] Dr. L. Guénée, Dr. C. Besnard
Laboratory of Crystallography, University of Geneva
24 quai E. Ansermet, 1211 Geneva 4 (Switzerland)

[c] Prof. Dr. S. Petoud
Centre de Biophysique Moléculaire, CNRS UPR 4301
Rue Charles-Sadron, 45071 Orléans Cedex 2 (France)
E-mail: Stephane.Petoud@cnrs-orleans.fr

Supporting information for this article is available on the WWW under http://dx.doi.org/10.1002/chem.201102827.

te)$_3$][8c,e] and 2) the detection of remarkable luminescence quantum yields for [Eu(terpy)(β-diketonate)$_3$] in the solid state,[1,8] little is known about the structures, speciations, and stabilities of these ternary complexes in solution. This lack of reliable information is common in lanthanide coordination chemistry and, during our quest for identifying unsaturated neutral [LnX$_3$] units for cascade complexation with semi-rigid tridentate ligands **L1**–**L8** (Scheme 2), we were often faced with drastic limitations, owing to unexpected solution behaviors.[9–11] For instance, when X = NO_3^- or $CF_3CO_2^-$, the desired mononuclear nine-coordinate complexes [Ln(**L1**)(X)$_3$] that were observed in the solid state systematically dimerized in aprotic polar solvents (see the Supporting Information, Figure S1).[9,10] For X = SCN^-, the situation was even worse, with the formation of intricate mixtures of charged complexes, $[Ln(\mathbf{L1})(SCN)_4]^-$ and $[Ln(\mathbf{L1})_2(SCN)_2]^+$, which prevented the isolation of the neutral targets, [Ln(**L1**)(SCN)$_3$].[11,12] To identify and further exploit a neutral [LnX$_3$] lanthanide carrier, we turned our attention toward X = β-diketonate, and, more precisely, toward the highly soluble [Ln(hfac)$_3$] compounds (hfac = hexafluoroacetylacetonate), which are known to be rather robust toward dissociation, dimerization, and hydrolysis.[1,13] Being aware of the reports of some faint thermodynamic affinities of [Ln(β-diketonate)$_3$] toward didentate 1,10-phenanthroline in polar solvents,[14] we first embarked on the quantitative exploration of the intermolecular cascade reaction of these units with the related tridentate N-heterocyclic ligands **L2** and **L3**.

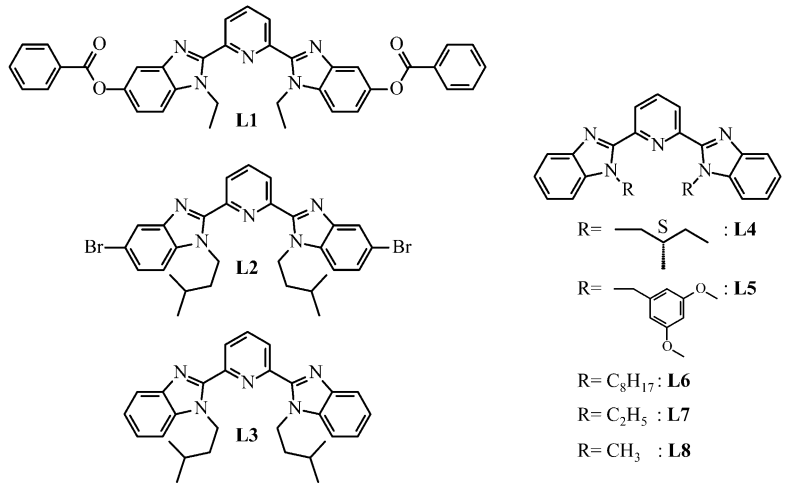

Scheme 2. Chemical structures of ligands **L1**–**L8** in their *trans–trans* conformations.

Results and Discussion

Synthesis, characterization, and molecular structures of ligands L2 and L3 and of complexes [Ln(L*k*)(hfac)$_3$] (*k* = 2, 3; Ln = La, Eu, Gd, Lu, Y): Although attractive for solubility and chirality reasons, the substitution of branched neopentyl (**L4**)[15] or 3,5-dimethoxybenzyl groups (**L5**)[16] at the 1-position of the benzimidazole side-arms in ligands **L4** and **L5** drastically limits the affinity of these ligands for trivalent lanthanides. Structural investigations have attributed this negative effect to the steric bulk of these substituents when the tridentate ligand adopts the planar *cis–cis* conformation required for its coordination to Ln^{III} (see Figure 2).[15,16] Indeed, the connection of more-compact linear lipophilic octyl chains (**L6**) endows sufficient stability in [Ln(**L6**)$(NO_3)_3$] for their quantitative formation in acetonitrile at millimolar concentrations, although difficult isolation, purification, and characterization of these waxy materials hinders detailed photophysical investigations and further exploitations.[17] With this in mind, we envisioned the use of 3-methyl-1-butyl residues in **L2** and **L3** for optimizing their solubility in organic solvents whilst minimizing the structural expansion responsible for the thermodynamic penalty in the associated complexes (Scheme 3). Compound **L3** was obtained by a standard acidic activation of the carboxylic groups in the presence of *o*-phenylenediamine to give compound **3**, which was then deprotonated and alkylated.[18] Because the latter procedure mixed the 5- and 6-positions within each benzimidazole ring,[18] the stereospecific connection of two bromine atoms at the 5,5′-positions of the benzimidazole rings in **L2** relied on an alternative two-step reductive Phillips-modified coupling strategy (Scheme 3).[19]

Because of the average planar C_{2v}-symmetrical arrangement adopted by the free ligands in solution, we only detected five signals for the aromatic protons in the ^{1}H NMR spectrum of compound **L2** (six signals for **L3**, see Figure 3a, Figure 4a; also see the Supporting Information, Tables S1 and S2), together with pairs of enantiotopic methyl groups for H9 and H10 (atom numbering is given in Scheme 3; herein H9 and H10 refer to the H atoms bonded to C9 and C10, respectively).[16] The lack of a nuclear Overhauser enhancement effect (NOE) between alkyl protons H6 and pyridine protons H1 or H2 suggested that the three coordinated nitrogen atoms adopted the standard *trans–trans* geometry, which optimized the intramolecular electric dipolar interactions (Scheme 3).[20] The crystal structure of ligand **L3** confirmed this suggestion and showed two slightly different molecules in the asymmetric unit, both of which adopted the expected *transoid* conformation (N47 was *trans* to N44 whilst N80 was *trans* to N44, Figure 1). Typical bond lengths and angles were observed (see the Supporting Information, Table S3)[21] but the benzimidazole-pyridine-benzimidazole aromatic units were not strictly coplanar (interplanar angles 9.6–38.9°; see the Supporting Information, Table S4 and Figure S2) because of the residual helical twists imposed by the

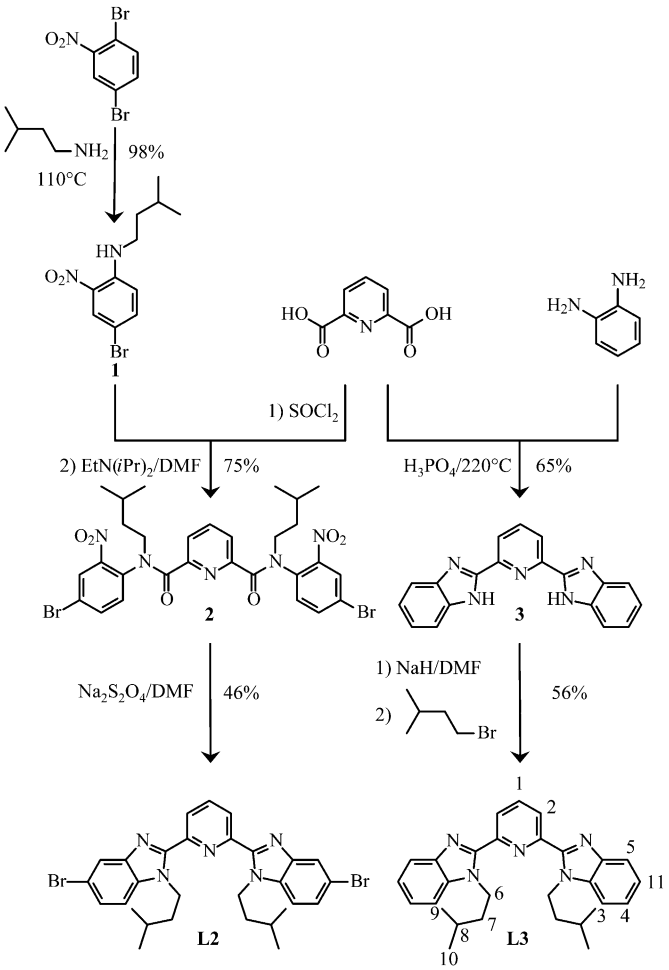

Scheme 3. Syntheses of ligands **L2** and **L3** with atom numbering.

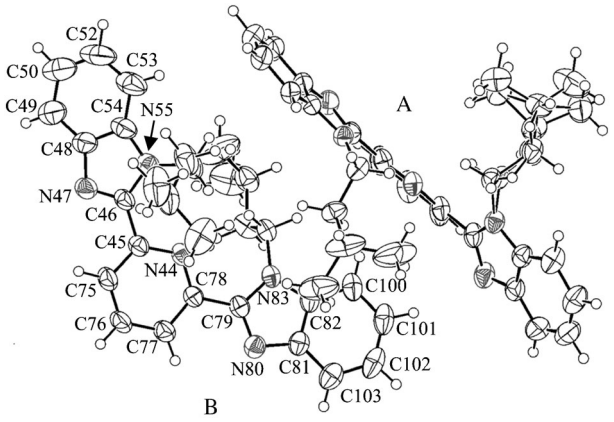

Figure 1. ORTEP of the molecular structures of two slightly different ligands (A and B) in the asymmetric unit of ligand **L3**. Thermal ellipsoids were set at 50% probability.

alkyl residues. This observation agreed with the interplanar angles of 23.4–27.2° reported for isomeric ligand **L4**.[15a]

The reactions of stoichiometric amounts of compound **L2** or **L3** with [Ln(hfac)$_3$(diglyme)] (Ln = La, Eu, Gd, Lu, Y)[3,22] in CH_2Cl_2/MeCN gave anhydrous ternary complexes [Ln(**L*k***)(hfac)$_3$] (yield: 40–60%; see the Supporting Information, Table S5). Upon slow evaporation, prisms suitable for X-ray analysis were obtained for Ln = La, Eu, and Lu (see the Supporting Information, Table S6). All of these compounds crystallized in the monoclinic crystal system ($P2_1/n$ space group for the large and mid-range La and Eu cations, $C2/c$ for the small Lu cation) and showed the formation of mononuclear complex [Ln(**L*k***)(hfac)$_3$]. Careful inspection of the crystal packing revealed that either weak intermolecular Br–π interactions in [Ln(**L2**)(hfac)$_3$] (Ln = La, Eu; see the Supporting Information, Figure S3) or faint aromatic π–π stacking in [Ln(**L3**)(hfac)$_3$] (Ln = La, Eu; see the Supporting Information, Figure S4) contributed to the cohesion of the crystal structures for the larger lanthanides, whilst no remarkable intermolecular interactions were observed for Ln = Lu, except for some short F···benzimidazole distances along the *b* axis (see the Supporting Information, Figure S5). We concluded that the geometries of the molecular complexes were weakly affected by packing forces, which justified the analysis of the coordination bond lengths in term of their chemical affinities.[24]

The six molecular structures for [Ln(**L*k***)(hfac)$_3$] were very similar (Figure 2; also see the Supporting Information, Figure S6) and their rigid cores were globally superimposable across the lanthanide series (see the Supporting Information, Figures S7–S9). Each metal atom in [Ln(**L*k***)(hfac)$_3$] (k = 2, 3; Ln = La, Eu, Lu) was nine-coordinated by the three nitrogen atoms of the bound aromatic ligand (*cis–cis* conformation) and the six oxygen atoms of three didentate hexafluoroacetylacetonate anions (Figure 2). One didentate hfac$^-$ ion was almost located within the coordinating plane defined by the metal and the three bound nitrogen atoms, whilst the two remaining hfac$^-$ ions were arranged on both sides of this plane, thereby leading to a highly distorted coordination geometry around the metal centers. To minimize the steric constraints produced by the alkyl chains that were located close to the hydrogen atoms of the central pyridine rings,[16,17] the polyaromatic tridentate aromatic ligands deviated from planarity (interplanar pyridine-benzimidazole angles of 9.8–31.4° (average: 18(10)°) for [Ln(**L2**)(hfac)$_3$] and 14.6–27.0° (average: 21(5)°) for [Ln(**L3**)(hfac)$_3$]; see the Supporting Information, Tables S7–S9 and S10–S12, respectively). In contrast with the reported intramolecular interligand interactions within the analogous [Ln(*i*Pr-pybox)(hfac)$_3$] complexes (*i*Pr-pybox = 2,6-bis(5-isopropyloxazolin-2-yl)pyridine),[23] we did not detect any unusual short contacts between ligand **L2** (or **L3**) and hfac$^-$ ions that were bound to the same metal in [Ln(**L*k***)(hfac)$_3$]. However, thorough analysis of the bond lengths showed a systematic and intriguing contraction of both the Ln–O and Ln–N distances for a given metal on going from [Ln(**L2**)(hfac)$_3$] to [Ln(**L3**)(hfac)$_3$], whilst the bond angles displayed no special trends (see the Supporting Information, Table S7–S12). Thus, we resorted to the calculation of bond valences ($\nu_{Ln,N}$ and $\nu_{Ln,O}$) with Equation (1) for an easy comparison of the strength of the ligand–metal interactions in the various complexes (see the Supporting Information, Tables S13–S18):[11,24,25]

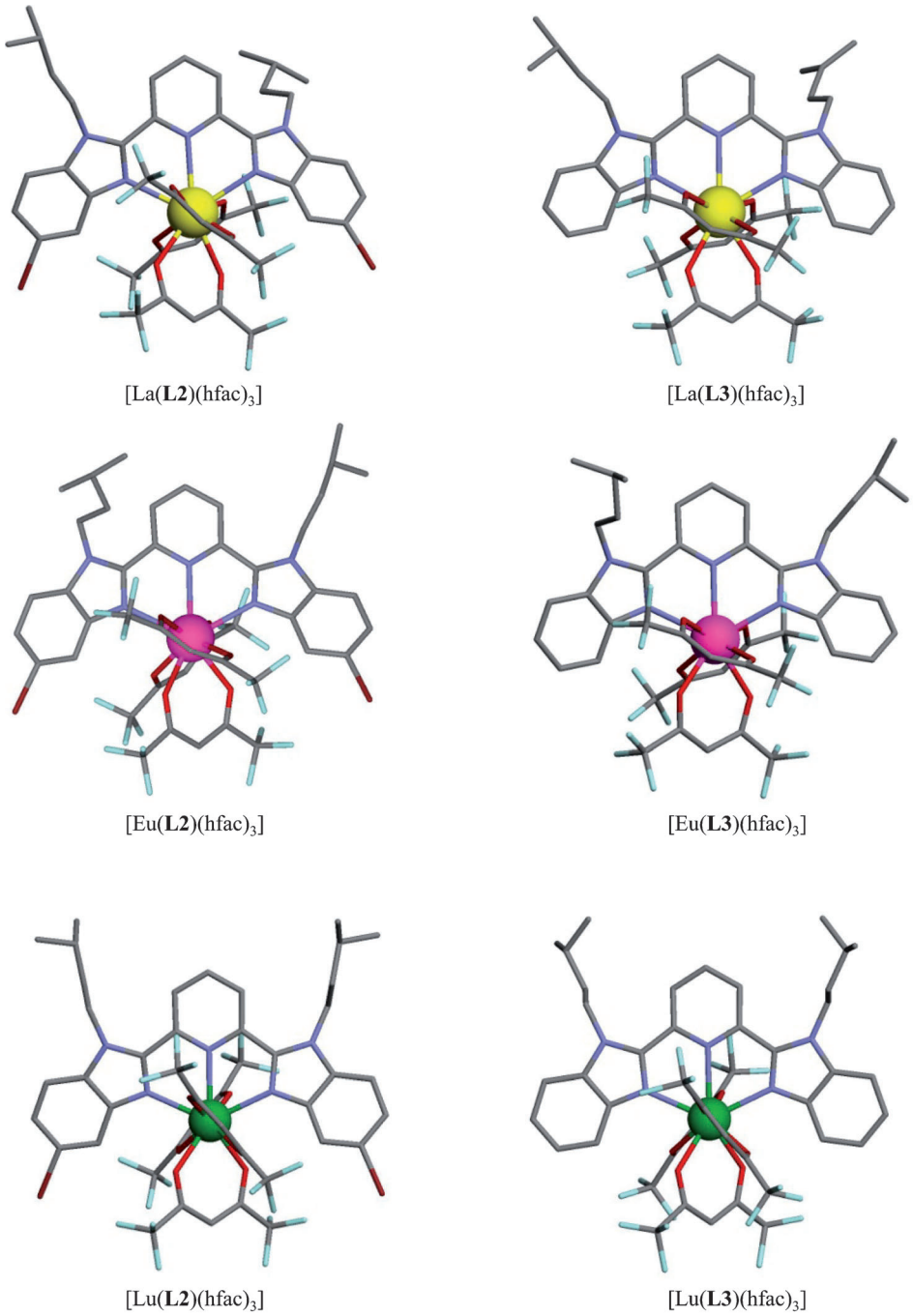

Figure 2. The molecular structures of complexes [Ln(**L2**)(hfac)$_3$] and [Ln(**L3**)(hfac)$_3$] (Ln = La, Eu, Lu) in the solid state. Colors: C gray, N dark blue, O red, F light blue, La yellow, Eu magenta, Lu green. H atoms are omitted for clarity. For atom numbering and thermal ellipsoids, see the Supporting Information, Figure S6.

$$\nu_{Ln,j} = \exp[(R_{Ln,j} - d_{Ln,j})/b] \quad (1)$$

where $d_{Ln,j}$ is the bond length, $R_{Ln,j}$ corresponds to the bond-valence parameters, and $b = 0.37$ Å is a universal scaling constant. From the average bond valences for [Ln(**L*k***)-(hfac)$_3$] (Table 1, entries 1–6), we found that $\nu_{Ln,O\text{-}hfac} > \nu_{Ln,N\text{-}ligand}$, which was in line with the preference of trivalent lanthanides for negatively charged oxygen donors. We also noted that: 1) $\nu_{Ln,O\text{-}hfac}$(**L2**) < $\nu_{Ln,O\text{-}hfac}$(**L3**) and $\nu_{Ln,N\text{-}ligand}$(**L2**) < $\nu_{Ln,N\text{-}ligand}$(**L3**) for a given metal, and 2) $\nu_{La,j} \geq \nu_{Eu,j} > \nu_{Lu,j}$ for each ligand along the lanthanide series (Table 1). These results suggested that: 1) the connection of bulky bromine atoms onto the aromatic ligand backbone expanded the coordination sphere and reduced interactions between the donor atoms and the central cation in [Ln(**L2**)(hfac)$_3$], and 2) the affinity of the ligands for the central cation decreased along the lanthanide series; this trend was opposite to the classically observed electrostatic trend.[26,27] As expected,[17] the replacement of the 2,6-bis(benzimidazol-2-yl)pyridine scaffolds in [Eu(**L3**)(hfac)$_3$] with the analogous terpyridine ligand in [Eu(4-phenyl-terpy)(hfac)$_3$] (Table 1, entry 7) or with 2,6-bis(oxazolinyl)pyridine ligand in [Eu(*i*Pr-pybox)(hfac)$_3$] (Table 1, entry 8) only had a minor impact on the geometry of the coordination sphere.[23] On the contrary, the replacement of electron-withdrawing fluoride atoms in the hfac$^-$ ions with bulky electron-donating methyl groups in dipivaloymethanate anions (dpm$^-$) significantly distanced the nitrogen atoms from the metal in [Eu(terpy)(dpm)$_3$] (Table 1, entry 9). Finally, the replacement of the six-membered chelate rings, which were produced by the didentate hfac$^-$ ions in [Ln(**L*k***)(hfac)$_3$], with the four-membered chelated rings that were produced by didentate nitrate anions in [Ln(**L*k***)(NO$_3$)$_3$] (Table 1, entries 10–13) decreased the global anion affinities ($\nu_{Ln,O\text{-}hfac} > \nu_{Ln,O\text{-}NO_3}$). In terms of bond-valence, [Ln(hfac)$_3$] is a promising candidate as a neutral lanthanide carrier in cascade complexation because: 1) hfac$^-$ ions strongly coordinated to the Ln^{III} centers, whilst 2) the electron-withdrawing CF$_3$ group limited charge-delocalization onto the cation to such an extent that the subsequent coordination of an additional neutral tridentate polyaromatic binding unit was still efficient.

Table 1. Average bond valences ($\nu_{Ln,j}$) and bond-valence sums ($V_{Ln,j}$)[a] in the crystal structures of [Ln(**L*k***)(hfac)$_3$], [Ln(**L*k***)(NO$_3$)$_3$], and related complexes.

Complex	$\nu_{Ln,N\text{-ligand}}$	$\nu_{Ln,O\text{-hfac}}$	$\nu_{Ln,O\text{-}NO_3}$	V_{Ln}	Reference
[La(**L2**)(hfac)$_3$]	0.32(4)	0.38(3)		3.22	this work
[Eu(**L2**)(hfac)$_3$]	0.32(3)	0.35(4)		3.05	this work
[Lu(**L2**)(hfac)$_3$]	0.31(3)	0.34(7)		2.96	this work
[La(**L3**)(hfac)$_3$]	0.36(3)	0.41(3)		3.53	this work
[Eu(**L3**)(hfac)$_3$]	0.35(2)	0.39(4)		3.37	this work
[Lu(**L3**)(hfac)$_3$]	0.31(5)	0.35(6)		3.00	this work
[Eu(4-Ph-terpy)(hfac)$_3$][b]	0.33(2)	0.37(2)		3.17	[8d]
[Eu(*i*Pr-pybox)(hfac)$_3$][c]	0.30(3)	0.35(3)		2.99	[23]
[Eu(terpy)(dpm)$_3$][d]	0.26(3)	0.39(5)		3.14	[8b]
[Lu(**L1**)(NO$_3$)$_3$]	0.37(4)		0.31(2)	2.96	[9a]
[Lu(**L6**)(NO$_3$)$_3$]	0.38(7)		0.32(2)	3.06	[17]
[Eu(**L8**)(NO$_3$)$_3$(CH$_3$OH)]	0.36(6)		0.28(5)	3.04	[17]
[Eu(**L4**)(NO$_3$)$_3$(CH$_3$CN)]	0.38(9)		0.27(3)	2.99	[15a]

[a] $V_{Ln} = \sum V_{Ln,j}$. [b] 4-Ph-terpy = 4′-phenyl-2,2′:6′,2″-terpyridine. [c] *i*Pr-pybox = 2,6-bis(5-isopropyl-oxazolin-2-yl)pyridine. [d] terpy = 2,2′:6′,2″-terpyridine, dpm = dipivaloylmethanate.

Speciation and structures of complexes [Ln(L*k*)(hfac)$_3$] (*k* = 2, 3; Ln = La, Eu, Lu, Y) in solution: Monitoring the titration of **L*k*** (*k* = 2, 3) with [Ln(hfac)$_3$(diglyme)] by ^{1}H NMR spectroscopy in $CDCl_3$ showed the stepwise disappearance of the signals for the free ligand and the appearance of ten new peaks for ligand **L2** (eleven peaks for **L3**), which were characteristic of the formation of the single C_{2v}-symmetrical complex [Ln(**L*k***)(hfac)$_3$] (Figure 3; also see the Supporting Information, Table S1 and Figure S10). At a total ligand concentration of 5 mM and [Ln(hfac)$_3$]/**L*k*** = 1.0, the signals for the free ligand disappeared, which agreed with Equilibrium (2), for which $\beta_{1,1}^{Ln(hfac)_3,\mathbf{Lk}} \geq 5\times10^5$ (in $CHCl_3$).[28] This value was in line with association constants of 10^7 that have been reported for the formation of [Ln(1,10-phenantroline)(hfac)$_3$] in dichloromethane.[29]

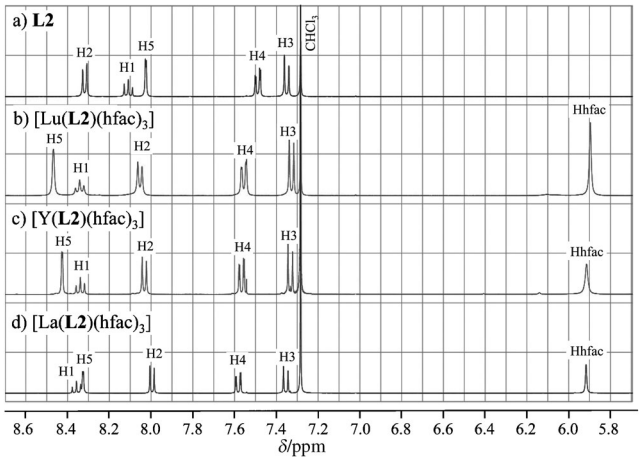

Figure 3. ^{1}H NMR spectra of a) ligand **L2** and its diamagnetic complexes b) [Lu(**L2**)(hfac)$_3$], c) [Y(**L2**)(hfac)$_3$], and d) [La(**L2**)(hfac)$_3$] in $CDCl_3$ (total ligand concentration: 5 mM, 293 K, atom numbering is given in Scheme 3).

$$Ln(hfac)_3 + \mathbf{Lk} \rightleftharpoons [Ln(\mathbf{Lk})(hfac)_3] \qquad \beta_{1,1}^{Ln(hfac)_3,\mathbf{Lk}} \qquad (2)$$

The downfield shift of H1 and the concomitant upfield shift of H2 in diamagnetic complexes [Ln(**L*k***)(hfac)$_3$] (*k* = 2,3; Ln = La, Y, Lu) were diagnostic for the complexation of the central pyridine ring to the cationic metal,[30] whilst the NOE effect between H2 and H6 attested to the *cis–cis* conformation that was adopted by the ligand upon coordination of the benzimidazole side-arms (Figure 2).[27a] However, contrary to the crystal structures, in which only a twofold axis could be considered, we observed an average pseudo-trigonal symmetry on the NMR timescale for complexes [Ln(**L*k***)(hfac)$_3$], with a single signal for the protons (Figure 3; also see the Supporting Information, Table S1) and for the fluorine atoms (see the Supporting Information, Figure S12 and Table S19) of the three didentate hexafluoroacetylacetonate anions. Such dynamic behavior is common for lanthanide complexes and a straightforward explanation involved fast exchange of the axial and equatorial didentate hfac$^-$ ions, which made them equivalent on the NMR timescale, thereby leading to a dynamically averaged C_{2v} symmetry for the remaining coordinated tridentate aromatic ligand in [Ln(**L*k***)(hfac)$_3$]. Confronted by closely related observations with [Ln(1,10-phenanthroline)(TTA)$_3$] (TTA = (4,4,4-trifluoro-1-2-thienyl)-1,3-butanedione), Destri and co-workers used paramagnetic NMR spectroscopy and pseudo-contact shift analysis for proposing an alternative trigonal structure in solution, in which the neutral heterocyclic ligand lay on one side of the C_3 axis of a distorted facial "static" trigonal prism that was produced by the [Ln(TTA)$_3$] moiety.[31] Fast rotation of the didentate phenanthroline ligand around the threefold axis on the NMR timescale was also required for producing local C_2 symmetry for the aromatic ligand. Extending this reasoning for [Ln(**L*k***)(hfac)$_3$] was difficult because the ^{13}C NMR (see the Supporting Information, Figure S11) and ^{19}F NMR patterns (see the Supporting Information, Figure S12) pointed to six equivalent CF_3 groups for the three coordinated hfac$^-$ anions (global C_{3h}, D_3, or D_{3h} point group) on the NMR timescale, which was incompatible with the formation of a "static" trigonal prism produced by the [Ln(hfac)$_3$] moiety with **L*k*** coordinated on one side of the threefold axis (C_3 or C_{3v} point group). As expected, the replacement of diamagnetic metals with paramagnetic Eu^{III} in [Eu(**L*k***)(hfac)$_3$] showed considerable lanthanide-induced shifts, with a maximum effect for H5 because of its location close to the metallic center (Figure 2, also see the Supporting Information, Table S1).[32] Repeating these titrations in more-polar CD_3CN provided similar results for Ln = Eu, Y, Lu with the exclusive formation of [Ln(**L*k***)(hfac)$_3$] (*k* = 2, 3), according to Equilibrium (2) (Figure 4; also see the Supporting Information, Figure S13 and Table S2). For the smaller Lu cation, we noted a significant reduction in $\beta_{1,1}^{Ln(hfac)_3,\mathbf{Lk}}$ in acetonitrile, and we detected non-negligible amounts of free ligand and free [Lu(hfac)$_3$] in slow exchange on the NMR timescale (total ligand concentration: 5 mM, [Lu(hfac)$_3$]/**L*k*** = 1.0; Figure 4b, also see the Supporting Information, Figure S13b). Surprisingly, ^{1}H NMR titration of **L*k*** with larger lanthanum cations showed the formation of two C_{2v}-symmetric complexes at

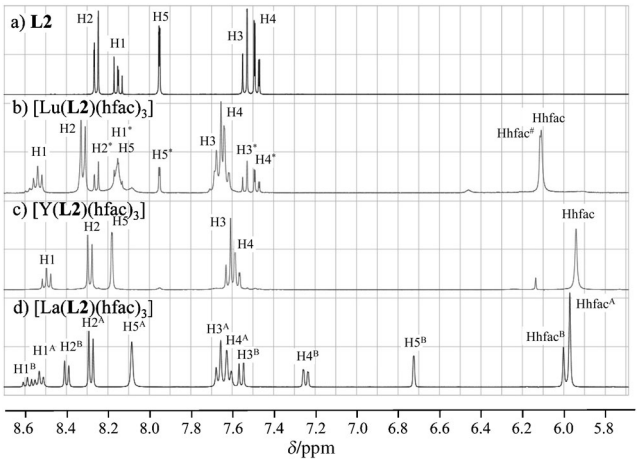

Figure 4. ^{1}H NMR spectra of a) ligand **L2** and its diamagnetic complexes b) [Lu(**L2**)(hfac)$_3$] (*=free ligand, #=free Lu(hfac)$_3$), c) [Y(**L2**)(hfac)$_3$], and d) [La(**L2**)(hfac)$_3$] in CD_3CN (total ligand concentration: 5 mM, 293 K, atom numbering is given in Scheme 3).

[La(hfac)$_3$]/**Lk**=1.0: [La(**Lk**)(hfac)$_3$]-A and [La(**Lk**)(hfac)$_3$]-B (Figure 4d; also see the Supporting Information, Figure S13d and Table S2).

Comparison of the ^{1}H NMR chemical shifts of lanthanum complexes with those of their analogous diamagnetic complexes [Y(**Lk**)(hfac)$_3$] and [Lu(**Lk**)(hfac)$_3$] unambiguously demonstrated that [La(**Lk**)(hfac)$_3$]-A could be assigned to the expected neutral mononuclear nine-coordinate complex [La(**Lk**)(hfac)$_3$]. The striking upfield shift observed for the aromatic protons H4, H5, and H11 in the second complex [La(**Lk**)(hfac)$_3$]-B suggested some local diamagnetic anisotropy produced by their specific location in the shielding cone of neighboring aromatic rings, as found in diamagnetic complexes $[Ln(\mathbf{L8})_2]^{3+}$[33] and $[Ln(\mathbf{L8})_3]^{3+}$,[27a] which contained two or three polyaromatic tridentate units. Accordingly, diffusion-ordered spectroscopy (DOSY NMR) displayed smaller translational self-diffusion coefficients for [La(**Lk**)(hfac)$_3$]-B, which was in agreement with the existence of larger molecular aggregates, including additional ligands (see the Supporting Information, Table S20). Quantitative analysis of the self-diffusion coefficients with the help of the Stokes–Einstein equation showed that the molecular weights increased by $\Delta MM^{H}_{B-A} = MM^{H}_{La-B} - MM^{H}_{La-A}$=578-(122) g mol^{-1} (**L2**), and by ΔMM^{H}_{B-A}=265(56) g mol^{-1} (**L3**) on going from [La(**Lk**)(hfac)$_3$] to [La(**Lk**)(hfac)$_3$]-B (see the Supporting Information, Table S20, Appendix 1).[34] These values matched reasonably well with the computed changes in molecular weight for the replacement of one hfac$^-$ anion with a tridentate neutral ligand to give the ten-coordinate cations $[La(\mathbf{L2})_2(hfac)_2]^+$ (ΔMM_{B-A}=402 g mol^{-1}) and $[La(\mathbf{L3})_2(hfac)_2]^+$ (ΔMM_{B-A}=244 g mol^{-1}), according to Equilibrium (3).

$$2\,[La(\mathbf{Lk})(hfac)_3] \rightleftharpoons [La(\mathbf{Lk})_2(hfac)_2]^+ + [La(hfac)_4]^- \qquad K^{La,\mathbf{Lk}}_{exch} \qquad (3)$$

MS (ESI) spectra of solutions of [La(**Lk**)(hfac)$_3$] in acetonitrile confirmed the proposed bi-exchange process, with the detection of prominent signals for $[La(\mathbf{Lk})_2(hfac)_2]^+$ (m/z 1771 for k=2 and 1456 for k=3, positive mode) and for $[La(hfac)_4]^-$ (m/z 967.3, negative mode), whilst ^{19}F NMR spectroscopy showed three singlets, which were assigned to [La(**Lk**)(hfac)$_3$] (δ=−77.52 ppm), $[La(\mathbf{Lk})_2(hfac)_2]^+$ (δ=−77.08 ppm), and $[La(hfac)_4]^-$ (δ=−77.46 ppm; see the Supporting Information, Table S19 and Figure S14). We concluded that, in acetonitrile, [La(**Lk**)(hfac)$_3$] co-existed with its ionized form, $[La(\mathbf{Lk})_2(hfac)_2]^+$ and $[La(hfac)_4]^-$, according to Equilibrium (3).[35] Because of the slow exchange on the NMR timescale, the integrated intensities of the same proton in **Lk**, [La(**Lk**)(hfac)$_3$], and $[La(\mathbf{Lk})_2(hfac)_2]^+$ along the titration of **Lk** with [La(hfac)$_3$] could be exploited for the estimation of thermodynamic constants $K^{La,\mathbf{Lk}}_{exch}$ ([Equilibrium (3)]) and $\beta^{La(hfac)_3,\mathbf{Lk}}_{1,1}$ ([Equilibrium (2)]; also see the Supporting Information, Appendix 2). At room temperature, we obtained $K^{La,\mathbf{L2}}_{exch}$=0.07(4) and $K^{La,\mathbf{L3}}_{exch}$=0.04(3) (see the Supporting Information, Table S21), which translated into $\frac{[La(\mathbf{Lk})_2(hfac)_2]}{[La(\mathbf{Lk})_2(hfac)_3]} = \sqrt{K^{La,\mathbf{Lk}}_{exch}}$=0.26(7) and 0.20(8) for ligands **L2** and **L3**, respectively; that is, a ligand speciation of about 70% in favor of the target complexes [La(**Lk**)(hfac)$_3$]. Variable-temperature NMR spectra for the most-soluble complex, [La(**L2**)(hfac)$_3$], showed a significant increase in the $\frac{[La(\mathbf{Lk})_2(hfac)_2]}{[La(\mathbf{Lk})_2(hfac)_3]}$ ratio at low temperatures (see the Supporting Information, Table S21 and Figure S15), from which a van′t Hoff plot gave $\Delta H^{\circ La,\mathbf{L2}}_{exch}$=−23(1) kJ mol^{-1}, $\Delta S^{\circ La,\mathbf{L2}}_{exch}$=−98(4) J mol^{-1}K^{-1}, and $\Delta G^{\circ La,\mathbf{L2}}_{exch}$=6(1) kJ mol^{-1} (see the Supporting Information, Figure S16). The considerable entropic penalty of Equilibrium (3) followed the charge-neutralization principle, which entropically strongly disfavors anion/cation dissociation in polar solvents.[36] Thus, the detection of non-negligible amounts of $[La(\mathbf{Lk})_2(hfac)_2]^+$ was driven by the enthalpic gain that accompanied the **Lk**/hfac bi-exchange process. Beyond the minor cooperative/anti-cooperative intramolecular interligand interactions that contributed to the latter equation (see below), we suspected that solvation processes played a crucial role in stabilizing the ionic products, $[La(\mathbf{Lk})_2(hfac)_2]^+$ and $[La(hfac)_4]^-$. To substantiate this hypothesis, we noted that the ^{1}H NMR titration of ligand **L2** with [La(hfac)$_3$] in CD_3NO_2, a solvent with a dielectric constant very similar to that of CD_3CN, also showed the concomitant formation of [La(**L2**)(hfac)$_3$], $[La(\mathbf{L2})_2(hfac)_2]^+$, and $[La(hfac)_4]^-$ (see the Supporting Information, Figure S17); this phenomenon stepwise disappears when non-polar $CDCl_3$ was added to CD_3CN (see the Supporting Information, Figure S18). Moreover, $K^{La,\mathbf{L2}}_{exch}$ was highly sensitive to the ionic strength of the solution, and $K^{La,\mathbf{L2}}_{exch}$=0.005 when 1.4 M $LiClO_4$ was added in CD_3CN. With this result in mind, we considered the values $\log(\beta^{La(hfac)_3,\mathbf{L2}}_{1,1})$=3.3(9) and $\log(\beta^{La(hfac)_3,\mathbf{L3}}_{1,1})$=3.6(9), which were estimated for Equilibrium (2) by using NMR data, to only be mere estimations for the thermodynamic stability constants extrapolated at infinite dilution. Finally, the reluctance of smaller lanthanides for reaching ten-coordination in $[Ln(\mathbf{L2})_2(hfac)_2]^+$ resulted in such a rapid decrease of

$K_{exch}^{La,Lk}$ along the lanthanide series that the latter complexes were only detected for Ln = La, Ce, and Pr.

Thermodynamic behavior of complexes [Ln(L*k*)(hfac)$_3$] (*k* = 2, 3; Ln = La, Nd, Sm, Eu, Gd, Tb, Tm, Lu, Y) in acetonitrile: Thermodynamic stability constants $\beta_{1,1}^{Ln(hfac)_3,Lk}$ for Equilibrium (2), but extrapolated at zero ionic strength, were obtained by spectrophotometric titrations of ligands **L2** and **L3** at low concentration (10^{-4} M in CH_3CN and 10^{-4} M diglyme) with [Ln(hfac)$_3$(diglyme)] (Ln = La, Nd, Sm, Eu, Gd, Tb, Tm, Lu, Y; $|Ln|_{tot}/|Lk|_{tot} = 0.1 \rightarrow 2.6$; see the Supporting Information, Figure S19). The *trans–trans*→*cis–cis* conformational change of the tridentate ligand, which accompanied the complexation process, induced some significant changes in the electronic structure,[37] which were easily monitored in the UV part of the absorption spectra (see the Supporting Information, Figure S19a).[16,18b,38] Correcting the spectrophotometric data for the absorption of free [Ln(hfac)$_3$] (see the Supporting Information, Appendix 3) showed the classical splitting of the ligand-centered π→π* transition, which resulted from the coordination of ligand **L*k*** to the metal center in [Ln(**L*k***)(hfac)$_3$] (33110 and 28170 cm^{-1}; see the Supporting Information, Figure S19b),[37–39] whilst the existence of isosbestic points was diagnostic for the existence of only two absorbing species in the solution (excluding [Ln(hfac)$_3$]; see the Supporting Information, Figure S19b). The single end-point for $|Ln|_{tot}/|Lk|_{tot} = 1.0$ (see the Supporting Information, Figure S19c) confirmed the operation of Equilibrium (2), and the spectrophotometric data were fitted with non-linear least-square techniques[40] to give the associated formation constants $\beta_{1,1}^{Ln(hfac)_3,Lk}$ (Table 2 and Figure 5).

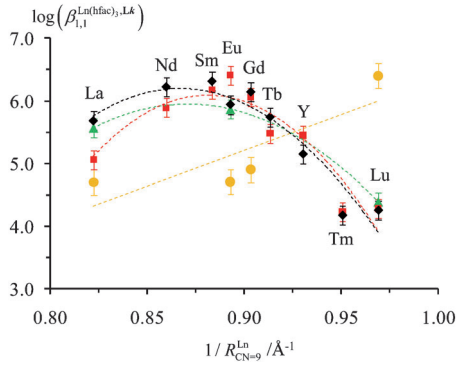

Figure 5. Variations of $\log(\beta_{1,1}^{Ln(hfac)_3,Lk})$ for ligands **L2** (red squares), **L3** (black diamonds), and **L8** (green triangles) as a function of the inverse of the nine-coordinate ionic radii for the lanthanide series.[41] The dashed lines are only guides for the eyes. The related variation of $\log(\beta_{1,1}^{Ln(NO_3)_3,L7})$ is taken from reference [11] (yellow disks).

As inferred from the bond-valence analysis in the solid state, $\beta_{1,1}^{Ln(hfac)_3,Lk}$ decreases across the lanthanide series (Figure 5), which demonstrates the operation of a counterintuitive trend for this system.[26,27] Because the replacement of the bulky 3-methy-1-butyl groups (ligands **L2** and **L3**) with simple methyl groups (**L8**) had a negligible impact on the thermodynamic constants (Figure 5), the switch from the standard electrostatic trend, which characterized the connection of **L*k*** to [Ln(NO$_3$)$_3$] (**L*k*** = **L7** or **L8**, [Equilibrium (4)]),[11] to the reverse behavior, for the addition of **L*k*** to [Ln(hfac)$_3$] (**L*k*** = **L2**, **L3**, or **L8**, [Equilibrium (2)]), was assigned to the choice of counteranions:

$$Ln(NO_3)_3 + Lk \rightleftharpoons [Ln(Lk)(NO_3)_3] \qquad \beta_{1,1}^{Ln(NO_3)_3,Lk} \qquad (4)$$

Table 2. Thermodynamic-formation constants ($\log\beta_{1,1}^{Ln(hfac)_3,Lk}$) and associated microscopic affinities ($\log(f_{Lk}^{Ln(hfac)_3})$ and $\Delta G_{Lk}^{Ln(hfac)_3}$) obtained by spectrophotometric titrations of ligands **L2**, **L3**, and **L8** with [Ln(hfac)$_3$(diglyme)] in MeCN (298 K).[a]

Ligand	Ln^{III}	$R_{CN=9}^{Ln}$[Å][b]	$\log\beta_{1,1}^{Ln(hfac)_3,Lk}$	$\log(f_{Lk}^{Ln(hfac)_3})$	$\Delta G_{Lk}^{Ln(hfac)_3}$ [kJ mol^{-1}]
L2	La	1.216	5.06(7)	4.60(7)	−26.3(6)
L2	Nd	1.163	5.89(13)	5.41(13)	−30.9(6)
L2	Sm	1.132	6.18(16)	5.70(16)	−33(1)
L2	Eu	1.120	6.41(12)	5.93(12)	−33.8(6)
L2	Gd	1.107	6.06(15)	5.58(15)	−32.0(6)
L2	Tb	1.095	5.48(8)	5.00(8)	−28.7(6)
L2	Y	1.075	5.45(8)	4.97(8)	−28.7(6)
L2	Tm	1.052	4.23(32)	3.75(32)	−21(1)
L2	Lu	1.032	4.28(30)	3.80(30)	−21(1)
L3	La	1.216	5.68(11)	5.20(11)	−29.8(6)
L3	Nd	1.163	6.22(9)	5.74(9)	−32.7(6)
L3	Sm	1.132	6.31(10)	5.83(10)	−33.2(6)
L3	Eu	1.120	5.94(9)	5.46(9)	−30.9(6)
L3	Gd	1.107	6.14(11)	5.66(11)	−32.0(6)
L3	Tb	1.095	5.74(7)	5.26(7)	−29.8(6)
L3	Y	1.075	5.15(5)	4.67(5)	−27.0(6)
L3	Tm	1.052	4.18(30)	3.70(30)	−21(2)
L3	Lu	1.032	4.26(24)	3.78(24)	−21(1)
L8	La	1.216	5.57(8)	5.09(8)	−29.2(6)
L8	Eu	1.120	5.87(6)	5.39(6)	−30.9(6)
L8	Lu	1.032	4.29(31)	3.91(31)	−21.8(2)

[a] MeCN contains a fixed total concentration (10^{-4} M) of diglyme for stabilizing [Ln(hfac)$_3$]. [b] Effective ionic radii for nine-coordinate Ln^{III}.[41]

Altogether, 1) the stability constants collected for [Ln(**L*k***)(hfac)$_3$] along the major part of the lanthanide series (i.e. $\log(\beta_{1,1}^{Ln(hfac)_3,Lk}) > \log(\beta_{1,1}^{Ln(NO_3)_3,Lk})$) combined with 2) the large solubility brought by the branched alkyl residues in **L2** and **L3**, and 3) the remarkable bowl-shaped thermodynamic selectivity[27a] make [Ln(hfac)$_3$] very attractive for the planned loading of multi-tridentate polymeric ligands that contain 2,6-bis(benzimidazol-2-yl)pyridine binding units. However, we noted that the trend $\beta_{1,1}^{Ln(hfac)_3,L2} < \beta_{1,1}^{Ln(hfac)_3,L3}$ suggested by the crystal-structure analysis was not pertinent in solution, probably as a result of compensating solvation effects.

A deeper insight into the thermodynamic complexation process benefitted from the site-binding model,[42] which deciphered the various energetic contributions to the formation of [Ln(**L*k***)(hfac)$_3$]. In Equation (5), the microscopic intermolecular affinity of ligand **L*k*** for the metal unit [Ln(hfac)$_3$] was estimated by the connection parameter $f_{Lk}^{Ln(hfac)_3}$ (Table 2, column 5), which was a microscopic describer that included desolvation processes, whilst the purely

entropic statistical factor $\omega_{1,1}^{\text{chiral}}\cdot\omega_{1,1}^{\text{Ln(hfac)}_3,\mathbf{Lk}}=3$ (associated with Equilibrium (2)) was obtained by the method of the symmetry numbers (Figure 6a).[43]

$$\beta_{1,1}^{\text{La(hfac)}_3,\mathbf{Lk}}=\omega_{1,1}^{\text{chiral}}\cdot\omega_{1,1}^{\text{Ln(hfac)}_3,\mathbf{Lk}}\cdot f_{1,1}^{\text{La(hfac)}_3,\mathbf{Lk}}=3f_{\mathbf{Lk}}^{\text{La(hfac)}_3} \quad (5)$$

After fixing the standard concentration of the reference state to 1 M,[44] the van't Hoff isotherm transformed $f_{\mathbf{Lk}}^{\text{Ln(hfac)}_3}$ into their free energy counterparts $-34\le\Delta G_{\text{con},\mathbf{Lk}}^{\text{Ln(hfac)}_3}\le -21\ \text{kJ mol}^{-1}$ across the lanthanide series for ligands **L2**, **L3**, and **L8** (Table 2, column 6). These values compared well with those reported for $\Delta G_{\mathbf{L7}}^{\text{Ln(NO}_3)_3}$, but were significantly less-negative than those found for $\Delta G_{\mathbf{L7}}^{\text{Ln(CF}_3\text{SO}_3)_3}$ and $\Delta G_{\mathbf{L7}}^{\text{Ln(ClO}_4)_3}$ in pure acetonitrile.[11] More detailed information could not be obtained from the determination of a single stability constant. However, the operation of Equilibrium (3) and the formation of the two ternary complexes $[\text{La}(\mathbf{Lk})(\text{hfac})_3]$ and $[\text{La}(\mathbf{Lk})_2(\text{hfac})_2]^+$ opens up new perspectives when one considers Equilibrium (2) to be the result of a cascade reaction of the solvated metal with ligands **Lk** and hfac^- ([Equilibrium (6)]).

$$\text{La}^{3+}+\mathbf{Lk}+3\,\text{hfac}^- \rightleftharpoons [\text{La}(\mathbf{Lk})(\text{hfac})_3] \qquad \beta_{1,1,3}^{\text{La},\mathbf{Lk},\text{hfac}} \quad (6)$$

Since the statistical factors only marginally contributed to the total free-energy change,[42] rough values were deduced by fixing an arbitrarily common coordination number of CN = 9 around each lanthanide atom, except for $[\text{La}(\mathbf{Lk})_2(\text{hfac})_2]^+$ (CN = 10) and $[\text{La}(\text{hfac})_4]^-$ (CN = 8; see the Supporting Information, Figure S20). Moreover, the donor atoms in the first coordination sphere were assumed to occupy the position of an idealized tricapped trigonal prism, whilst solvent molecules filled the vacant positions. With these assumptions in mind, Equilibrium (6) was transformed into Equilibrium (7), whose stability constant ($\beta_{1,1,3}^{\text{La},\mathbf{Lk},\text{hfac}}$) could be modeled by Equation (8) (Figure 6b, $f_{\mathbf{Lk}}^{\text{Ln}}$ and $f_{\text{hfac}}^{\text{Ln}}$ are the intermolecular microscopic affinities of each ligand for Ln^{3+} and $u_{\text{L,L}}=e^{-\left(\Delta E_{\text{L,L}}/RT\right)}$ are the Boltzmann factors that account for the intramolecular interligand interactions that occurred within the coordination sphere).[42]

$$[\text{La}(\text{CH}_3\text{CN})_9]^{3+}+\mathbf{Lk}+3\,\text{hfac}^- \rightleftharpoons [\text{La}(\mathbf{Lk})(\text{hfac})_3]+9\,\text{CH}_3\text{CN} \qquad \beta_{1,1,3}^{\text{La},\mathbf{Lk},\text{hfac}} \quad (7)$$

$$\beta_{1,1,3}^{\text{La},\mathbf{Lk},\text{hfac}}=48f_{\mathbf{Lk}}^{\text{La}}(f_{\text{hfac}}^{\text{La}})^3(u_{\mathbf{Lk},\text{hfac}})^3(u_{\text{hfac,hfac}})^3 \quad (8)$$

The same strategy was followed for modeling Equilibrium (9) with the stability constant given in Equation (10). This process was systematically repeated for the related equilibria, thereby leading to the formation of $[\text{La}(\mathbf{Lk})_n]^{3+}$ (n = 1–3; see the Supporting Information, S18–S23) and $[\text{La}(\text{hfac})_n]^{(3-n)+}$ (n = 1–4; see the Supporting Information, S24–S31, Appendix 4, and Figure S20).

$$[\text{La}(\text{CH}_3\text{CN})_9]^{3+}+2\,\mathbf{Lk}+2\,\text{hfac}^- \rightleftharpoons [\text{La}(\mathbf{Lk})_2(\text{hfac})_2]^+ +9\,\text{CH}_3\text{CN} \qquad \beta_{1,2,2}^{\text{La},\mathbf{Lk},\text{hfac}} \quad (9)$$

$$\beta_{1,2,2}^{\text{La},\mathbf{Lk},\text{hfac}}=72(f_{\mathbf{Lk}}^{\text{La}})^2(f_{\text{hfac}}^{\text{La}})^2(u_{\mathbf{Lk},\text{hfac}})^4(u_{\text{hfac,hfac}})(u_{\mathbf{Lk},\mathbf{Lk}}) \quad (10)$$

Once the experimental values for $\beta_{1,1}^{\text{La(hfac)}_3,\mathbf{Lk}}$ ([Equilibrium (2)], Table 2), $K_{\text{exch}}^{\text{La},\mathbf{Lk}}$ [Equilibrium (3)], $\beta_{1,0,3}^{\text{La},\mathbf{Lk},\text{hfac}}$ (see the Supporting Information, [Equilibrium (S28)] and Table S22), and $\beta_{1,0,4}^{\text{La},\mathbf{Lk},\text{hfac}}$ (see the Supporting Information, [Equilibrium (S30)] and Table S22) were in hand, the missing stability constants $\beta_{1,1,3}^{\text{La},\mathbf{Lk},\text{hfac}}$ [Equilibrium (7)] and $\beta_{1,2,2}^{\text{La},\mathbf{Lk},\text{hfac}}$ [Equilibrium (9)] were deduced by using Equations (11) and (2) (see the Supporting Information, Table S22).

$$\beta_{1,1,3}^{\text{La},\mathbf{Lk},\text{hfac}}=\beta_{1,0,3}^{\text{La},\mathbf{Lk},\text{hfac}}\cdot\beta_{1,1}^{\text{La(hfac)}_3,\mathbf{Lk}} \quad (11)$$

$$\beta_{1,2,2}^{\text{La},\mathbf{Lk},\text{hfac}}=\frac{(\beta_{1,1,3}^{\text{La},\mathbf{Lk},\text{hfac}})^2\cdot K_{\text{exch}}^{\text{La},\mathbf{Lk}}}{\beta_{1,0,4}^{\text{La},\mathbf{Lk},\text{hfac}}} \quad (12)$$

Multi-linear least-square fits of the nine Equations (Eq. (11) and (12) as well as Eq. (S18)–(S31) in the Supporting Information) converged for the five microscopic thermodynamic describers (Table 3), which satisfyingly reproduced the experimental formation constants (see the Supporting Information, Table S22 and Figure S21).[45]

Table 3. Fitted microscopic thermodynamic parameters for $\text{La}^{\text{III}}/\mathbf{Lk}/\text{hfac}^-$ (k = 2, 3; MeCN; 298 K).[a]

Entry	Parameters	L2	L3
1	$\log(f_{\mathbf{Lk}}^{\text{La}})$	5.5(4)	4.3(5)
2	$\Delta G_{\text{con},\mathbf{Lk}}^{\text{La}}$ [kJ mol^{-1}]	−31(2)	−25(3)
3	$\log(f_{\text{hfac}}^{\text{La}})$	6.2(3)	6.2(4)
4	$\Delta G_{\text{con,hfac}}^{\text{La}}$ [kJ mol^{-1}]	−35(2)	−35(2)
5	$\log(u_{\mathbf{Lk},\mathbf{Lk}}^{\text{La}})$	−0.4(4)	0.8(6)
6	$\Delta E_{\mathbf{Lk},\mathbf{Lk}}^{\text{La}}$ [kJ mol^{-1}]	2(3)	−5(3)
7	$\log(u_{\mathbf{Lk},\text{hfac}}^{\text{La}})$	−0.5(2)	0.1(2)
8	$\Delta E_{\mathbf{Lk},\text{hfac}}^{\text{La}}$ [kJ mol^{-1}]	3(1)	0(1)
9	$\log(u_{\text{hfac,hfac}}^{\text{La}})$	−0.4(2)	−0.4(3)
10	$\Delta E_{\text{hfac,hfac}}^{\text{La}}$ [kJ mol^{-1}]	2(1)	2(2)

[a] MeCN contains a fixed total concentration (10^{-4} M) of diglyme for stabilizing $[\text{Ln(hfac)}_3]$.

In line with the well-known oxophilicity of trivalent lanthanides and the preference for charge-neutralization in polar solvents, the intermolecular connection of the hfac^- anion to La^{3+} ($\Delta G_{\text{con,hfac}}^{\text{La}}=-RT\ln\left(f_{\text{hfac}}^{\text{La}}\right)=-35(2)\ \text{kJ mol}^{-1}$, Table 3, entry 4) made a prominent contribution to the stability of $[\text{La}(\mathbf{Lk})(\text{hfac})_3]$. The related interactions with the neutral tridentate N-donor ligands **Lk** with La^{3+} were slightly less favorable ($-31\le\Delta G_{\text{con},\mathbf{Lk}}^{\text{La}}=-RT\ln(f_{\mathbf{Lk}}^{\text{La}})\le -25\ \text{kJ mol}^{-1}$, Table 3, entry 2), but they closely matched those found for the connection of **Lk** onto $[\text{La(hfac)}_3]$ ($-30\le\Delta G_{\text{con},\mathbf{Lk}}^{\text{La(hfac)}_3}=-RT\ln(f_{\mathbf{Lk}}^{\text{La(hfac)}_3})\le -26\ \text{kJ mol}^{-1}$, Table 2), which was in agreement with a negligible influence of the charge neutralization brought by the complexation of hfac^- ions on the cascade reaction with ligands **L2** and **L3**. As

a)

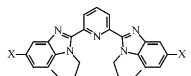

$$[Ln(hfac)_3(CH_3CN)_3] + \mathbf{L}\boldsymbol{k} \rightleftharpoons[\beta_{1,1}^{Ln(hfac)_3,\mathbf{L}\boldsymbol{k}}] [Ln(\mathbf{L}\boldsymbol{k})(hfac)_3] + 3\,CH_3CN \quad (2)$$

Point groups:	C_{3v}	C_{2v}	C_{2v}	C_{3v}
σ^{ext}:	3	2	2	3
σ^{int}:	3^9	3^4	3^{10}	1
σ^{chiral}:	1	1	1	1

$$\omega_{1,1}^{chiral} = \frac{\sigma_{Ln(hfac)_3}^{chiral}\cdot\sigma_{Lk}^{chiral}}{\sigma_{Ln\text{-}Lk}^{chiral}\cdot\left(\sigma_{CH_3CN}^{chiral}\right)^3} = \frac{1\cdot1}{1\cdot1^3} = 1 \qquad \omega_{1,1}^{Ln(hfac)_3,\mathbf{L}\boldsymbol{k}} = \frac{\left(\sigma_{Ln(hfac)_3}^{ext}\sigma_{Ln(hfac)_3}^{int}\right)\cdot\left(\sigma_{Lk}^{ext}\sigma_{Lk}^{int}\right)}{\left(\sigma_{Ln\text{-}Lk}^{ext}\sigma_{Ln\text{-}Lk}^{ext}\right)\cdot\left(\sigma_{CH_3CN}^{ext}\sigma_{CH_3CN}^{int}\right)^3} = \frac{3\cdot3^9\cdot2\cdot3^4}{2\cdot3^{10}\cdot3^3} = 3$$

$$\Rightarrow \beta_{1,1}^{Ln(hfac)_3,\mathbf{L}\boldsymbol{k}} = \omega_{1,1}^{chiral}\omega_{1,1}^{Ln(hfac)_3,\mathbf{L}\boldsymbol{k}} f_{1,1}^{Ln(hfac)_3,\mathbf{L}\boldsymbol{k}} = 3 f_{\mathbf{L}\boldsymbol{k}}^{Ln(hfac)_3} \quad (5)$$

b)

$$[Ln(CH_3CN)_9]^+ + \mathbf{L}\boldsymbol{k} + 3\,hfac^- \rightleftharpoons[\beta_{1,1,3}^{Ln,\mathbf{L}\boldsymbol{k},hfac}] [Ln(\mathbf{L}\boldsymbol{k})(hfac)_3] + 9\,CH_3CN \quad (7)$$

Point groups:	D_{3h}	C_{2v}	C_{2v}	C_{2v}	C_{3v}
σ^{ext}:	6	2	2	2	3
σ^{int}:	3^9	3^4	3^2	3^{10}	1
σ^{chiral}:	1	1	1	1	1

$$\omega_{1,1}^{chiral} = \frac{1\cdot1\cdot1^3}{1\cdot1^9} = 1 \qquad \omega_{1,1,3}^{Ln,\mathbf{L}\boldsymbol{k},hfac} = \frac{6\cdot3^9\cdot2\cdot3^4\cdot\left(2\cdot3^2\right)^3}{2\cdot3^{10}\cdot3^9} = 48$$

$$\Rightarrow \beta_{1,1,3}^{Ln,\mathbf{L}\boldsymbol{k},hfac} = 48 f_{\mathbf{L}\boldsymbol{k}}^{Ln}\left(f_{hfac}^{Ln}\right)^3\left(u_{\mathbf{L}\boldsymbol{k},hfac}\right)^3\left(u_{hfac,hfac}\right)^3 \quad (8)$$

Figure 6. Application of the site-binding model,[42] which shows the determination of symmetry numbers (σ^{ext}, σ^{int}, σ^{chiral}),[43] for a) Equilibrium (2) and b) Equilibrium (7). The symmetry point groups are those expected for idealized arrangements of the donor groups of the ligands in the first coordination sphere of the lanthanide.

a corollary, the intramolecular heteroligand interactions $\Delta E_{\mathbf{L}\boldsymbol{k},hfac}^{La} = -RT\ln(u_{\mathbf{L}\boldsymbol{k},hfac}^{La})$ were negligible (Table 3, entry 8); this trend was mirrored by the homoligand **L*k*–L*k*** ($\Delta E_{\mathbf{L}\boldsymbol{k},\mathbf{L}\boldsymbol{k}}^{La}$; Table 3, entry 6) and hfac–hfac ($\Delta E_{hfac,hfac}^{La}$; Table 3, entry 10) interactions within experimental errors. Finally, the introduction of Equations (8), (10), and (S31) from the Supporting Information into Equation (12) gave:

$$K_{exch}^{La,\mathbf{L}\boldsymbol{k}} = \frac{3}{4}\frac{(u_{hfac,hfac}^{La})\cdot(u_{\mathbf{L}\boldsymbol{k},\mathbf{L}\boldsymbol{k}}^{La})}{(u_{\mathbf{L}\boldsymbol{k},hfac}^{La})^2} \quad (13)$$

which was transformed by using the van't Hoff isotherm into the standard mixing rule [Eq. (14)]:[45]

$$\begin{aligned}\Delta E_{\mathbf{L}\boldsymbol{k},hfac}^{mix} &= \Delta G_{exch}^{La,\mathbf{L}\boldsymbol{k}} + RT\ln\left(\frac{3}{4}\right)\\ &= \Delta E_{hfac,hfac}^{La,\mathbf{L}\boldsymbol{k}} + \Delta E_{\mathbf{L}\boldsymbol{k},\mathbf{L}\boldsymbol{k}}^{La} - 2\Delta E_{\mathbf{L}\boldsymbol{k},hfac}^{La}\end{aligned} \quad (14)$$

Under statistical conditions, the sum of the homoligand interactions ($\Delta E_{hfac,hfac}^{La} + \Delta E_{\mathbf{L}\boldsymbol{k},\mathbf{L}\boldsymbol{k}}^{La}$) exactly overcame the scaled heteroligand interactions ($2\Delta E_{\mathbf{L}\boldsymbol{k},hfac}^{La}$), and $\Delta E_{\mathbf{L}\boldsymbol{k},hfac}^{mix} = 0$.[45] This result was close to that found for [La(**L2**)(hfac)$_3$] ($\Delta E_{\mathbf{L2},hfac}^{mix} = -1(3)$ kJ mol^{-1}) and for [La(**L3**)(hfac)$_3$] ($\Delta E_{\mathbf{L3},hfac}^{mix} = -2(4)$ kJ mol^{-1}). On the contrary, the decrease in $K_{exch}^{Ln,\mathbf{L}\boldsymbol{k}}$ for the smaller lanthanide cations corresponded to a considerable anti-cooperative process ($\Delta E_{\mathbf{L}\boldsymbol{k},hfac}^{mix} \gg 0$) produced by the sum of the homoligand interactions, which became more repulsive than their heteroligand counterpart ($\Delta E_{hfac,hfac}^{La} + \Delta E_{\mathbf{L}\boldsymbol{k},\mathbf{L}\boldsymbol{k}}^{La} > 2\Delta E_{\mathbf{L}\boldsymbol{k},hfac}^{La}$). This trend was assigned to an increase in $\Delta E_{\mathbf{L}\boldsymbol{k},\mathbf{L}\boldsymbol{k}}^{Ln}$ for the heavier lanthanide cations.

Photophysical properties of complexes [Ln(L*k*)(hfac)$_3$] (*k* = 2, 3; Ln = La, Eu, Gd): Taking $\log(\Delta\beta_{1,1}^{Ln(hfac)_3,\mathbf{L}\boldsymbol{k}}) \approx 5.5$ for Equilibrium (2) with Ln = Eu, Gd, Tb, we predicted that partial ligand-decomplexation amounted to 6% at millimolar concentrations, but reached 16% (10^{-4} M) and 43% (10^{-5} M) at the concentrations typically used for recording unbiased photophysical data. Therefore, we limited the investigation of the luminescent properties to solid-state samples, for which quantitative complexation had been firmly established by X-ray diffraction, whilst the absorption electronic spectra (recorded in 10^{-4} M MeCN solution) were systematically corrected for partial dissociation (see the Supporting Information, Appendix 5). According to the standard procedure,[4,46] the ligand-centered photophysical properties were deduced for the Gd complexes [Gd(**L*k***)(hfac)$_3$] because paramagnetic Gd^{III} induced a mixing of the ligand and metal wavefunctions that was very similar to that expected for the complexation of luminescent Eu^{III} (heavy-atom effect and paramagnetic coupling),[47] without possessing accessible low-lying metal-centered excited states.[48] However, the situation for the ternary complex [Gd(**L*k***)(hfac)$_3$] was delicate because both types of ligands (i.e. **L*k*** and hfac$^-$) possessed delocalized π-aromatic chromophores, which may contribute to the light-harvesting and sensitization processes.

The electronic absorption spectrum of coordinated hfac$^-$ ions in [Gd(hfac)$_3$(diglyme)] showed a broad band envelope for the spin-allowed $^1n,^1\pi\rightarrow{}^1\pi^*$ transitions, centered at 33200 cm^{-1} with a shoulder at lower energy (30000 cm^{-1}, Figure 7a). Excitation into the hfac($^1\pi\pi^*$) level at $\tilde{\nu}_{exc}$ = 33330 cm^{-1} produced short-lived fluorescence (0-0 phonon transition at $E_{0\text{-}0}(^1\pi\pi^*) = 27000$ cm^{-1}, Figure 7b) and long-lived phosphorescence ($E_{0\text{-}0}(^3\pi\pi^*) = 21550$ cm^{-1}, $\tau(^3\pi\pi^*) = 1.17(2)$ ms at 77 K, Figure 7c; also see the Supporting Information, Table S23). To decipher the photophysical consequences of the subsequent cascade reaction of [Gd(hfac)$_3$(diglyme)] with **L*k***, we first noted that the intensity of the $^1\pi\rightarrow{}^1\pi^*$ transitions, centered on the non-coordinated tridentate ligand **L*k***, was similar to that observed for [Gd(hfac)$_3$(diglyme)], but red-shifted by about 2000 cm^{-1}

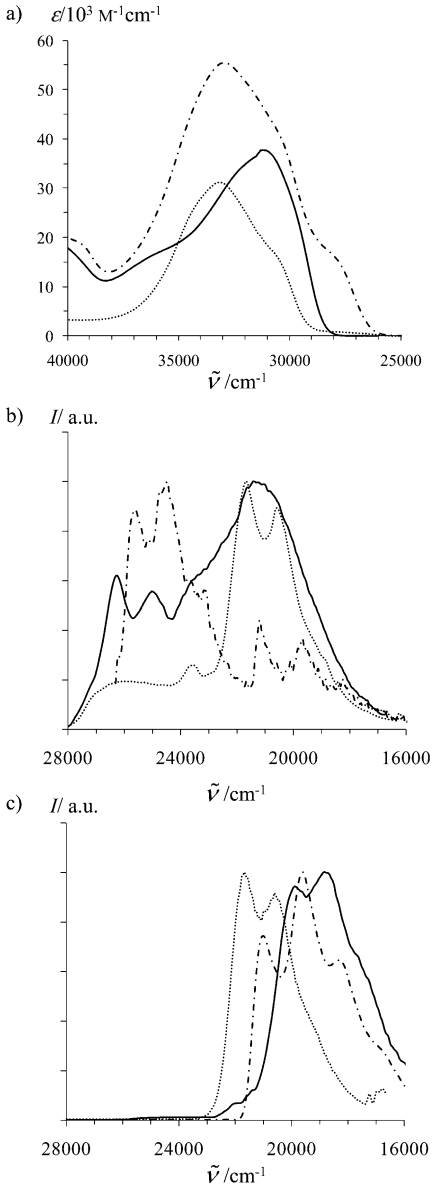

Figure 7. a) Absorption (10^{-4} M in CH_3CN, 293 K, corrected for partial dissociation, see the Supporting Information), b) fluorescence (solid-state, 77 K) and c) phosphorescence spectra (solid-state, 77 K, delay time after excitation flash: 0.05 ms) recorded for **L2** (——, $\tilde{\nu}_{exc}=31250\ cm^{-1}$), [Gd(hfac)$_3$(diglyme)] (-----, $\tilde{\nu}_{exc}=33330\ cm^{-1}$), and [Gd(**L2**)(hfac)$_3$] (–•–•, $\tilde{\nu}_{exc}=27780\ cm^{-1}$). All emission spectra were arbitrarily normalized to 1.

(Table S23, Figure 7a); this pattern was retained in their emission spectra (Figure 7b; also see the Supporting Information, Table S23).[49] Upon complexation of **L*k*** to [Gd(hfac)$_3$], the characteristics of each of the contributing chromophores were easily recognized in the absorption spectra of [Gd(**L*k***)(hfac)$_3$] (Figures 7a; also see the Supporting Information, Figure S23a).

Interestingly, the additional splitting of the **L*k***-centered $^1\pi\rightarrow{}^1\pi^*$ transitions[37] produced a low-energy component at 27740 cm^{-1},[18b] which was exploited for the selective excitation of the coordinated tridentate ligands in [Ln(**L*k***)(hfac)$_3$] (Ln = Gd, Eu; Figures 7a, also see the Supporting Information, Figure S23a).[50] Therefore, irradiation of [Gd(**L2**)(hfac)$_3$] and [Gd(**L3**)(hfac)$_3$] at $\tilde{\nu}_{exc}=27780\ cm^{-1}$ produced similar emission spectra, which reflected the electronic structure of the coordinated tridentate ligands without significant contributions from the hfac ligands (0–0 phonon transition for fluorescence at $E_{0\text{-}0}(^1\pi\pi^*)\approx25400\ cm^{-1}$ (Figures 7b, see the Supporting Information, Figure S23b), and long-lived phosphorescence at $E_{0\text{-}0}(^3\pi\pi^*)\approx21000\ cm^{-1}$, $\tau(^3\pi\pi^*)=0.4$–1.0 ms at 77 K (Figures 7c; also see the Supporting Information, Figure S23c and Table S23).

When Gd^{III} was replaced with emissive Eu^{III} in the complexes [Eu(**L*k***)(hfac)$_3$], irradiation in the **L*k***-centered excited states at $\tilde{\nu}_{exc}=27780\ cm^{-1}$ produces faint residual ligand-centered fluorescence ($^1\pi\pi^*\rightarrow{}^1\pi\pi$) together with an intense red signal that arose from **L*k***→Eu energy-transfer followed by Eu($^5D_1$) and Eu($^5D_0$)-centered luminescence (Figure 8).

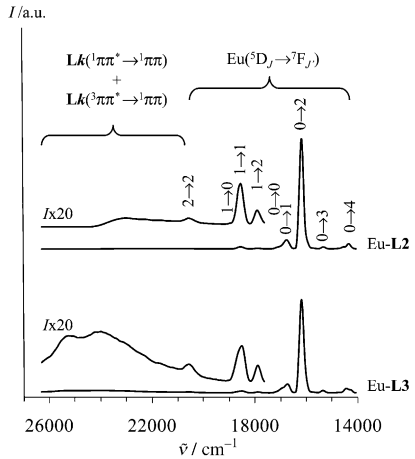

Figure 8. Solid-state luminescence emission spectra of [Eu(**L*k***)(hfac)$_3$] ($k=2$, 3; 77 K; $\tilde{\nu}_{exc}=27780\ cm^{-1}$).

The intensities of the Eu($^5D_1\rightarrow{}^7F_J$) transitions were extremely small compared to the luminescence arising from the Eu($^5D_0\rightarrow{}^7F_J$) transitions, and the emission spectra were dominated by the hypersensitive forced electric dipolar Eu($^5D_0\rightarrow{}^7F_2$) transition, centered at 16240 cm^{-1}. These two spectral characteristics have been well-documented for low-symmetry tris-β-diketonate Eu^{III} complexes (Figure 8).[1,2,51] The experimental absolute quantum yields Φ_{Eu}^{L} (determined upon excitation of the ligand excited states and monitoring of the Eu^{3+} emission) reached 29(2)% for [Eu(**L2**)(hfac)$_3$] and 30(2)% for [Eu(**L3**)(hfac)$_3$] (solid-state, 293 K) and testified to the efficiency of the sensitization process brought by tridentate ligands **L2** or **L3**. The latter quantum yields were marginally smaller than the $40\% \le \Phi_{Eu}^{L} \le 60\%$ recently reported for optimized [Eu(**L**)(β-diketonate)$_3$] complexes, where **L** were chelating N-donor or O-donor ligands and β-diketonate was the unsymmetrical 2-thienoyltrifluoroacetonate.[1,2,31,52] Interestingly, the Eu($^5D_0$) excited lifetime of $\tau_{obs}^{Eu}=0.97(1)$ ms observed for [Eu(**L2**)(hfac)$_3$] and [Eu(**L3**)(hfac)$_3$] (solid-state, 293 K; see the Supporting Informa-

tion, Table S23) was close to the radiative Eu($^5D_0$) lifetime ($\tau_r^{Eu} = 1.13$ ms) recently estimated for [Eu(hfac)$_3$(H$_2$O)$_2$] under the same experimental conditions.[54c] The subsequent rough estimation of the intrinsic Eu-centered quantum yields ($\Phi_{Eu}^{Eu} = \tau_{obs}^{Eu}/\tau_r^{Eu} = 0.97/1.13 = 0.86$) in [Eu(**L2**)(hfac)$_3$] and [Eu(**L3**)(hfac)$_3$] confirmed the standard statement that the global quantum yield (Φ_{Eu}^{L}) in ternary complexes [Eu(**L**)(hfac)$_3$] was limited by the sensitization process, which combined the efficiencies of the successive inter-system crossing $^1\pi^* \rightarrow {}^3\pi^*$ and **L**→Eu (^5D_j) energy-transfer processes (see the Supporting Information, Figure S24).[52]

Conclusion

The replacement of didentate nitrate (X = NO_3^-) or carboxylate groups (X = $CF_3CO_2^-$, both four-membered chelating anions) with didentate hexafluoroacetylacetonate (X = hfac$^-$, a six-membered chelating anion) around trivalent lanthanide atoms of the formula [LnX$_3$] offers remarkable advantages for cascade reactions with tridentate N-heterocyclic ligands:

1) The thermodynamic affinities of the tridentate **L*k*** ligands for [Ln(hfac)$_3$] with large and mid-range trivalent lanthanides (Ln = La–Ho; MeCN; 293 K; Figure 5) were 1–2 orders of magnitude larger than those found upon reaction with [Ln(CF$_3$CO$_2$)$_3$][10] and [Ln(NO$_3$)$_3$].[11]
2) The bowl-shaped best-fit curve displayed by $\log(\beta_{1,1}^{Ln(hfac)_3,\mathbf{Lk}})$ along the lanthanide series contrasted with the standard monotonous electrostatic behavior displayed by $\log(\beta_{1,1}^{Ln(NO_3)_3,\mathbf{Lk}})$. The crossing of the two curves at around Ln = Ho reversed the selectivity for the heavier cations (Ln = Tm–Lu), which preferred complexation with [Ln(NO$_3$)$_3$] (Figure 5). The anomalously long Lu–N bond-lengths for the smallest Lu^{III} cation in the crystal structure of [Lu(**L*k***)(hfac)$_3$] confirmed the operation of this rare anti-electrostatic trend in the solid state. However, nine-coordination was retained for the complete series of [Lu(**L*k***)(hfac)$_3$]; this trend was in contrast to the change in coordination numbers (CN = 10→9→8) found for [Ln(**L*k***)(NO$_3$)$_3$].[9,11]
3) The negligible values observed for the microscopic inter-ligand interactions that operated in the coordination sphere of the largest La^{III} cation in [La(**L*k***)(hfac)$_3$] were responsible for the concomitant formation of [La(**L*k***)$_2$(hfac)$_2$]$^+$ (10-coordinate) and [La(hfac)$_4$]$^-$ in MeCN at room temperature, through a solvent-dependent enthalpy-driven **L*k***/hfac bi-exchange process. Because of the increasing **L*k***–**L*k*** repulsive interactions that accompanied the contraction of the lanthanide ionic radius in [Ln(**L*k***)$_2$(hfac)$_2$]$^+$, the latter side-reaction was strictly limited to the largest cations Ln = La, Ce, and Pr in MeCN. Replacement of MeCN with CHCl$_3$ restored the exclusive formation of [Ln(**L*k***)(hfac)$_3$] in solution for the complete lanthanide series.
4) The exclusive detection of monomeric, strongly luminescent [Eu(**L*k***)(hfac)$_3$] units in solution, even though their analogous compounds [Eu(**L*k***)(NO$_3$)$_3$] and [Eu(**L*k***)(CF$_3$CO$_2$)$_3$] only existed as complicate mixtures of monomers and dimers, represented a decisive argument for the exploitation of [Ln(hfac)$_3$] as neutral lanthanide carriers for the planned metallic loading of linear multisite polymers that incorporate 2,6-bis(benzimidazole-2-yl)pyridine binding units.

Experimental Section

Chemicals were purchased from Strem, Acros, Fluka AG, and Aldrich, and used without further purification unless otherwise stated. The hexafluoroacetylacetonate salts, [Ln(hfac)$_3$C$_8$H$_{14}$O$_3$], were prepared from their corresponding oxide (Aldrich, 99.99%).[22] MeCN and CH$_2$Cl$_2$ were distilled over calcium hydride. Silica gel plates (Merck 60 F$_{254}$) were used for thin layer chromatography (TLC) and Fluka silica gel 60 (0.04–0.063 mm) or Acros neutral activated alumina (0.050–0.200 mm) was used for preparative column chromatography.

Preparation of *N*-3-methylbutyl-(4-bromo-2-nitrophenyl)amine (1): 2,5-Dibromonitrobenzene (**6**, 19.97 g, 71.09 mmol) and 3-methylbutylamine (70% in water) were heated in an autoclave at 110°C for 24 h. The dark mixture was evaporated to dryness, extracted with CH$_2$Cl$_2$ (100 mL), and successively washed with half-saturated aqueous NH$_4$Cl solution (3× 50 mL) and water (50 mL). The organic layer was dried (Na$_2$SO$_4$), the solvent was evaporated, and the resulting oil was crystallized from *n*-hexane to give 20.02 g (69.72 mmol, yield 98%) of compound **1** as orange crystals. ^{1}H NMR (CDCl$_3$, 400 MHz): $\delta = 1.00$ (d, 6H, $^3J = 6.6$ Hz), 1.65 (q, 2H, $^3J = 7.2$ Hz), 1.78 (n, 1H, $^3J = 6.7$ Hz), 3.32 (q, 2H, $^3J = 7.2$ Hz), 6.79 (d, 1H, $^3J = 9.2$ Hz), 7.51 (dd, 1H, $^3J = 9.2$ Hz, $^4J = 2.3$ Hz), 8.34 ppm (s, 1H, $^4J = 2.3$ Hz). MS (ESI, CH$_2$Cl$_2$): *m*/*z*: 288.1 [*M*+H]$^+$.

Preparation of pyridine-2,6-dicarboxylic acid bis[(4-bromo-2-nitrophenyl)-(3-methylbutyl)amide] (2): Pyridine-2,6-dicarboxylic acid (2.99 g, 17.89 mmol) and DMF (30 μL) were heated to reflux in freshly distilled thionyl chloride (15 mL) for 1 h. Excess thionyl chloride was distilled from the reaction mixture, which was then co-evaporated with dry CH$_2$Cl$_2$ (3×20 mL) and dried under vacuum. The solid was re-dissolved in freshly distilled CH$_2$Cl$_2$ (20 mL) and a solution of *N*-3-methylbutyl-(4-bromo-2-nitrophenyl)-amine (**1**, 5.01 g, 17.45 mmol) in CH$_2$Cl$_2$ (20 mL) was slowly added under an inert atmosphere. The resulting mixture was heated to reflux for 24 h and the pH value was kept close to pH 9 by adding small amounts of *N*,*N*-diisopropylethylamine. The mixture was partitioned between CH$_2$Cl$_2$ (60 mL) and half-saturated aqueous NH$_4$Cl (60 mL). The organic layer was separated and the aqueous phase was further extracted with fresh CH$_2$Cl$_2$ (2×60 mL). The combined organic phases were dried with anhydrous sodium sulfate, evaporated to dryness, and the crude product was purified by column chromatography on silica gel (CH$_2$Cl$_2$/MeOH, 100:0→99.5:0.5) to give 4.4 g (6.24 mmol, yield 75%) of compound **2** as a yellow powder. MS (ESI, CH$_2$Cl$_2$): *m*/*z*: 704.8 [*M*+H]$^+$.

Preparation of 2,6-bis[1-(3-methylbutyl)-5-bromobenzimidazol-2-yl]pyridine (L2): Pyridine-2,6-dicarboxylic acid bis[(4-bromo-2-nitrophenyl)(3-methylbutyl)amide] (**2**, 0.5037 g, 0.714 mmol) was dissolved in DMF (3 mL) and a solution of Na$_2$S$_2$O$_4$ (85%, 1.35 g, 6.56 mmol) in EtOH (3 mL) was added. The slurry solution was heated to 85°C, then deionized water (3 mL) was added and the resulting mixture was heated to reflux for 20 h under an inert atmosphere. The reaction was allowed to cool to RT and KOH (4M, 5 mL) was added to the solution. The solvents were evaporated under vacuum, the crude product was dissolved in CH$_2$Cl$_2$ (30 mL), washed with water (3×20 mL), dried with anhydrous sodium sulfate, and evaporated to dryness. Purification by column chromatography on silica gel (CH$_2$Cl$_2$/MeOH, 100:0→99:1) gave 199.7 mg

(0.327 mmol, yield 46%) of ligand **L2** as a white powder. ^{1}H NMR ($CDCl_3$, 400 MHz): δ=0.69 (d, 12H, ^3J=6.6 Hz), 1.38 (n, 2H, ^3J=6.6 Hz), 1.60 (q, 4H, ^3J=7.4 Hz), 4.67 (t, 4H, ^3J=7.7 Hz), 7.33 (d, 2H, ^3J=8.6 Hz), 7.47 (d, 2H, ^3J=8.6 Hz), 8.01 (s, 2H), 8.09 (t, 1H, ^3J=7.9 Hz), 8.30 ppm (d, 2H, ^3J=7.9 Hz); ^{13}C NMR ($CDCl_3$, 100 MHz): δ=22.10 (primary C); 38.73, 43.64 (secondary C); 25.73, 111.48, 123.12, 125.82, 126.60, 138.42, 149.58, 150.87 (tertiary C); 115.71, 135.06, 144.00 ppm (quaternary C); MS (ESI, CH_2Cl_2): m/z: 608.5 $[M+H]^+$; elemental analysis calcd (%) for $C_{29}H_{31}N_5Br_2$: C 57.16, H 5.13, N 11.49; found: C 56.95, H 5.15, N 11.29.

Preparation of 2,6-bis(benzimidazol-2-yl)pyridine (3):[18] Pyridine 2,6-dicarboxylic acid (10.43 g, 62 mmol) was stirred with *o*-phenylenediamine (15 g, 13.8 mmol) in syrupy polyphosphoric acid (120 mL) at 220°C for 5 h. The colored melt was poured onto 3.5 L of vigorously stirring cold water. When cooled, the bulky blue–green precipitate was collected by filtration and slurried in a hot aqueous sodium carbonate solution (10%, 1.5 L). The resulting solid was filtered and recrystallized from MeOH to give colorless prisms (12.6 g, 40.3 mmol, 65% yield). ^{1}H NMR ([D$_6$]DMSO, 400 MHz): δ=7.23 (t, 2H, ^3J=7.3 Hz), 7.31 (t, 2H, ^3J=7.3 Hz), 7.69 (d, 2H, ^3J=7.3 Hz), 7.73 (d, 2H, ^3J=7.3 Hz), 8.13 (t, 1H, ^3J=7.8 Hz), 7.23 ppm (d, 2H, ^3J=7.8 Hz).

Preparation of 2,6-bis[1-(3-methylbutyl)benzimidazol-2-yl]pyridine (L3): 2,6-Bis(benzimidazol)pyridine (**3**, 2 g, 6.42 mmol) was dissolved in dry DMF (100 mL) under a N_2 atmosphere. The solution was cooled to 0°C and a suspension of sodium hydride (640 mg, 16.06 mmol) in DMF (5 mL) was added. After stirring for 2 h at room temperature, 1-bromo-2-methylbutane (2.91 g, 19.27 mmol) was added and the solution was stirred for a further 24 h at room temperature under an inert atmosphere. Water (100 mL) was added and the aqueous phase was extracted with CH_2Cl_2 (5×50 mL). The combined organic phases were washed with water (5×50 mL), dried (Na_2SO_4), and evaporated to dryness, and the crude product was purified by column chromatography on silica gel (CH_2Cl_2/MeOH, 99.9:0.1→99:1) followed by crystallization in hot *n*-hexane to give 1.615 g of 2,6-bis[1-(3-methylbutyl)benzimidazol-2-yl]pyridine (**L3**, 3.57 mmol, yield 56%) as transparent crystals. ^{1}H NMR ($CDCl_3$, 400 MHz): δ=0.72 (d, 12H, ^3J=6.6 Hz), 1.42 (n, 2H, ^3J=6.6 Hz), 1.65 (dd, 4H, ^3J=7.1, ^3J=8.2 Hz), 4.74 (t, 4H, ^3J=7.8 Hz), 7.39 (m, 4H), 7.49 (d, 2H, ^3J=7.1 Hz), 7.90 (d, 2H, ^3J=7.1 Hz), 8.09 (t, 1H, ^3J=7.9 Hz), 8.34 ppm (d, 2H, ^3J=7.9 Hz); ^{13}C NMR ($CDCl_3$, 100 MHz): δ=22.16 (primary C); 38.79, 43.47(secondary C); 25.78, 110.27, 122.80, 123.57, 125.58, 138.26, 149.95, 150.09 (tertiary C); 120.33, 136.14, 142.76 ppm (quaternary C); MS (ESI, CH_2Cl_2): m/z: 452.4 $[M+H]^+$; elemental analysis calcd (%) for $C_{29}H_{33}N_5$: C 77.13, H 7.37, N 15.51; found: C 77.09, H 7.39, N 15.52.

Preparation of complexes [Ln(L*k*)(hfac)$_3$] (*k*=2, 3; Ln=La, Eu, Gd, Lu, Y): Stoichiometric amounts of **L*k*** and [Ln(hfac)$_3$(diglyme)] were reacted in MeCN/CH_2Cl_2 (1:1) at RT. Slow evaporation of CH_2Cl_2 provided single-crystals of anhydrous [Ln(**L*k***)(hfac)$_3$] suitable for X-ray diffraction that gave satisfactory elemental analysis data (see the Supporting Information, Table S5).

Spectroscopic measurements: ^{1}H, ^{19}F and ^{13}C NMR spectra were recorded at 293 K on Bruker Avance 400 MHz and Bruker DRX-300 MHz spectrometers. Chemical shifts are given in ppm with respect to TMS. DOSY- NMR data used the pulse sequence implemented in the Bruker program ledbpgp2s[53] which employed stimulated echo, bipolar gradients and longitudinal eddy current delay as the z filter. The four 2 ms gradient pulses had sine-bell shapes and amplitudes ranging linearly from 2.5 to 50 G cm^{-1} in 32 steps. The diffusion delay was in the range 60–140 ms depending on the analyte diffusion coefficient, and the no. of scans was 32. The processing was done using a line broadening of 5 Hz and the diffusion coefficients were calculated with the Bruker processing package. VT-^{1}H NMR measurements of samples were measured on a Bruker Avance 400 spectrometer equipped with a variable temperature unit. The integrated intensities of the relevant peaks were obtained by deconvoluting using Matlab or Excel (one Lorentz function per peak) after Fourier transform and phasing of the spectrum using mnova. Fitting of van't Hoff plots was done using Excel. Pneumatically-assisted electrospray (ESI-MS) mass spectra were recorded from 10^{-4} M solutions on an Applied Biosystems API 150EX LC/MS System equipped with a Turbo Ionspray source. Elemental analyses were performed by K. L. Buchwalder from the Microchemical Laboratory of the University of Geneva. Electronic absorption spectra in the UV/Vis were recorded at 20°C from solutions in CH2Cl2 with a Perkin–Elmer Lambda 900 spectrometer using quartz cells of 10 or 1 mm path length. Excitation and emission spectra as well as lifetime measurements were recorded on a Perkin–Elmer LS-50B spectrometer equipped for low-temperature measurements. Luminescence spectra in the visible were measured using a Jobin Yvon-Horiba Fluorolog-322 spectrofluorimeter equipped with a Hamamatsu R928. Spectra were corrected for both excitation and emission responses (excitation lamp, detector and both excitation and emission monochromator responses). Quartz tube sample holders were employed. Quantum yield measurements of the solid state samples were measured on quartz tubes with the help an integration sphere developed by Frédéric Gumy and Jean-Claude G. Bünzli (Laboratory of Lanthanide Supramolecular Chemistry, École Polytechnique Féderale de Lausanne (EPFL), BCH 1402, CH- 1015 Lausanne, Switzerland) commercialized by GMP S.A. (Renens, Switzerland).

X-ray crystallography: For a summary of the crystal data, intensity measurements, and structure refinements for ligand **L3**, [Ln(**L2**)(hfac)$_3$], and [Ln(**L3**)(hfac)$_3$] (Ln=La, Eu, Lu), see the Supporting Information, Table S6. All crystals were mounted on quartz fibers with protection oil. Cell dimensions and intensities were measured between 120–200 K on a Stoe IPDS diffractometer with graphite-monochromated $Mo_{K\alpha}$ radiation (λ=0.71073 Å). Data were corrected for Lorentz and polarization effects and for absorption. The structures were solved by direct methods (SIR92[54] or SIR97)[55] or by charge-flipping methods (superflip).[56] All other calculation were performed with ShelX97[57] or Crystals[58] systems and ORTEP[59] programs. CCDC-843152 (**L3**), CCDC-843153 ([La(**L2**)(hfac)$_3$]), CCDC-843154 ([Eu(**L2**)(hfac)$_3$]), CCDC-843155 ([Lu(**L2**)(hfac)$_3$]), CCDC-843156 ([La(**L3**)(hfac)$_3$]), CCDC-843157 ([Eu(**L2**)(hfac)$_3$]), contain the supplementary crystallographic data for this paper. These data can be obtained free of charge from The Cambridge Crystallographic Data Centre via www.ccdc.cam.ac.uk/data_request/cif.

The Supporting Information contains details for the calculation of hydrodynamic molecular weights (Appendix 1), for the determination of stability constants (Appendix 2), for the correction of electronic absorption spectra (Appendices 3 and 5), and for thermodynamic modeling (Appendix 4). Tables of ^{1}H NMR spectroscopic shifts, elemental analysis, crystal data, geometric parameters and bond valences, self-diffusion coefficients, and photophysical data are also provided. Figures showing molecular structures with atom numbering, molecular superimpositions, crystal packing, symmetry numbers, ^{1}H, ^{13}C, and ^{19}F NMR spectra, and electronic absorption and emission spectra are also given.

Acknowledgements

Financial support from the Swiss National Science Foundation is gratefully acknowledged. S.P. acknowledges supports from la Ligue contre le Cancer and from the Institut National de la Santé et de la Recherche Médicale (INSERM). The work in France was carried out within the COST Action D38.

[1] H. F. Brito, O. M. L. Malta, M. C. F. C. Felinto, E. E. S. Teotonio, *The Chemistry of Metal Enolates*, Wiley, **2009**, Chap. 3, pp. 131–184.
[2] K. Binnemans in *Handbook on the Physics and Chemistry of Rare Earths, Vol. 35* (Eds: K. A. Gschneidner, J.-C. G. Bünzli, V. K. Pecharsky), Elsevier North Holland, Amsterdam, **2005**, pp. 107–272.
[3] G. Malandrino, I. L. Fragalà, *Coord. Chem. Rev.* **2006**, *250*, 1605–1620.
[4] a) J. Kido, Y. Okamoto, *Chem. Rev.* **2002**, *102*, 2357–2368; b) R. C. Evans, P. Douglas, C. J. Winscom, *Coord. Chem. Rev.* **2006**, *250*, 2093–2126; c) A. de Bettencourt-Dias, *Dalton Trans.* **2007**, 2229–

2241; d) K. Binnemans, *Chem. Rev.* **2009**, *109*, 4283–4374; e) M. A. Katkova, M. N. Bochkarev, *Dalton Trans.* **2010**, *39*, 6599–6612.

[5] X.-Y. Chen, X. Yang, B. J. Holliday, *J. Am. Chem. Soc.* **2008**, *130*, 1546–1547.

[6] A. Valore, E. Cariati, S. Righetto, D. Roberto, F. Tessore, R. Ugo, I. L. Fragalà, M. E. Fragalà, G. Malandrino, F. De Angelis, L. Belpassi, I. Ledoux-Rak, K.-H. Thi, J. Zyss, *J. Am. Chem. Soc.* **2010**, *132*, 4966–4970.

[7] a) P. A. Vigato, V. Peruzzo, S. Tamburini, *Coord. Chem. Rev.* **2009**, *253*, 1099–1201; b) G. Zucchi, V. Murugesan, D. Tondelier, D. Aldakov, T. Jeon, F. Yang, P. Thuery, M. Ephritikhine, B. Geffroy, *Inorg. Chem.* **2011**, *50*, 4851–4856, and references therein.

[8] a) M. L. Melby, N. J. Rose, E. Abramson, J. C. Caris, *J. Am. Chem. Soc.* **1964**, *86*, 5117–5125; b) R. C. Holz, L. C. Thompson, *Inorg. Chem.* **1988**, *27*, 4640–4644; c) Y. Fukuda, A. Nakao, K. Hayashi, *J. Chem. Soc. Dalton Trans.* **2002**, 527–533; d) X.-L. Li, L.-X. Shi, L.-Y. Zhang, H.-M. Wen, Z.-N. Chen, *Inorg. Chem.* **2007**, *46*, 10892–10900; e) X.-L. Li, F.-R. Dai, L.-Y. Zhang, Y.-M. Zhu, Q. Peng, Z.-N. Chen, *Organometallics* **2007**, *26*, 4483–4490.

[9] a) E. Terazzi, S. Torelli, G. Bernardinelli, J.-P. Rivera, J.-M Bénech, C. Bourgogne, B. Donnio, D. Guillon, D. Imbert, J.-C. G. Bünzli, A. Pinto, D. Jeannerat, C. Piguet, *J. Am. Chem. Soc.* **2005**, *127*, 888–903; b) T. B. Jensen, E. Terazzi, K. Buchwalder, L. Guénée, H. Nozary, K. Schenk, B. Heinrich, B. Donnio, D. Guillon, C. Piguet, *Inorg. Chem.* **2010**, *49*, 8601–8619.

[10] H. Nozary, S. Torelli, L. Guénée, E. Terazzi, G. Bernardinelli, B. Donnio, D. Guillon, C. Piguet, *Inorg. Chem.* **2006**, *45*, 2989–3003.

[11] A. Escande, L. Guénée, K.-L. Buchwalder, C. Piguet, *Inorg. Chem.* **2009**, *48*, 1132–1147. The thermodynamic-formation constants for [Ln(**L7**)(NO$_3$)$_3$] were obtained from the titration of solutions of ligand (10^{-4} M) with [Ln(NO$_3$)$_3$(H$_2$O)$_3$] in MeCN solvent with water (3×10^{-4} M); this procedure was comparable to that for [Ln(**L*k***)(hfac)$_3$], where water was replaced by diglyme (10^{-4} M). Therefore, a comparison of the stability constants $\beta_{1,1}^{\mathrm{Ln(NO_3)_3},\mathbf{L7}}$ and $\beta_{1,1}^{\mathrm{Ln(hfac)_3},\mathbf{Lk}}$ (Figure 5) is acceptable.

[12] Similar mixtures of [La(terpy)$_2$(NO$_3$)$_2$]$^+$ and [La(terpy)(NO$_3$)$_4$]$^-$ were reported for [La(terpy)(NO$_3$)$_3$] in wet MeCN, see: M. Fréchette, C. Bensimon, *Inorg. Chem.* **1995**, *34*, 3520–3527.

[13] a) R. Amano, A. Sato, S. Suzuki, *Chem. Lett.* **1980**, 537–540; b) A.-S. Chauvin, F. Gumy, I. Matsubayashi, Y. Hasegawa, J.-C. G. Bünzli, *Eur. J. Inorg. Chem.* **2006**, 473–480.

[14] a) W. H. Watson, R. J. Williams, N. R. Stemple, *J. Inorg. Nucl. Chem.* **1972**, *34*, 501–508; b) K. Iftikhar, M. Sayeed, N. Ahmad, *Inorg. Chem.* **1982**, *21*, 80–84; c) S. T. Frey, M. L. Gong, W. deW. Horrocks, Jr., *Inorg. Chem.* **1994**, *33*, 3229–3234; d) S. Yajima, Y. Hasegawa, *Bull. Chem. Soc. Jpn.* **1998**, *71*, 2825–2829.

[15] a) G. Muller, J.-C. G. Bünzli, K. J. Schenk, C. Piguet, G. Hopfgartner, *Inorg. Chem.* **2001**, *40*, 2642–2651; b) G. Muller, J. P. Riehl, K. J. Schenk, G. Hopfgartner, C. Piguet, J.-C. G. Bünzli, *Eur. J. Inorg. Chem.* **2002**, 3101–3110; c) G. Muller, C. L. Maupin, J. P. Riehl, H. Birkedal, C. Piguet, J.-C. G. Bünzli, *Eur. J. Inorg. Chem.* **2003**, 4065–4072.

[16] a) C. Piguet, J.-C. G. Bünzli, G. Bernardinelli, C. G. Bochet, P. Froidevaux, *J. Chem. Soc. Dalton Trans.* **1995**, 83–97.

[17] a) C. Piguet, A. F. Williams, G. Bernardinelli, E. Moret, J.-C. G. Bünzli, *Helv. Chim. Acta* **1992**, *75*, 1697–1717.

[18] a) A. W. Addison, P. J. Burke, *J. Heterocycl. Chem.* **1981**, *18*, 803–805; b) C. Piguet, B. Bocquet, E. Müller, A. F. Williams, *Helv. Chim. Acta* **1989**, *72*, 323–337.

[19] a) C. Piguet, B. Bocquet, G. Hopfgartner, *Helv. Chim. Acta* **1994**, *77*, 931–942; b) B. M. McKenzie, A. K. Miller, R. J. Wojtecki, J. C. Johnson, K. A. Burke, K. A. Tzeng, P. T. Mather, S. J. Rowan, *Tetrahedron* **2008**, *64*, 8488–8495; c) J. Duchek, A. Vasella, *Helv. Chim. Acta* **2011**, *94*, 977–985.

[20] C. Marie, M. Miguirditchian, D. Guillaumont, A. Tosseng, C. Berthon, P. Guilbaud, M. Duvail, J. Bisson, D. Guillaneux, M. Pipelier, D. Dubreuil, *Inorg. Chem.* **2011**, *50*, 6557–6566.

[21] F. H. Allen, O. Kennard, D. G. Watson, L. Brammer, A. G. Orpen, R. Taylor, *J. Chem. Soc. Perkin Trans. 2* **1987**, S1–S19.

[22] a) W. J. Evans, D. G. Giarikos, M. A. Johnston, M. A. Greci, J. W. Ziller, *J. Chem. Soc. Dalton Trans.* **2002**, 520–526; b) G. Malandrino, R. Lo Nigro, I. L. Fragalà, C. Benelli, *Eur. J. Inorg. Chem.* **2004**, 500–509.

[23] J. Yuasa, T. Ohno, K. Miyata, H. Tsumatori, Y. Hasegawa, T. Kawai, *J. Am. Chem. Soc.* **2011**, *133*, 9892–9902.

[24] a) I. D. Brown, D. Altermatt, *Acta Crystallogr. B* **1985**, *41*, 244–247; b) N. E. Breese, M. O'Keeffe, *Acta Crystallogr. B* **1991**, *47*, 192–197; c) I. D. Brown, *Acta Crystallogr. B* **1992**, *48*, 553–572; d) I. D. Brown, *The Chemical Bond in Inorganic Chemistry*, Oxford University Press, **2002**; e) I. D. Brown, *Chem. Rev.* **2009**, *109*, 6858–6919.

[25] a) A. Trzesowska, R. Kruszynski, T. J. Bartczak, *Acta Crystallogr. B Structural Science* **2004**, B60, 174–178; b) A. Trzesowska, R. Kruszynski, T. J. Bartczak, *Acta Crystallogr. B* **2005**, *61*, 429–434; c) F. Zocchi, *J. Mol. Struct.* **2007**, *805*, 73–78.

[26] a) G. R. Choppin in *Lanthanide Probes in Life, Chemical and Earth Sciences* (Eds.: J.-C. G. Bünzli, G. R. Choppin), Elsevier, Amsterdam, **1989**, Chap. 1, pp. 1–41; b) C. Piguet, J.-C. G. Bünzli, *Chem. Soc. Rev.* **1999**, *28*, 347–358.

[27] a) S. Petoud, J.-C. G. Bünzli, F. Renaud, C. Piguet, K. J. Schenk, G. Hopfgartner, *Inorg. Chem.* **1997**, *36*, 5750–5760; b) Z. Kolarik, *Chem. Rev.* **2008**, *108*, 4208–4252.

[28] Assuming that the non-detection of resolved signals for the free ligand indicates that its concentration corresponds to less than 2% of the complex concentration, Equation (2) predicts that $\beta_{1,1}^{\mathrm{Ln(hfac)_3},\mathbf{Lk}} > 4.9\times10^5$ for $|\mathbf{Lk}|_{\mathrm{tot}} = |\mathrm{Ln(hfac)_3}|_{\mathrm{tot}} = 5\times10^{-3}$ M (standard concentration of the reference state: 1 M).

[29] M. D. Ward, *Coord. Chem. Rev.* **2007**, *251*, 1663–1677.

[30] D. K. Lavallee, M. D. Baughman, M. D. Phillips, *J. Am. Chem. Soc.* **1977**, *99*, 718–724.

[31] C. Freund, W. Porzio, U. Giovanella, F. Vignali, M. Pasini, S. Destri, A. Mech, S. Di Pietro, L. Di Bari, P. Mineo, *Inorg. Chem.* **2011**, *50*, 5417–5429.

[32] The paramagnetic pseudo-contact shift depended on $(r_{\mathrm{Ln-H}})^{-3}$, see: C. Piguet, C. F. G. C. Geraldes in *Handbook on the Physics and Chemistry of Rare Earths, Vol. 33* (Eds.: K. A. Gschneidner, J.-C. G. Bünzli, V. K. Pecharsky), Elsevier North Holland, Amsterdam, **2003**, pp. 353–463.

[33] T. Le Borgne, P. Altmann, N. André, J.-C. G. Bünzli, G. Bernardinelli, P.-Y. Morgantini, J. Weber, C. Piguet, *Dalton Trans.* **2004**, 723–733.

[34] a) A. Macchioni, G. Ciancaleoni, C. Zuccaccia, D. Zuccaccia, *Chem. Soc., Rev.* **2008**, *37*, 479–489; b) N. Dalla Favera, L. Guénée, G. Bernadinelli, C. Piguet, *Dalton Trans.* **2009**, 7625–7638.

[35] The integrations of the ^{1}H NMR signals indicated an accidental equivalence of the hfac protons in [La(**L*k***)(hfac)$_3$] and [Ln(hfac)$_4$]$^-$ at 400 MHz, whilst [La(**Lk**)$_2$(hfac)$_2$]$^+$ gave a separate signal for these protons at lower field.

[36] R. J. Motekaitis, A. E. Martell, R. A. Hancock, *Coord. Chem. Rev.* **1994**, *133*, 39–65, and the references therein.

[37] K. Nakamoto, *J. Phys. Chem.* **1960**, *64*, 1420–1425.

[38] a) C. Piguet, C. G. Bochet, A. F. Williams, *Helv. Chim. Acta* **1993**, *76*, 372–384; b) C. Piguet, J.-C. G. Bünzli, G. Bernardinelli, A. F. Williams, *Inorg. Chem.* **1993**, *32*, 4139–4149.

[39] S. G. Telfer, T. McLean, M. R. Waterland, *Dalton Trans.* **2011**, *40*, 3097–3108.

[40] a) H. Gampp, M. Maeder, C. J. Meyer, A. Zuberbühler, *Talanta*, **1985**, 32, 1133–1139; b) H. Gampp, M. Maeder, C. J. Meyer, A. Zuberbühler, *Talanta* **1986**, *33*, 943–951.

[41] a) R. D. Shannon, *Acta Crystallogr. Sect. A* **1976**, *32*, 751–767; b) P. D'Angelo, A. Zitolo, V. Migliorati, G. Chillemi, M. Duvail, P. Vitorge, S. Abadie, R. Spezia, *Inorg. Chem.* **2011**, *50*, 4572–4579.

[42] a) J. Hamacek, M. Borkovec, C. Piguet, *Chem. Eur. J.* **2005**, *11*, 5217–5226; b) J. Hamacek, M. Borkovec, C. Piguet, *Chem. Eur. J.* **2005**, *11*, 5227–5237; c) J. Hamacek, M. Borkovec, C. Piguet, *Dalton Trans.* **2006**, 1473–1490; d) J. W. Steed, J. L. Atwood, *Supramolecular Chemistry,* 2nd ed., Wiley, Chichester, **2009**, 610–616; e) C. Piguet, *Chem. Commun.* **2010**, *46*, 6209–6231.

[43] G. Ercolani, C. Piguet, M. Borkovec, J. Hamacek, *J. Phys. Chem. B* **2007**, *111*, 12195–12203, and references therein.
[44] D. Munro, *Chem. Br.* **1977**, *13*, 100–105.
[45] a) M. Borkovec, J. Hamacek, C. Piguet, *Dalton Trans.* **2004**, 4096–4105; b) M. Borkovec, G. J. M. Koper, C. Piguet, *Curr. Opin. Colloid Interface Sci.* **2006**, *11*, 280–289.
[46] N. M. Shavaleev, S. V. Eliseeva, R. Scopelliti, J.-C. G. Bünzli, *Inorg. Chem.* **2010**, *49*, 3929–3936.
[47] a) S. Tobita, M. Arakawa, I. Tanaka, *J. Phys. Chem.* **1984**, *88*, 2697–2702; b) S. Tobita, M. Arakawa, I. Tanaka, *J. Phys. Chem.* **1985**, *89*, 5649–5654.
[48] W. T. Carnall, P. R. Fields, K. Rajnak, *J. Chem. Phys.* **1968**, *49*, 4443–4446.
[49] The introduction of heavy bromine atoms did not drastically affect the energy of the **Lk**($^1\pi\pi^*$) and **Lk**($^3\pi\pi^*$) excited levels in going from **L3** to **L2**, but it strongly favored $^1\pi\pi^*\rightarrow{}^3\pi\pi^*$ intersystem crossing, with the detection of a much-stronger phosphorescence for ligand **L2** (see the Supporting Information, Figure S22).
[50] Irradiation of [Gd(hfac)3(diglyme)] at $\tilde{\nu}_{exc}=27780\,cm^{-1}$ showed a faint emission.
[51] J.-C. G. Bünzli, E. Moret, V. Foiret, K. J. Schenk, M. Z. Wang, L. P. Jin, *J. Alloys Compd.* **1994**, *207–208*, 107–111.
[52] a) K. Miyata, Y. Hasegawa, Y. Kuramochi, T. Nakagawa, T. Yokoo, T. Kawai, *Eur. J. Inorg. Chem.* **2009**, 4777–4785; b) Z.-N. Chen, F. Ding, F. Hao, M. Guan, Z.-Q. Bian, B. Ding, C.-H. Huang, *New J. Chem.* **2010**, *34*, 487–494; c) S. V. Eliseeva, D. N. Pleshkov, K. A. Lyssenko, L. S. Lepnev, J.-C. G. Bünzli, N. P. Kuzmina, *Inorg. Chem.* **2011**, *50*, 5137–5144.
[53] D. Wu, A. Chen, C. S. Johnson Jr., *J. Magn. Reson. A* **1995**, *115*, 260–264.
[54] A. Altomare, G. Cascarano, C. Giacovazzo, A. Guagliardi, *J. Appl. Crystallogr.* **1993**, *26*, 343–350.
[55] A. Altomare, M. C. Burla, M. Camalli, G. Cascarano, C. Giacovazzo, A. Guagliardi, G. Moliterni, G. Polidori, R. Spagna, *J. Appl. Crystallogr.* **1999**, *32*, 115–119.
[56] L. Palatinus, G. Chapuis, *J. Appl. Crystallogr.* **2007**, *40*, 786–790.
[57] G. M. Sheldrick, SHELXL97 Program for the Solution and Refinement of Crystal Structures, University of Göttingen, Germany, **1997**.
[58] P. W. Betteridge, J. R. Carruthers, R. I. Cooper, K. Prout, D. J. Watkin, *J. Appl. Crystallogr.* **2003** *36*, 1487.
[59] C. K. Johnson, ORTEP II; Report ORNL-5138, Oak Ridge National Laboratory, Tennessee, **1976**.

Received: September 9, 2011
Published online: April 30, 2012

CHEMISTRY
A EUROPEAN JOURNAL

Supporting Information

N-Heterocyclic Tridentate Aromatic Ligands Bound to [Ln(hexafluoroacetylacetonate)$_3$] Units: Thermodynamic, Structural, and Luminescent Properties

Amir Zaïm,[a] Homayoun Nozary,[a] Laure Guénée,[b] Céline Besnard,[b] Jean-François Lemonnier,[a] Stéphane Petoud,*[c] and Claude Piguet*[a]

chem_201102827_sm_miscellaneous_information.pdf

Appendix 1 Quantitative analysis of the self-diffusion coefficients obtained for [La(L*k*)(hfac)$_3$] and [La(L*k*)(hfac)$_3$]-B in acetonitrile.

The application of the Stokes-Einstein equation (S1), corrected for microfrictional theory,[34] gives hydrodynamic radii r_x^H (Table S20, column 6), from which the pseudo-spherical hydrodynamic volumes $V_x^H = (4/3)\pi\left(r_x^H\right)^3$ (Table S20, column 7) of [La(**L*k***)(hfac)$_3$] and [La(**L*k***)(hfac)$_3$]-B can be estimated in solution (k_B is Boltzmann constant, η = 3.65·10^{-4} kg·m^{-1}·s^{-1} is the viscosity of acetonitrile at 293 K, r_{solv}^H is the hydrodynamic radius of the solvent molecules).[S1]

$$D_x = \left(\frac{k_B T}{6\pi\eta r_x^H}\right)\left[1 + 0.695\left(\frac{r_{solv}^H}{r_x^H}\right)^{2.234}\right] \qquad \text{(S1)}$$

Assuming that the molecular densities $\rho_x^{mol} = \left(MM_x^{mol} / N_{Av}\right) / V_x^{mol}$ (Table S20, column 4, N_{Av} is Avogadro number) computed in the solid state with the help of the van der Waals volumes V_x^{mol} estimated for [La(**L*k***)(hfac)$_3$] (Table S20, column 3) are good approximations for the molecular densities in solution $\rho_x^H \approx \rho_x^{mol}$, eq (S2) provides the hydrodynamic molecular weights MM_x^H of the particles in solution (Table S20, column 8).

$$MM_x^H = \rho_x^H \cdot V_x^H \cdot N_{Av} \qquad \text{(S2)}$$

At this level of approximation, it is no so suprising that MM_x^H found for the monuclear nine-coordinated [La(**L*k***)(hfac)$_3$] complexes in solution deviate by ~ 20% from those deduced from the solid state elemental analyses (Table S20, columns 2 and 8). However, the comparison of the MM_x^H values found for [La(**L*k***)(hfac)$_3$]-A (= [La(**L*k***)(hfac)$_3$]) and [La(**L*k***)(hfac)$_3$]-B in the same sample tube is more pertinent since it only assumes that $\rho_{La\text{-}A}^H \approx \rho_{La\text{-}B}^H$ without special reference to solid state structures. We thus deduce that the molecular weights increase by $\Delta MM_{B\text{-}A}^H = MM_{La\text{-}B}^H - MM_{La\text{-}A}^H$ = 578(122) g/mol (**L2**), and by $\Delta MM_{B\text{-}A}^H$ = 265(56) g/mol (**L3**) on going from [La(**L*k***)(hfac)$_3$] to [La(**L*k***)(hfac)$_3$]-B (Table S20, column 8).

[S1] $r_{solv}^H / r_x^H = D_x / D_{solv}$ for globular objects with $D_{solv} \approx D_{CD2HCN}$ = 5.63·10^{-9} m^2·s^{-1} at 293 K.[34b].

Appendix 2. **Speciation obtained from ^{1}H NMR titrations of L*k* with [La(hfac)$_3$] in CD_3CN**.

For a given stoichiometric $\left|\mathrm{La}\right|_{\mathrm{tot}} / \left|\mathbf{L}\boldsymbol{k}\right|_{\mathrm{tot}}$ ratio, the integrated intensities of the ^{1}H NMR signals recorded for the same proton in **L*k*** (I_{Lk}), [La(**L*k***)(hfac)$_3$] ($I_{\mathrm{La\text{-}Lk}}$) and $[\mathrm{La}(\mathbf{L}\boldsymbol{k})_2(\mathrm{hfac})_2]^+$ ($I_{\mathrm{La\text{-}2Lk}}$) can be combined and scaled with respect to the $\left|\mathrm{La}(\mathbf{L}\boldsymbol{k})(\mathrm{hfac})_3\right|$ by using eqs (S3) and (S4).

$$\left|\mathbf{L}\boldsymbol{k}\right| = \left(\frac{I_{\mathrm{LK}}}{I_{\mathrm{La\text{-}Lk}}}\right)\left|\mathrm{La}(\mathbf{L}\boldsymbol{k})(\mathrm{hfac})_3\right| \tag{S3}$$

$$\left|\mathrm{La}(\mathbf{L}\boldsymbol{k})_2(\mathrm{hfac})_2\right| = \left(\frac{I_{\mathrm{La\text{-}2Lk}}}{2I_{\mathrm{La\text{-}Lk}}}\right)\left|\mathrm{La}(\mathbf{L}\boldsymbol{k})(\mathrm{hfac})_3\right| \tag{S4}$$

Introducing eqs (S3) and (S4) into the mass balance eq (S5) yields eq (S6) after straightforward algebraic transformations.

$$\left|\mathbf{L}\boldsymbol{k}\right|_{\mathrm{tot}} = \left|\mathbf{L}\boldsymbol{k}\right| + \left|\mathrm{La}(\mathbf{L}\boldsymbol{k})(\mathrm{hfac})_3\right| + 2\left|\mathrm{La}(\mathbf{L}\boldsymbol{k})_2(\mathrm{hfac})_2\right| \tag{S5}$$

$$\left|\mathrm{La}(\mathbf{L}\boldsymbol{k})(\mathrm{hfac})_3\right| = \left|\mathbf{L}\boldsymbol{k}\right|_{\mathrm{tot}}\left(\frac{I_{\mathrm{La\text{-}Lk}}}{I_{\mathrm{Lk}} + I_{\mathrm{La\text{-}Lk}} + I_{\mathrm{La\text{-}2Lk}}}\right) \tag{S6}$$

Introducing eq (S6) into eqs (S3) and (S4) gives the speciation of the free ligand (eq S7) and of $[\mathrm{La}(\mathbf{L}\boldsymbol{k})_2(\mathrm{hfac})_2]^+$ (eq S8).

$$\left|\mathbf{L}\boldsymbol{k}\right| = \left|\mathbf{L}\boldsymbol{k}\right|_{\mathrm{tot}}\left(\frac{I_{\mathrm{Lk}}}{I_{\mathrm{Lk}} + I_{\mathrm{La\text{-}Lk}} + I_{\mathrm{La\text{-}2Lk}}}\right) \tag{S7}$$

$$\left|\mathrm{La}(\mathbf{L}\boldsymbol{k})_2(\mathrm{hfac})_2\right| = \frac{\left|\mathbf{L}\boldsymbol{k}\right|_{\mathrm{tot}}}{2}\left(\frac{I_{\mathrm{La\text{-}2Lk}}}{I_{\mathrm{Lk}} + I_{\mathrm{La\text{-}Lk}} + I_{\mathrm{La\text{-}2Lk}}}\right) \tag{S8}$$

Since $\left|\mathrm{La}(\mathbf{L}\boldsymbol{k})_2(\mathrm{hfac})_2\right| = \left|\mathrm{La(hfac)_4}\right|$ according to equilibrium (3), the missing concentration $\left|\mathrm{La(hfac)_3}\right|$ (eq S10) can be deduced from the mass balance written for the metal concentrations (eq S9).

$$\left|\mathrm{La(hfac)_3}\right| = \left|\mathrm{La}\right|_{\mathrm{tot}} - \left|\mathrm{La(hfac)_4}\right| - \left|\mathrm{La}(\mathbf{L}\boldsymbol{k})(\mathrm{hfac})_3\right| - \left|\mathrm{La}(\mathbf{L}\boldsymbol{k})_2(\mathrm{hfac})_2\right| \tag{S9}$$

$$\left|\mathrm{La(hfac)_3}\right| = \left|\mathrm{La}\right|_{\mathrm{tot}} - \left|\mathbf{L}\boldsymbol{k}\right|_{\mathrm{tot}}\left(\frac{I_{\mathrm{La\text{-}Lk}} + I_{\mathrm{La\text{-}2Lk}}}{I_{\mathrm{Lk}} + I_{\mathrm{La\text{-}Lk}} + I_{\mathrm{La\text{-}2Lk}}}\right) \tag{S10}$$

The final introduction of the concentrations expressed in eqs (S6)-(S8) and (S10) into the laws of mass action associated with equilibrium (2) and (3) yields eq (S11) and (S12), respectively (the standard concentration of the reference state is set at 1 M in eq S11).

$$\beta_{1,1}^{\mathrm{La(hfac)_3},\mathbf{L}\boldsymbol{k}} = \frac{\left|\mathrm{La}(\mathbf{L}\boldsymbol{k})(\mathrm{hfac})_3\right|}{\left|\mathrm{La(hfac)_3}\right|\cdot\left|\mathbf{L}\boldsymbol{k}\right|} = \frac{I_{\mathrm{La\text{-}Lk}}}{I_{\mathrm{Lk}}}\left(\frac{I_{\mathrm{Lk}} + I_{\mathrm{La\text{-}Lk}} + I_{\mathrm{La\text{-}2Lk}}}{\left|\mathrm{La}\right|_{\mathrm{tot}}\left(I_{\mathrm{Lk}} + I_{\mathrm{La\text{-}Lk}} + I_{\mathrm{La\text{-}2Lk}}\right) - \left|\mathbf{L}\boldsymbol{k}\right|_{\mathrm{tot}}\left(I_{\mathrm{La\text{-}Lk}} + I_{\mathrm{La\text{-}2Lk}}\right)}\right) \tag{S11}$$

$$K_{\mathrm{exch}}^{\mathrm{La},\mathbf{L}\boldsymbol{k}} = \frac{\left|\mathrm{La}(\mathbf{L}\boldsymbol{k})_2(\mathrm{hfac})_2\right|\cdot\left|\mathrm{La(hfac)_4}\right|}{\left|\mathrm{La}(\mathbf{L}\boldsymbol{k})(\mathrm{hfac})_3\right|^2} = \frac{\left|\mathrm{La}(\mathbf{L}\boldsymbol{k})_2(\mathrm{hfac})_2\right|^2}{\left|\mathrm{La}(\mathbf{L}\boldsymbol{k})(\mathrm{hfac})_3\right|^2} = \frac{1}{4}\left(\frac{I_{\mathrm{La\text{-}2Lk}}}{I_{\mathrm{La\text{-}Lk}}}\right)^2 \tag{S12}$$

Appendix 3. **Correction of the rough spectrophotometric data for the residual absorption of [Ln(hfac)$_3$]**.

For a given stoichiometric ratio $x = \left|\mathrm{Ln}\right|_{\mathrm{tot}} / \left|\mathbf{Lk}\right|_{\mathrm{tot}}$, the absorbance A_x^λ recorded at the wavelength λ for a mixture produced by equilibrium (2) can be expressed with the Lambert-Beer relationship (eq S13, l is the pathlength of the incident light within the solution, ε_i^λ is the molar absorption coefficient of species i at the wavelength λ).

$$\frac{A_x^\lambda}{l} = \varepsilon_{\mathrm{Ln(hfac)_3}}^\lambda \left|\mathrm{Ln(hfac)_3}\right| + \varepsilon_{\mathrm{Lk}}^\lambda \left|\mathbf{Lk}\right| + \varepsilon_{\mathrm{Ln\text{-}Lk}}^\lambda \left|\mathrm{Ln}(\mathbf{Lk})(\mathrm{hfac})_3\right| \qquad \text{(S13)}$$

The introduction of the mass balances given in eqs (S14)-(S15) into eq (S13) yields eq (S16), which can be easily rearranged to give eq (S17).

$$\left|\mathrm{Ln}\right|_{\mathrm{tot}} = \left|\mathrm{Ln(hfac)_3}\right| + \left|\mathrm{Ln}(\mathbf{Lk})(\mathrm{hfac})_3\right| \qquad \text{(S14)}$$

$$\left|\mathbf{Lk}\right|_{\mathrm{tot}} = \left|\mathbf{Lk}\right| + \left|\mathrm{Ln}(\mathbf{Lk})(\mathrm{hfac})_3\right| \qquad \text{(S15)}$$

$$\frac{A_x^\lambda}{l} = \varepsilon_{\mathrm{Ln(hfac)_3}}^\lambda \left(\left|\mathrm{Ln}\right|_{\mathrm{tot}} - \left|\mathrm{Ln}(\mathbf{Lk})(\mathrm{hfac})_3\right|\right) + \varepsilon_{\mathrm{Lk}}^\lambda \left(\left|\mathbf{Lk}\right|_{\mathrm{tot}} - \left|\mathrm{Ln}(\mathbf{Lk})(\mathrm{hfac})_3\right|\right) + \varepsilon_{\mathrm{Ln\text{-}Lk}}^\lambda \left|\mathrm{Ln}(\mathbf{Lk})(\mathrm{hfac})_3\right| \qquad \text{(S16)}$$

$$F\left(\lambda, \left|\mathrm{Ln}\right|_{\mathrm{tot}}, \left|\mathbf{Lk}\right|_{\mathrm{tot}}\right) = \frac{A_x^\lambda}{l} - \varepsilon_{\mathrm{Ln(hfac)_3}}^\lambda \left(\frac{\left|\mathrm{Ln}\right|_{\mathrm{tot}}}{\left|\mathbf{Lk}\right|_{\mathrm{tot}}}\right) = \varepsilon_{\mathrm{Lk}}^\lambda + \frac{\left(\varepsilon_{\mathrm{Ln\text{-}Lk}}^\lambda - \varepsilon_{\mathrm{Lk}}^\lambda - \varepsilon_{\mathrm{Ln(hfac)_3}}^\lambda\right)}{\left|\mathbf{Lk}\right|_{\mathrm{tot}}} \left|\mathrm{Ln}(\mathbf{Lk})(\mathrm{hfac})_3\right| \qquad \text{(S17)}$$

During the spectrophotometric titration, $F\left(\lambda, \left|\mathrm{Ln}\right|_{\mathrm{tot}}, \left|\mathbf{Lk}\right|_{\mathrm{tot}}\right)$ is a constant at a specific wavelength λ_0 for which $\left(\varepsilon_{\mathrm{Ln\text{-}Lk}}^{\lambda_0} - \varepsilon_{\mathrm{Lk}}^{\lambda_0} - \varepsilon_{\mathrm{Ln(hfac)_3}}^{\lambda_0}\right) = 0$. This condition has non-negligible probability to occur only for the formation of a single additional absorbing complex. We also note that any graphical representation of $F\left(\lambda, \left|\mathrm{Ln}\right|_{\mathrm{tot}}, \left|\mathbf{Lk}\right|_{\mathrm{tot}}\right)$ as a function of $1/\left|\mathbf{Lk}\right|_{\mathrm{tot}}$ becomes constant after the final end point of the titration.

Appendix 4. Equilibria and associated thermodynamic models for the formation constants of $[La(L\boldsymbol{k})_n]^{3+}$ (n = 1-3) and $[La(hfac)_n]^{(3-n)+}$ (n = 1-4).

$$[La(CH_3CN)_9]^{3+} + \mathbf{L}\boldsymbol{k}^{-} \rightleftharpoons [La(\mathbf{L}\boldsymbol{k})(CH_3CN)_6]^{3+} + 3\ CH_3CN \quad \beta_{1,1,0}^{La,\mathbf{L}\boldsymbol{k},hfac} \quad (S18)$$

$$\beta_{1,1,0}^{La,\mathbf{L}\boldsymbol{k},hfac} = 6 f_{\mathbf{L}\boldsymbol{k}}^{La} \quad (S19)$$

$$[La(CH_3CN)_9]^{3+} + 2\ \mathbf{L}\boldsymbol{k}^{-} \rightleftharpoons [La(\mathbf{L}\boldsymbol{k})_2(CH_3CN)_3]^{3+} + 6\ CH_3CN \quad \beta_{1,2,0}^{La,\mathbf{L}\boldsymbol{k},hfac} \quad (S20)$$

$$\beta_{1,2,0}^{La,\mathbf{L}\boldsymbol{k},hfac} = 12\left(f_{\mathbf{L}\boldsymbol{k}}^{La}\right)^2 u_{\mathbf{L}\boldsymbol{k},\mathbf{L}\boldsymbol{k}} \quad (S21)$$

$$[La(CH_3CN)_9]^{3+} + 3\ \mathbf{L}\boldsymbol{k}^{-} \rightleftharpoons [La(\mathbf{L}\boldsymbol{k})_3]^{3+} + 9\ CH_3CN \quad \beta_{1,3,0}^{La,\mathbf{L}\boldsymbol{k},hfac} \quad (S22)$$

$$\beta_{1,3,0}^{La,\mathbf{L}\boldsymbol{k},hfac} = 16\left(f_{\mathbf{L}\boldsymbol{k}}^{La}\right)^3 \left(u_{\mathbf{L}\boldsymbol{k},\mathbf{L}\boldsymbol{k}}\right)^3 \quad (S23)$$

$$[La(CH_3CN)_9]^{3+} + hfac^{-} \rightleftharpoons [La(hfac)(CH_3CN)_7]^{2+} + 2\ CH_3CN \quad \beta_{1,0,1}^{La,\mathbf{L}\boldsymbol{k},hfac} \quad (S24)$$

$$\beta_{1,0,1}^{La,\mathbf{L}\boldsymbol{k},hfac} = 12 f_{hfac}^{La} \quad (S25)$$

$$[La(CH_3CN)_9]^{3+} + 2\ hfac^{-} \rightleftharpoons [La(hfac)_2(CH_3CN)_5]^{+} + 4\ CH_3CN \quad \beta_{1,0,2}^{La,\mathbf{L}\boldsymbol{k},hfac} \quad (S26)$$

$$\beta_{1,0,2}^{La,\mathbf{L}\boldsymbol{k},hfac} = 48\left(f_{hfac}^{La}\right)^2 u_{hfac,hfac} \quad (S27)$$

$$[La(CH_3CN)_9]^{3+} + 3\ hfac^{-} \rightleftharpoons [La(hfac)_3(CH_3CN)_3] + 6\ CH_3CN \quad \beta_{1,0,3}^{La,\mathbf{L}\boldsymbol{k},hfac} \quad (S28)$$

$$\beta_{1,0,3}^{La,\mathbf{L}\boldsymbol{k},hfac} = 64\left(f_{hfac}^{La}\right)^3 \left(u_{hfac,hfac}\right)^3 \quad (S29)$$

$$[La(CH_3CN)_9]^{3+} + 4\ hfac^{-} \rightleftharpoons [La(hfac)_4]^{-} + 9\ CH_3CN \quad \beta_{1,0,4}^{La,\mathbf{L}\boldsymbol{k},hfac} \quad (S30)$$

$$\beta_{1,0,4}^{La,\mathbf{L}\boldsymbol{k},hfac} = 24\left(f_{hfac}^{La}\right)^4 \left(u_{hfac,hfac}\right)^6 \quad (S31)$$

The experimental $\beta_{1,j,0}^{La,\mathbf{L}\boldsymbol{k},hfac}$ (j = 1-3, eqs S18, S20, S22) and $\beta_{1,0,l}^{La,\mathbf{L}\boldsymbol{k},hfac}$ (l = 1-4, eqs S24, S26, S28, S30) values were determined by spectrophotometric titrations of $Ln(CF_3SO_3)_3$ with $\mathbf{L}\boldsymbol{k}$ or $Me_4(hfac)$ in acetonitrile containining 10^{-4} M of diglyme (Table S22).[S2]

[S2] The triflate anion is considered as mainly non-coordinating in acetonitrile, see J.-C. G. Bünzli, A. Milicic-Tang, in *Handbook on the Physics and Chemistry of Rare Earths*; K. A. Gschneidner, L. Eyring, Eds.; Elsevier, **1995**; Vol. 21, 322-394.

Appendix 5. Correction of the absorption spectrum of [Ln(L*k*)(hfac)$_3$] for partial dissociation in solution.

$$Ln(hfac)_3 + \mathbf{L}k \rightleftharpoons [Ln(\mathbf{L}k)(hfac)_3] \qquad \beta_{1,1}^{Ln(hfac)_3,\mathbf{L}k} \qquad (2)$$

Once the formation constant $\beta_{1,1}^{Ln(hfac)_3,\mathbf{L}k}$ is at hand (eq 2), the speciation in solution is easily obtained from the mass balances given in eqs S32 and S33, combined with the law of mass action eq S34 (C_{Lk} and C_{Ln} are the total concentrations of ligand, respectively of metallic unit Ln(hfac)$_3$ and $|Ln|$ stands for $|Ln(hfac)_3|$).

$$C_{Lk} = |Lk| + |LnLk| \Rightarrow |LnLk| = C_{Lk} - |Lk| \qquad (S32)$$

$$C_{Ln} = |Ln| + |LnLk| \Rightarrow |Ln| = C_{Ln} - |LnLk| = C_{Ln} - \left(C_{Lk} - |Lk|\right) \qquad (S33)$$

$$\beta_{1,1}^{Ln(hfac)_3,\mathbf{L}k} = \frac{|LnLk|}{|Lk||Ln|} \qquad (S34)$$

Introduction of eqs S32 and S33 into eq S34 yields

$$\beta_{1,1}^{Ln(hfac)_3,\mathbf{L}k} = \frac{C_{Lk} - |Lk|}{|Lk|\left(C_{Ln} - C_{Lk} + |Lk|\right)} \qquad (S35)$$

Straightforward algebraic transformations eventually lead to

$$\beta_{1,1}^{Ln(hfac)_3,\mathbf{L}k}|Lk|^2 + \left[\beta_{1,1}^{Ln(hfac)_3,\mathbf{L}k}\left(C_{Ln} - C_{Lk}\right) + 1\right]|Lk| - C_{Lk} = 0 \qquad (S36)$$

For any mixture of ligand and metal, the solution of the quadratic eq S36 provides the concentration of the free ligand, from which those of the free metal and free complex can be deduced with eqs S32 and S33. The total absorbance A_{tot} at a wavelength λ is given by the Lambert-Beer relationship (eq S37), where $\varepsilon_{Ln}^{\lambda}$, $\varepsilon_{Lk}^{\lambda}$ and $\varepsilon_{LnLk}^{\lambda}$ are the molar absorption coefficients of Ln(hfac)$_3$, **L*k*** and [Ln(**L*k***)(hfac)$_3$], respectively, and l is the pathlength of the analytic cell. According that the absorption spectra of Ln(hfac)$_3$ (Fig. 7a) and of **L*k*** (Fig 7a and S22a) can be recorded independently, the absorption spectrum of the pure complex corrected for dissociation is deduced from the experimental absorbance A_{tot} recorded for any C_{Ln}/C_{Lk} mixture by using eq S38.

$$A_{tot} = l\sum_n \varepsilon_n^{\lambda}|n| = l\left[\left(\varepsilon_{Ln}^{\lambda}|Ln|\right) + \left(\varepsilon_{Lk}^{\lambda}|Lk|\right) + \left(\varepsilon_{LnLk}^{\lambda}|LnLk|\right)\right] \qquad (S37)$$

$$\varepsilon_{LnLk}^{\lambda} = \frac{\left(A_{tot}/l\right) - \varepsilon_{Ln}^{\lambda}|Ln| - \varepsilon_{Lk}^{\lambda}|Lk|}{|LnLk|} \qquad (S38)$$

Table S1. ^{1}H NMR Shifts (in ppm with Respect to TMS) for the Ligands **L2**-**L3** and Their Complexes [Ln(**L*k***)(hfac)$_3$] in $CDCl_3$ at 293 K (Ln = La, Eu, Lu, Y). [a]

	H1	H2	H3	H4	H5	H6	H7	H8	H9,10	H11	Hhfac
L2	8.09	8.29	7.33	7.46	8.00	4.66	1.60	1.38	0.68	-	-
L3	8.06	8.31	7.36	7.46	7.88	4.72	1.63	1.40	0.69	7.36	-
[La(**L2**)(hfac)$_3$]	8.36	8.00	7.35	7.58	8.32	4.52	1.95	1.85	1.10	-	5.92
[La(**L3**)(hfac)$_3$]	8.33	7.98	7.39	7.47	8.13	4.54	1.99	1.88	1.12	7.47	5.87
[Eu(**L2**)(hfac)$_3$]	6.90	6.46	9.38	10.61	25.79	6.06	3.23	2.49	1.43	-	1.57
[Eu(**L3**)(hfac)$_3$]	6.91	6.39	9.24	10.3	24.17	5.95	3.18	2.48	1.44	11.68	1.55
[Lu(**L2**)(hfa)$_3$]	8.32	8.03	7.30	7.53	8.44	4.55	1.95	1.90	1.13	-	5.87
[Lu(**L3**)(hfa)$_3$]	8.29	8.01	7.34	7.42	8.24	4.57	1.99	1.92	1.14	7.42	5.83
[Y(**L2**)(hfac)$_3$]	8.32	8.01	7.31	7.54	8.40	4.54	1.96	1.89	1.12	-	5.89
[Y(**L3**)(hfac)$_3$]	8.31	8.02	7.36	7.45	8.22	4.58	2.01	1.93	1.15	7.45	5.87

[a] Numbering is given in Scheme 3.

Table S2. ^{1}H NMR Shifts (in ppm with Respect to TMS) for the Ligands **L2**-**L3** and Their Complexes [Ln(**L*k***)(hfac)$_3$] in CD_3CN at 293 K (Ln = La, Eu, Lu, Y). [a]

	H1	H2	H3	H4	H5	H6	H7	H8	H9,10	H11	Hhfac
L2	8.18	8.28	7.57	7.51	7.98	4.73	1.61	1.40	0.66	-	
L3	8.13	8.26	7.59	7.31	7.76	4.74	1.60	1.39	0.64	7.36	
[La(**L2**)(hfac)$_3$]-A	8.51	8.26	7.64	7.59	8.06	4.62	1.83	1.70	0.96	-	5.95
[La(**L2**)(hfac)$_3$]-B	8.56	8.37	7.53	7.22	6.70	4.73	1.83	1.70	1.06	-	5.98
[La(**L3**)(hfac)$_3$]-A	8.50	8.24	7.69	7.31	7.82	4.63	1.86	1.73	0.98	7.46	5.90
[La(**L3**)(hfac)$_3$]-B	8.50	8.34	7.49	7.11	6.87	4.69	1.86	1.73	1.03	6.63	5.97
[Eu(**L2**)(hfac)$_3$]	7.78	7.10	9.80	8.72	21.47	5.99	2.82	2.21	1.20	-	2.67
[Eu(**L3**)(hfac)$_3$]	7.87	7.08	8.44	9.41	19.59	5.86	2.73	2.12	1.20	10.34	3.02
[Lu(**L2**)(hfa)$_3$]	8.54	8.32	7.66	7.62	8.15	4.69	1.89	1.84	1.06	-	6.11
[Lu(**L3**)(hfa)$_3$]	8.52	8.31	7.48	7.31	7.71	4.72	1.89	1.84	1.06	7.36	6.12
[Y(**L2**)(hfac)$_3$]	8.50	8.29	7.62	7.57	8.18	4.66	1.86	1.78	1.01	-	5.94
[Y(**L3**)(hfac)$_3$]	8.48	8.28	7.68	7.29	7.97	4.68	1.88	1.81	1.03	7.45	5.90

[a] Numbering is shown in Scheme 3.

Table S3 Selected Bond Distances (Å) and Bond Angles (°) in **L3**.[a]

Bond distances (Å)

Atom 1	Atom 2	Distance	Atom 1	Atom 2	Distance
C63a	C58a	1.533(3)	C90b	C89b	1.543(5)
C59a	C58a	1.523(4)	C91b	C89b	1.522(5)
C58a	C57a	1.510(4)	C89b	C85b	1.519(3)
C57a	C56a	1.536(4)	C85b	C84b	1.512(3)
C56a	N55a	1.475(3)	C84b	N83b	1.461(3)
N55a	C54a	1.373(3)	N83b	C82b	1.386(2)
N55a	C46a	1.371(2)	N83b	C79b	1.380(3)
C54a	C53a	1.396(3)	C82b	C100b	1.397(3)
C54a	C48a	1.402(3)	C82b	C81b	1.401(3)
C53a	C52a	1.388(5)	C100b	C101b	1.381(3)
C52a	C50a	1.389(5)	C101b	C102b	1.401(4)
C50a	C49a	1.366(4)	C102b	C103b	1.364(4)
C49a	C48a	1.407(4)	C103b	C81b	1.399(3)
C48a	N47a	1.383(3)	C81b	N80b	1.387(3)
N47a	C46a	1.315(3)	N80b	C79b	1.320(3)
C46a	C45a	1.482(3)	C79b	C78b	1.482(3)
C45a	C75a	1.391(3)	C78b	C77b	1.396(3)
C45a	N44a	1.343(2)	C78b	N44b	1.330(3)
C75a	C76a	1.376(3)	C77b	C76b	1.381(3)
C76a	C77a	1.384(3)	C76b	C75b	1.379(3)
C77a	C78a	1.395(3)	C75b	C45b	1.384(3)
C78a	N44a	1.344(2)	C45b	N44b	1.350(2)
C78a	C79a	1.469(2)	C45b	C46b	1.486(3)
C79a	N80a	1.313(2)	C46b	N47b	1.321(3)
C79a	N83a	1.389(2)	C46b	N55b	1.369(2)
N80a	C81a	1.385(2)	N47b	C48b	1.380(3)
C81a	C103a	1.401(3)	C48b	C49b	1.395(3)
C81a	C82a	1.403(3)	C48b	C54b	1.400(3)
C103a	C102a	1.390(3)	C49b	C50b	1.364(4)
C102a	C101a	1.398(4)	C50b	C52b	1.391(4)
C101a	C100a	1.375(3)	C52b	C53b	1.378(3)

C100a	C82a	1.394(3)	C53b	C54b	1.397(3)
C82a	N83a	1.388(2)	C54b	N55b	1.378(2)
N83a	C84a	1.465(3)	N55b	C56b	1.448(5)
C84a	C85a	1.515(3)	C56b	C57b	1.504(6)
C85a	C89a	1.530(3)	C57b	C58b	1.504(5)
C89a	C90a	1.486(4)	C58b	C59b	1.530(6)
C89a	C91a	1.517(4)	C58b	C63b	1.528(6)

Angles (°)

At. 1	At. 2	At. 3	angle	At. 1	At. 2	At. 3	angle
C63a	C58a	C59a	109.6(3)	C90b	C89b	C91b	112.2(3)
C63a	C58a	C57a	110.0(2)	C90b	C89b	C85b	108.8(3)
C59a	C58a	C57a	111.5(2)	C91b	C89b	C85b	111.7(3)
C58a	C57a	C56a	115.3(2)	C89b	C85b	C84b	114.1(2)
C57a	C56a	N55a	113.94(18)	C85b	C84b	N83b	111.99(15)
C56a	N55a	C54a	123.74(18)	C84b	N83b	C82b	123.78(16)
C56a	N55a	C46a	130.2(2)	C84b	N83b	C79b	130.12(15)
C54a	N55a	C46a	105.64(18)	C82b	N83b	C79b	105.44(15)
N55a	C54a	C53a	131.9(2)	N83b	C82b	C100b	131.52(17)
N55a	C54a	C48a	106.18(17)	N83b	C82b	C81b	106.22(16)
C53a	C54a	C48a	121.9(3)	C100b	C82b	C81b	122.21(18)
C54a	C53a	C52a	116.1(3)	C82b	C100b	C101b	116.58(19)
C53a	C52a	C50a	122.4(2)	C100b	C101b	c102b	121.5(2)
C52a	C50a	C49a	121.6(3)	C101b	C102b	C103b	121.7(2)
C50a	C49a	C48a	117.7(3)	C102b	C103b	C81b	118.3(2)
C49a	C48a	C54a	120.2(2)	C82b	C81b	C103b	119.72(19)
C49a	C48a	N47a	130.0(2)	C82b	C81b	N80b	109.85(17)
C54a	C48a	N47a	109.8(2)	C103b	C81b	N80b	130.4(2)
C48a	N47a	C46a	104.43(17)	C81b	N80b	C79b	104.81(17)
N55a	C46a	N47a	113.96(18)	N83b	C79b	N80b	113.65(17)
N55a	C46a	C45a	125.56(18)	N83b	C79b	C78b	125.72(16)
N47a	C46a	C45a	120.43(16)	N80b	C79b	C78b	120.63(17)
C46a	C45a	C75a	119.13(16)	C79b	C78b	C77b	118.17(17)
C46a	C45a	N44a	117.69(16)	C79b	C78b	N44b	119.04(16)
C75a	C45a	N44a	123.14(18)	C77b	C78b	N44b	122.79(17)

C45a	C75a	C76a	118.55(17)	C78b	C77b	C76b	118.55(19)
C75a	C76a	C77a	119.38(17)	C77b	C76b	C75b	119.44(18)
C76a	C77a	C78a	118.60(18)	C76b	C75b	C45b	118.32(18)
C77a	C78a	N44a	122.68(16)	C75b	C45b	N44b	123.13(19)
C77a	C78a	C79a	118.51(16)	C75b	C45b	C46b	119.34(17)
N44a	C78a	C79a	118.80(15)	N44b	C45b	C46b	117.52(16)
C78a	N44a	C45a	117.63(15)	C45b	N44b	C78b	117.75(16)
C78a	C79a	N80a	121.24(16)	C45b	C46b	N47b	121.78(16)
C78a	C79a	N83a	125.49(16)	C45b	C46b	N55b	124.86(17)
N80a	C79a	N83a	113.26(15)	N47b	C46b	N55b	113.36(17)
C79a	N80a	C81a	105.14(16)	C46b	N47b	C48b	104.76(15)
N80a	C81a	C103a	129.2(2)	N47b	C48b	C49b	130.89(19)
N80a	C81a	C82a	110.22(16)	N47b	C48b	C54b	109.96(18)
C103a	C81a	C82a	120.51(18)	C49b	C48b	C54b	119.1(2)
C81a	C103a	C102a	116.6(2)	C48b	C49b	C50b	118.7(2)
C103a	C102a	C101a	122.2(2)	C49b	C50b	C52b	121.3(2)
C102a	C101a	C100a	121.7(2)	C50b	C52b	C53b	122.0(2)
C101a	C100a	C82a	116.6(2)	C52b	C53b	C54b	116.2(2)
C81a	C82a	C100a	122.39(18)	C48b	C54b	C53b	122.48(18)
C81a	C82a	N83a	105.67(15)	C48b	C54b	N55b	105.85(17)
C100a	C82a	N83a	131.9(2)	C53b	C54b	N55b	131.65(18)
C79a	N83a	C82a	105.70(15)	C54b	N55b	C46b	106.04(15)
C79a	N83a	C84a	130.34(15)	C54b	N55b	C56b	123.6(3)
C82a	N83a	C84a	123.30(15)	C46b	N55b	C56b	126.8(3)
N83a	C84a	C85a	112.02(15)	N55b	C56b	C57b	111.26(10)
C84a	C85a	C89a	113.48(18)	C56b	C57b	C58b	114.27(10)
C85a	C89a	C90a	112.0(2)	C57b	C58b	C59b	110.49(10)
C85a	C89a	C91a	109.3(2)	C57b	C58b	C63b	111.90(10)
C90a	C89a	C91a	110.0(3)	C59b	C58b	C63b	110.38(10)

[a] Numbering scheme is given in Fig. S1.

Table S4 Selected Least-Squares Planes Data for in **L3**.

Least-Squares Planes

Least-squares planes description	Abbreviation	Max. deviation/Å	Atom
Pyridine, N44a	Pya	0.008	C78a
Benzimidazole, N47a, N55a	bz1a	0.013	C49a
Benzimidazole, N80a, N83a	bz2a	0.029	C101a
Pyridine, N44b	Pyb	0.007	C77b
Benzimidazole, N47b, N55b	bz1b	0.036	C49b
Benzimidazole, N80b, N83b	bz2b	0.025	C102b

Interplanar angles (°)[a]

	bz2a	Pya	bz1b	bz2b
bz1a	39.75	37.05		
bz2a		9.62		
Pyb			38.53	15.76
bz1b				47.75

[a] Typical uncertainties: 0.05°.

Table S5 Elemental Analyses for [Ln(**L*k***)(hfac)$_3$] Complexes (*k* = 2, 3; Ln = La, Eu, Gd, Lu, Y).

Compound	MM/ g·mol^{-1}	%C found	%H found	%N found	%C calc	%H calc	%N calc
[La(**L2**)(hfac)$_3$]	1369.46	38.56	2.46	5.00	38.59	2.50	5.11
[Eu(**L2**)(hfac)$_3$]	1382.52	38.02	2.57	4.99	38.23	2.48	5.07
[Gd(**L2**)(hfac)$_3$]	1387.81	38.03	2.48	5.00	38.08	2.47	5.05
[Lu(**L2**)(hfac)$_3$]	1405.52	37.51	2.52	5.08	37.60	2.44	4.98
[Y(**L2**)(hfac)$_3$]	1319.46	39.96	2.63	5.27	40.05	2.60	5.31
[La(**L3**)(hfac)$_3$]	1211.67	43.54	2.82	5.72	43.62	2.99	5.78
[Eu(**L3**)(hfac)$_3$]	1224.73	42.81	2.80	5.63	43.15	2.96	5.72
[Gd(**L3**)(hfac)$_3$]	1230.02	42.68	2.72	5.71	42.07	2.95	5.69
[Lu(**L3**)(hfac)$_3$]	1247.73	42.34	2.89	5.49	42.35	2.91	5.61
[Y(**L3**)(hfac)$_3$]	1161.67	45.34	2.92	5.98	45.49	3.12	6.03

Table S6 Summary of Crystal Data, Intensity Measurements and Structure Refinements for **L3**, [Ln(**L2**)(hfac)$_3$] and [Ln(**L3**)(hfac)$_3$] (Ln = La, Eu, Lu).

Compound	**L3**	[La(**L2**)(hfac)$_3$]	[Eu(**L2**)(hfac)$_3$]	[Lu(**L2**)(hfac)$_3$]	[La(**L3**)(hfac)$_3$]	[Eu(**L3**)(hfac)$_3$]	[Lu(**L3**)(hfac)$_3$]
Emprical formula	$C_{58}H_{66}N_{10}$	$C_{44}H_{34}Br_2F_{18}LaN_5O_6$	$C_{44}H_{34}Br_2F_{18}EuN_5O_6$	$C_{44}H_{34}Br_2F_{18}LuN_5O_6$	$C_{44}H_{36}F_{18}LaN_5O_6$	$C_{44}H_{36}F_{18}EuN_5O_6$	$C_{44}H_{36}F_{18}LuN_5O_6$
Formula weight	903.20	1369.46	1382.52	1405.75	1210.66	1224.72	1247.75
Temperature/K	200	120	120	120	120	120	180
Crystal system	Orthorhombic	Monoclinic	Monoclinic	Monoclinic	Monoclinic	Monoclinic	Monoclinic
Space group	*Pca*2$_1$	*P*2$_1$/*n*	*P*2$_1$/*n*	*C*2/*c*	*P*2$_1$/*n*	*P*2$_1$/*n*	*C*2/*c*
a/Å	27.842 (7)	12.6691 (4)	12.6691 (4)	22.4798 (14)	12.0145 (8)	11.9006 (7)	21.8994 (11)
b/Å	9.477 (4)	25.5451 (11)	25.5451 (11)	13.2382 (8)	25.4880 (13)	25.3270 (17)	13.1128 (10)
c/Å	19.702 (5)	15.7845 (5)	15.7845 (5)	16.9991 (9)	15.8152 (11)	15.6843 (8)	19.8307 (10)
α/°	90	90	90	90	90	90	90
β/°	90	98.241 (3)	98.241 (3)	90.484 (5)	110.712 (5)	109.189 (4)	121.236 (3)
γ/°	90	90	90	90	90	90	90
Volume/ Å^3	5199 (3)	5055.6 (3)	5055.6 (3)	5058.6 (5)	4530.0(5)	4464.7(5)	4869.1 (5)
Z	4	4	4	4	4	4	4
ρ/Mg m^{-3}	1.154	1.799	1.816	1.846	1.775	1.822	1.702
μ/mm^{-1}	0.070	2.54	2.94	3.649	1.07	1.54	2.148
*R*1 (all data)[a]	0.0432,	0.033	0.043	0.025	0.03	0.032	0.0455
w*R*2 (all data)[b]	0.077	0.056	0.066	0.04	0.056	0.064	0.1479

Radiation : Mo-Kα (μ = 0.71073 Å). Monochromator : highly oriented graphite.[a] $R[F^2>2\sigma(F^2)]$. [b] w$R(F^2)$.

Table S7 Selected Bond Distances (Å), Bond Angles (°) in [La(**L2**)(hfac)$_3$].

Bond Distances (Å)

Atoms 1-2	Distance	Atoms 1-2	Distance	Atoms 1-2	Distance
La-O20	2.553(2)	La-O16	2.521(2)	La-N47	2.644(2)
La-O2	2.504(2)	La-O30	2.481(2)	La-N44	2.732(2)
La-O6	2.522(2)	La-O34	2.484(2)	La-N80	2.675(2)

Chelate Angles (°)

Atoms 1-2-3	Angle	Atoms 1-2-3	Angle	Atoms 1-2-3	Angle
N47-La-N44	60.24(7)	N47-La-N80	121.14(7)	N44-La-N80	60.93(7)
O30-La-O34	69.85(7)	O16-La-O20	67.78(6)	O2-La-O6	67.51(7)

N-La-O Angles (°)

Atoms 1-2-3	Angle	Atoms 1-2-3	Angle	Atoms 1-2-3	Angle
N44-La-O16	81.74(7)	N44-La-O20	109.84(7)	N44-La-O34	154.84(7)
N80-La-O16	66.08(7)	N80-La-O20	133.78(7)	N80-La-O34	144.60(7)
N47-La-O16	106.51(7)	N47-La-O20	70.30(7)	N47-La-O34	137.73(7)
N44-La-O30	135.31(7)	N44-La-O6	69.35(7)	N44-La-O2	113.35(7)
N80-La-O30	144.60(7)	N80-La-O6	90.25(7)	N80-La-O2	71.03(7)
N47-La-O30	82.86(7)	N47-La-O6	68.18(7)	N47-La-O2	133.91(7)

Selected Least-Squares Planes Data

Least-Squares Planes

Least-squares planes description	Abbreviation	Max. deviation/Å	Atom
Pyridine	py	0.021	C78
N44, C78, C77, C76, C75, C45			
Benzimidazole	bz1	0.034	C46
C46, N55, C54, C53, C52, C50, C49, C48, N47			
Benzimidazole	bz2	0.024	C102
N80, C79, N83, C82, C81, C103, C102, C101, C100			
Hexafluoroacetylacetonate	hfac1	0.016	C18
O16, C17, C18, C19, O20			
Hexafluoroacetylacetonate	hfac2	0.018	C3
O2, C3, C4, C5, O6			
Hexafluroacetylacetonate	hfac3	0.006	C33
C33, O34, C32, C31, O30			

Interplanar angles (°)[a]

	bz2	py	hfac1	hfac2	hfac3
bz1	42.31	15.10	47.69	86.45	43.53
bz2		31.33	79.93	47.11	12.87
py			62.49	78.17	33.78
hfac1				76.91	72.49
hfac2					42.92

[a] Typical uncertainties: 0.5°

Table S8 Selected Bond Distances (Å), Bond Angles (°) in [Eu(**L2**)$(hfac)_3$].

Bond Distances (Å)

Atoms 1-2	Distance	Atoms 1-2	Distance	Atoms 1-2	Distance
Eu-O20	2.502(3)	Eu-O16	2.442(3)	Eu-N47	2.541(4)
Eu-O2	2.458(3)	Eu-O30	2.380(3)	Eu-N44	2.613(4)
Eu-O6	2.431(3)	Eu-O34	2.377(3)	Eu-N80	2.589(4)

Chelate Angles (°)

Atoms 1-2-3	Angle	Atoms 1-2-3	Angle	Atoms 1-2-3	Angle
N47-Eu-N44	62.57(11)	N47-Eu-N80	125.30(12)	N44-Eu-N80	62.74(12)
O30-Eu-O34	73.40(11)	O16-Eu-O20	68.55(11)	O2-Eu-O6	68.42(11)

N-Eu-O Angles (°)

Atoms 1-2-3	Angle	Atoms 1-2-3	Angle	Atoms 1-2-3	Angle
N44-Eu-O16	79.79(12)	N44-Eu-O20	111.91(11)	N44-Eu-O34	151.16(11)
N80-Eu-O16	66.95(12)	N80-Eu-O20	135.40(12)	N80-Eu-O34	94.33(11)
N47-Eu-O16	104.11(11)	N47-Eu-O20	69.12(12)	N47-Eu-O34	137.22(11)
N44-Eu-O30	135.43(12)	N44-Eu-O6	69.29(11)	N44-Eu-O2	114.47(11)
N80-Eu-O30	143.97(12)	N80-Eu-O6	90.84(12)	N80-Eu-O2	70.33(11)
N47-Eu-O30	84.73(12)	N47-Eu-O6	69.22(12)	N47-Eu-O2	134.79(12)

Selected Least-Squares Planes Data

Least-Squares Planes

Least-squares planes description	Abbreviation	Max. deviation/Å	Atom
Pyridine	py	0.024	C45
N44, C78, C77, C76, C75, C45			
Benzimidazole	bz1	0.042	C46
C46, N55, C54, C53, C52, C50, C49, C48, N47			
Benzimidazole	bz2	0.028	C102
N80, C79, N83, C82, C81, C103, C102,C101, C100			
Hexafluoroacetylacetonate	hfac1	0.023	C19
O16, C17, C18, C19, O20			
Hexafluoroacetylacetonate	hfac2	0.024	C3
O2, C3, C4, C5, O6			
Hexafluroacetylacetonate	hfac3	0.019	C33
C33, O34, C32, C31, O30			

Interplanar angles (°)[a]

	bz2	py	hfac1	hfac2	hfac3
bz1	41.18	14.08	46.09	83.85	40.51
bz2		30.55	75.67	45.92	14.92
py			59.50	75.98	34.78
hfac1				83.41	64.77
hfac2					43.41

[a] Typical uncertainties: 0.5°

Table S9 Selected Bond Distances (Å), Bond Angles (°) in [Lu(**L2**)$(hfac)_3$].

Bond Distances (Å)

Atoms 1-2	Distance	Atoms 1-2	Distance	Atoms 1-2	Distance
Lu-O2’	2.3107(18)	Lu-O6’	2.457(2)	Lu-N27	2.459(2)
Lu-O2	2.3107(18)	Lu-O19’	2.2950(18)	Lu-N33	2.525(3)
Lu-O6	2.457(2)	Lu-O19	2.2950(18)	Lu-N27’	2.459(2)

Chelate Angles (°)

Atoms 1-2-3	Angle	Atoms 1-2-3	Angle	Atoms 1-2-3	Angle
N27-Lu-N33	65.32(5)	N27-Lu-N27’	130.64(11)	N33-Lu-N27’	65.32(5)
O19-Lu-O19’	78.71(9)	O6’-Lu-O2’	69.91(7)	O2-Lu-O6	69.91(7)

N-Lu-O Angles (°)

Atoms 1-2-3	Angle	Atoms 1-2-3	Angle	Atoms 1-2-3	Angle
N33-Lu-O6’	117.31(5)	N33-Lu-O2’	67.29(5)	N33-Lu-O19’	140.65(5)
N27’-Lu-O6’	134.96(7)	N27’-Lu-O2’	71.32(7)	N27’-Lu-O19’	83.10(7)
N27-Lu-O6’0	71.12(7)	N27-Lu-O2’	89.88(7)	N27-Lu-O19’	139.98(7)
N33-Lu-O19	140.65(5)	N33-Lu-O6	117.31(5)	N33-Lu-O2	67.29(5)
N27’-Lu-O19	139.98(7)	N27’-Lu-O6	71.12(7)	N27’-Lu-O2	89.88(7)
N27-Lu-O19	83.10(7)	N27-Lu-O6	134.96(7)	N27-Lu-O2	71.32(7)

Selected Least-Squares Planes Data

Least-Squares Planes

Least-squares planes description	Abbreviation	Max. deviation/Å	Atom
Pyridine	py	0.080	C32
N33, C32, C34, C35, C34', C32'			
Benzimidazole	bz1	0.018	N30
N27, C31, N30, C29, C28, C57, C56, C55, C54			
Benzimidazole	bz2	0.018	N30'
N27', C31', N30', C29', C28', C57', C56', C55', C54'			
Hexafluoroacetylacetonate	hfac1	0.04	C3
O2, C3, C4, C5, O6			
Hexafluoroacetylacetonate	hfac2	0.04	C3'
O2', C3', C4', C5', O6'			
Hexafluroacetylacetonate	hfac3	0.02	C20
O19, C20,C21, C20', O19'			

Interplanar angles (°)[a]

	bz2	py	hfac1	hfac2	hfac3
bz1	19.68	9.84	76.20	89.34	34.82
bz2		9.84	89.34	76.20	34.82
py			82.69	82.69	33.60
hfac1				83.23	72.44
hfac2					72.44

[a] Typical uncertainties: 0.5°

Table S10 Selected Bond Distances (Å), Bond Angles (°) in [La(**L3**)$(hfac)_3$].

Bond Distances (Å)

Atoms 1-2	Distance	Atoms 1-2	Distance	Atoms 1-2	Distance
La-O20	2.5044(18)	La-O16	2.4890(18)	La-N47	2.617(2)
La-O2	2.5120(19)	La-O30	2.4648(18)	La-N44	2.685(2)
La-O6	2.4620(19)	La-O34	2.4407(18)	La-N80	2.629(2)

Chelate Angles (°)

Atoms 1-2-3	Angle	Atoms 1-2-3	Angle	Atoms 1-2-3	Angle
N47-La-N44	60.63(7)	N47-La-N80	121.03(7)	N44-La-N80	60.40(7)
O30-La-O34	68.80(6)	O16-La-O20	67.15(6)	O2-La-O6	66.90(6)

N-La-O Angles (°)

Atoms 1-2-3	Angle	Atoms 1-2-3	Angle	Atoms 1-2-3	Angle
N44-La-O16	80.20(6)	N44-La-O20	109.93(6)	N44-La-O34	144.69(6)
N80-La-O16	67.30(6)	N80-La-O20	134.43(6)	N80-La-O34	88.37(6)
N47-La-O16	102.29(6)	N47-La-O20	68.27(6)	N47-La-O34	146.19(6)
N44-La-O30	146.15(6)	N44-La-O6	76.19(6)	N44-La-O2	107.58(6)
N80-La-O30	140.47(6)	N80-La-O6	101.35(7)	N80-La-O2	68.83(6)
N47-La-O30	92.74(6)	N47-La-O6	64.76(6)	N47-La-O2	131.65(6)

Selected Least-Squares Planes Data

Least-Squares Planes

Least-squares planes description	Abbreviation	Max. deviation/Å	Atom
Pyridine	py	0.016	C75
N44, C78, C77, C76, C75, C45			
Benzimidazole	bz1	0.014	C48
C46, N55, C54, C53, C52, C50, C49, C48, N47			
Benzimidazole	bz2	0.017	C100
N80, C79, N83, C82, C81, C103, C102,C101, C100			
Hexafluoroacetylacetonate	hfac1	0.08	C19
O16, C17, C18, C19, O20			
Hexafluoroacetylacetonate	hfac2	0.07	C3
O2, C3, C4, C5, O6			
Hexafluroacetylacetonate	hfac3	0.016	C31
C33, O34, C32, C31, O30			

Interplanar angles (°)[a]

	bz2	py	hfac1	hfac2	hfac3
bz1	40.68	22.30	39.10	80.60	38.94
bz2		26.70	77.16	42.37	8.33
py			61.06	68.92	29.91
hfac1				71.30	72.61
hfac2					41.80

[a] Typical uncertainties: 0.5°

Table S11 Selected Bond Distances (Å), Bond Angles (°) in [Eu(**L3**)$(hfac)_3$].

Bond Distances (Å)

Atoms 1-2	Distance	Atoms 1-2	Distance	Atoms 1-2	Distance
Eu-O20	2.424(2)	Eu-O16	2.394(2)	Eu-N47	2.539(2)
Eu-O2	2.440(2)	Eu-O30	2.369(2)	Eu-N44	2.570(3)
Eu-O6	2.371(2)	Eu-O34	2.345(2)	Eu-N80	2.541(3)

Chelate Angles (°)

Atoms 1-2-3	Angle	Atoms 1-2-3	Angle	Atoms 1-2-3	Angle
N47-Eu-N44	62.75(8)	N47-Eu-N80	62.47(8)	N44-Eu-N80	125.21(8)
O30-Eu-O34	72.25(7)	O16-Eu-O20	68.80(7)	O2-Eu-O6	68.33(7)

N-Eu-O Angles (°)

Atoms 1-2-3	Angle	Atoms 1-2-3	Angle	Atoms 1-2-3	Angle
N44-Eu-O16	78.72(8)	N44-Eu-O20	112.19(8)	N44-Eu-O34	143.82(8)
N80-Eu-O16	66.92(8)	N80-Eu-O20	135.54(8)	N80-Eu-O34	86.03(8)
N47-Eu-O16	101.56(8)	N47-Eu-O20	67.85(8)	N47-Eu-O34	143.96(8)
N44-Eu-O30	143.70(8)	N44-Eu-O6	73.60(8)	N44-Eu-O2	109.50(8)
N80-Eu-O30	140.24(8)	N80-Eu-O6	99.60(8)	N80-Eu-O2	68.37(8)
N47-Eu-O30	88.69(8)	N47-Eu-O6	65.47(8)	N47-Eu-O2	133.38(8)

Selected Least-Squares Planes Data

Least-Squares Planes

Least-squares planes description	Abbreviation	Max. deviation/Å	Atom
Pyridine	py	0.016	C75
N44, C78, C77, C76, C75, C45			
Benzimidazole	bz1	0.018	C54
C46, N55, C54, C53, C52, C50, C49, C48, N47			
Benzimidazole	bz2	0.025	C103
N80, C79, N83, C82, C81, C103, C102,C101, C100			
Hexafluoroacetylacetonate	hfac1	0.092	C19
O16, C17, C18, C19, O20			
Hexafluoroacetylacetonate	hfac2	0.087	C3
O2, C3, C4, C5, O6			
Hexafluroacetylacetonate	hfac3	0.025	C31
C33, O34, C32, C31, O30			

Interplanar angles (°)[a]

	bz2	Py	hfac1	hfac2	hfac3
bz1	39.74	20.62	40.08	79.72	38.94
bz2		25.69	75.29	43.10	10.69
py			66.69	68.79	30.62
hfac1				76.94	69.59
hfac2					40.84

[a] Typical uncertainties: 0.5°

Table S12 Selected Bond Distances (Å), Bond Angles (°) in [Lu(**L3**)(hfac)$_3$].

Bond Distances (Å)

Atoms 1-2	Distance	Atoms 1-2	Distance	Atoms 1-2	Distance
Lu-O20	2.309(4)	Lu-O60’	2.428(4)	Lu-N27	2.447(4)
Lu-O20’	2.309(4)	Lu-O19’	2.297(4)	Lu-N33	2.553(5)
Lu-O60	2.428(4)	Lu-O19	2.297(4)	Lu-N27’	2.447(4)

Chelate Angles (°)

Atoms 1-2-3	Angle	Atoms 1-2-3	Angle	Atoms 1-2-3	Angle
N27-Lu-N33	65.10(9)	N27-Lu-N270	130.20(13)	N33-Lu-N27’	65.10(9)
O19-Lu-O19’	79.01(14)	O60-Lu-O20	70.49(12)	O20’-Lu-O60’	70.49(13)

N-Lu-O Angles (°)

Atoms 1-2-3	Angle	Atoms 1-2-3	Angle	Atoms 1-2-3	Angle
N33-Lu-O60	119.27(7)	N33-Lu-O20	68.80(7)	N33-Lu-O19’	140.50(10)
N27’-Lu-O60	138.44(15)	N27’-Lu-O20	74.48(13)	N27’-Lu-O19’	138.20(13)
N27-Lu-O60	70.34(13)	N27-Lu-O20	87.88(14)	N27-Lu-O19’	84.51(13)
N33-Lu-O19	140.50(10)	N33-Lu-O60	119.27(7)	N33-Lu-O20’	68.80(7)
N27’-Lu-O19	84.51(13)	N27’-Lu-O60	138.44(15)	N27’-Lu-O20’	74.48(13)
N27-Lu-O19	138.20(13)	N27-Lu-O60	70.34(13)	N27-Lu-O20’	87.88(14)

Selected Least-Squares Planes Data

Least-Squares Planes

Least-squares planes description	Abbreviation	Max. deviation/Å	Atom
Pyridine N33, C32a, C34a, C35, C34b', C32b'	pya	0.089	C35
Pyridine N33, C32b, C34b, C35, C34a', C32a'	pyb	0.089	C35
Benzimidazole N27, C31, N30, C29, C28, C57, C56, C55, C54	bz1	0.016	C55
Benzimidazole N27', C31', N30', C29', C28', C57', C56', C55', C54'	bz2	0.014	C31'
Hexafluoroacetylacetonate O20, C3, C4, C5, O60	hfac1	0.049	C3
Hexafluoroacetylacetonate O20', C3', C4', C5', O60'	hfac2	0.049	C3'
Hexafluroacetylacetonate O19', C20,C21, C20', O19	hfac3	0.038	C20

Interplanar angles (°)[a]

	bz2	Pya	Pyb	hfac1	hfac2	hfac3
bz1	7.16	6.24	13.35	84.19	88.85	47.75
bz2		13.35	6.24	88.85	84.19	47.75
pya			19.46	79.41	87.96	49.44
pyb				87.96	79.41	49.44
hfac1					80.94	58.71
hfac2						58.71

[a] Typical uncertainties: 0.5°

Table S13 Bond Distances ($\delta_{i,j}$) Bond Valences ($\nu_{\mathrm{Ln},j}$)[a] and Total Atom Valence (V_{Ln})[b] in the Crystal Structure of [La(**L2**)(hfac)$_3$].

Atom [c]	Donor type	$\delta_{\mathrm{La},j}$ / Å	$\nu_{\mathrm{La},j}$	
N47	bzim	2.644	0.355	
N44	py	2.732	0.280	Average N-heterocyclic
N80	bzim	2.675	0.327	0.32(3)
O2	hfac	2.504	0.382	
O6	hfac	2.522	0.364	
O16	hfac	2.521	0.365	
O20	hfac	2.553	0.335	
O30	hfac	2.481	0.407	Average O-hfac
O34	hfac	2.484	0.403	0.38(3)
		V_{La}	3.217	

[a] $\nu_{\mathrm{Ln},j} = e^{\left[\left(R_{\mathrm{Ln}j} - \delta_{\mathrm{Ln},j}\right)/b\right]}$, whereby $\delta_{\mathrm{Ln},j}$ is the Ln-donor atom j distance. The valence bond parameters $R_{\mathrm{Ln,N}}$ and $R_{\mathrm{Ln,O}}$ are taken from refs [25] and b = 0.37Å. [b] $V_{\mathrm{Ln}} = \sum_j \nu_{\mathrm{Ln},j}$.[22] [c] Numbering taken from Figure S6a.

Table S14 Bond Distances ($\delta_{i,j}$) Bond Valences ($\nu_{\mathrm{Ln},j}$)[a] and Total Atom Valence (V_{Ln})[b] in the Crystal Structure of [Eu(**L2**)(hfac)$_3$].

Atom [c]	Donor type	$\delta_{\mathrm{Eu},j}$ / Å	$\nu_{\mathrm{Eu},j}$	
N47	bzim	2.541	0.358	
N44	py	2.613	0.295	Average N-heterocyclic
N80	bzim	2.589	0.315	0.32(3)
O2	hfac	2.458	0.321	
O6	hfac	2.431	0.346	
O16	hfac	2.442	0.336	
O20	hfac	2.502	0.285	
O30	hfac	2.380	0.397	Average O-hfac
O34	hfac	2.377	0.400	0.35(4)
		V_{Eu}	3.052	

[a] $\nu_{\mathrm{Ln},j} = e^{\left[\left(R_{\mathrm{Ln}j} - \delta_{\mathrm{Ln},j}\right)/b\right]}$, whereby $\delta_{\mathrm{Ln},j}$ is the Ln-donor atom j distance. The valence bond parameters $R_{\mathrm{Ln,N}}$ and $R_{\mathrm{Ln,O}}$ are taken from refs [25] and b = 0.37Å. [b] $V_{\mathrm{Ln}} = \sum_j \nu_{\mathrm{Ln},j}$.[22] [c] Numbering taken from Figure S6b.

Table S15 Bond Distances ($\delta_{i,j}$) Bond Valences （$\nu_{\mathrm{Ln},j}$)[a] and Total Atom Valence (V_{Ln})[b] in the Crystal Structure of [Lu(**L2**)(hfac)$_3$].

Atom [c]	Donor type	$\delta_{\mathrm{Lu},j}$ / Å	$\nu_{\mathrm{Lu},j}$	
N27	bzim	2.459	0.328	
N33	py	2.525	0.274	Average N-heterocyclic
N27’	bzim	2.459	0.328	0.31(3)
O2	hfa	2.3107	0.374	
O2’	hfa	2.3107	0.374	
O6	hfa	2.457	0.252	
O6’	hfa	2.457	0.252	
O19	hfa	2.295	0.390	Average O-hfac
O19’	hfa	2.295	0.390	0.34(7)
		V_{Lu}	2.962	

[a] $\nu_{\mathrm{Ln},j} = e^{\left[\left(R_{\mathrm{Ln}j} - \delta_{\mathrm{Ln},j}\right)/b\right]}$, whereby $\delta_{\mathrm{Ln},j}$ is the Ln-donor atom j distance. The valence bond parameters $R_{\mathrm{Ln,N}}$ and $R_{\mathrm{Ln,O}}$ are taken from refs [25] and b = 0.37Å. [b] $V_{\mathrm{Ln}} = \sum_j \nu_{\mathrm{Ln},j}$.[22] [c] Numbering taken from Figure S6c.

Table S16 Bond Distances ($\delta_{i,j}$) Bond Valences （$\nu_{\mathrm{Ln},j}$)[a] and Total Atom Valence (V_{Ln})[b] in the Crystal Structure of [La(**L3**)(hfac)$_3$].

Atom [c]	Donor type	$\delta_{\mathrm{Eu},j}$ / Å	$\nu_{\mathrm{Eu},j}$	
N47	bzim	2.617	0.382	
N44	py	2.685	0.318	Average N-heterocyclic
N80	bzim	2.629	0.370	0.36(3)
O2	hfac	2.512	0.374	
O6	hfac	2.462	0.428	
O16	hfac	2.489	0.398	
O20	hfac	2.5044	0.382	
O30	hfac	2.4648	0.425	Average O-hfac
O34	hfac	2.4407	0.453	0.41(3)
		V_{La}	3.529	

[a] $\nu_{\mathrm{Ln},j} = e^{\left[\left(R_{\mathrm{Ln}j} - \delta_{\mathrm{Ln},j}\right)/b\right]}$, whereby $\delta_{\mathrm{Ln},j}$ is the Ln-donor atom j distance. The valence bond parameters $R_{\mathrm{Ln,N}}$ and $R_{\mathrm{Ln,O}}$ are taken from refs [25] and b = 0.37Å. [b] $V_{\mathrm{Ln}} = \sum_j \nu_{\mathrm{Ln},j}$.[22] [c] Numbering taken from Figure S6d.

Table S17 Bond Distances ($\delta_{i,j}$) Bond Valences （$\nu_{\mathrm{Ln},j}$)[a] and Total Atom Valence (V_{Ln})[b] in the Crystal Structure of [Eu(**L3**)(hfac)$_3$].

Atom [c]	Donor type	$\delta_{\mathrm{Lu},j}$ / Å	$\nu_{\mathrm{Lu},j}$	
N47	bzim	2.539	0.360	
N44	py	2.570	0.331	Average N-heterocyclic
N80	bzim	2.541	0.358	0.35(1)
O2	hfa	2.440	0.337	
O6	hfa	2.371	0.407	
O16	hfa	2.394	0.382	
O20	hfa	2.424	0.352	
O30	hfa	2.369	0.409	Average O-hfac
O34	hfa	2.345	0.436	0.39(4)
		V_{Eu}	3.372	

[a] $\nu_{\mathrm{Ln},j} = e^{\left[\left(R_{\mathrm{Ln}j} - \delta_{\mathrm{Ln},j}\right)/b\right]}$, whereby $\delta_{\mathrm{Ln},j}$ is the Ln-donor atom j distance. The valence bond parameters $R_{\mathrm{Ln,N}}$ and $R_{\mathrm{Ln,O}}$ are taken from refs [25] and b = 0.37Å. [b] $V_{\mathrm{Ln}} = \sum_j \nu_{\mathrm{Ln},j}$.[22] [c] Numbering taken from Figure S6e.

Table S18 Bond Distances ($\delta_{i,j}$) Bond Valences （$\nu_{\mathrm{Ln},j}$)[a] and Total Atom Valence (V_{Ln})[b] in the Crystal Structure of [Lu(**L3**)(hfac)$_3$].

Atom [c]	Donor type	$\delta_{\mathrm{Eu},j}$ / Å	$\nu_{\mathrm{Eu},j}$	
N27	bzim	2.447	0.338	
N33	py	2.553	0.254	Average N-heterocyclic
N27’	bzim	2.447	0.338	0.31(4)
O2	hfac	2.309	0.376	
O2’	hfac	2.309	0.376	
O6	hfac	2.428	0.273	
O6’	hfac	2.428	0.273	
O19	hfac	2.297	0.388	Average O-hfac
O19’	hfac	2.297	0.388	0.35(5)
		V_{Lu}	3.00	

[a] $\nu_{\mathrm{Ln},j} = e^{\left[\left(R_{\mathrm{Ln}j} - \delta_{\mathrm{Ln},j}\right)/b\right]}$, whereby $\delta_{\mathrm{Ln},j}$ is the Ln-donor atom j distance. The valence bond parameters $R_{\mathrm{Ln,N}}$ and $R_{\mathrm{Ln,O}}$ are taken from refs [25] and b = 0.37Å. [b] $V_{\mathrm{Ln}} = \sum_j \nu_{\mathrm{Ln},j}$.[22] [c] Numbering taken from Figure S6f.

Table S19 ^{19}F NMR Shifts for the Complexes [Ln(**L*k***)(hfac)$_3$] in CD_3CN at 293 K (Ln = La, Y). [a].

	δ in $CDCl_3$ /ppm	δ in CD_3CN /ppm
[Y(**L2**)(hfac)$_3$]	-76.94	[b]
[Y(**L3**)(hfac)$_3$]	-76.96	[b]
[La(**L2**)(hfac)$_3$]	-77.01	-77.51
[La(**L2**)$_2$(hfac)$_2$]$^+$	-	-77.08
[La(hfac)$_4$]$^-$	-	-77.46
[La(**L3**)(hfac)$_3$]	-77.06	-77.53
[La(**L3**)$_2$(hfac)$_2$]$^+$	-	-77.07
[La(hfac)$_4$]$^-$	-	-77.46

[a] Numbering is given in Scheme 3. [b] Not recorded.

Table S20 Experimental Molecular Weights (MM_x, Table S5), Solid-State Molecular Volumes (V_x^{mol})[a] and Translational Self-diffusion Coefficients (D_x), and Calculated Solid-State Molecular Densities (ρ_x^{mol}, eq S2), Hydrodynamic Radii (r_x^H, eq S1), Hydrodynamic Volumes (V_x^H) and Hydrodynamic Molecular Weights (MM_x^H, eq S2) for [La(**L*k***)(hfac)$_3$]-A and [La(**L*k***)(hfac)$_3$]-B in CD_3CN at 293 K (**L*k*** = **L2**, **L3**).

Compds	MM_x /g·mol^{-1}	V_x^{mol} /Å^3	ρ_x^{mol} /g·cm^{-3}	D_x /m^{2}s^{-1}	r_x^H /Å	V_x^H /Å^3	MM_x^H /g·mol^{-1}
[La(**L2**)(hfac)$_3$]-A	1369.46	793.7	2.87	1.13(4)·10^{-9}	5.4(3)	652(56)	1124(112)
[La(**L2**)(hfac)$_3$]-B	-	-	-	0.97(4)·10^{-9}	6.2(3)	986(86)	1702(170)
[La(**L3**)(hfac)$_3$]-A	1211.67	724.8	2.78	1.20(3)·10^{-9}	5.1(2)	539(47)	901(90)
[La(**L3**)(hfac)$_3$]-B	-		-	1.10(4)·10^{-9}	5.5(3)	697(60)	1166(117)

[a] The solid-state molecular volumes of the complexes were deduced from the building of the van der Waals surfaces around the molecular structures.

Table S21 Integrated VT ^{1}H NMR Intensities for a Given Proton, and Calculated Exchange Constants $K_{exch}^{La,\mathbf{L3}}$ (eq S12) for equilibrium (3) Obtained for the Complex [La(**L2**)(hfac)$_3$] in CD_3CN (0.01 M).

T /K	I_{L3}	$I_{La\text{-}L3}$	$I_{La\text{-}2L3}$	$K_{exch}^{La,\mathbf{L2}}$
233	0	32(3)	68(3)	1.1(2)
243	0	39(3)	61(3)	0.61(8)
253	0	46(2)	54(2)	0.34(3)
263	0	51(2)	49(2)	0.23(2)
273	0	56(3)	44(3)	0.15(2)
283	0	61(3)	39(3)	0.10(1)
293	0	64(3)	36(3)	0.08(1)
303	0	69(5)	31(5)	0.05(1)
313	0	68(4)	32(4)	0.06(1)
323	0	70(4)	30(4)	0.046(9)

Table S22 Experimental and Computed Thermodynamic Formation Constants (log($\beta_{i,j,l}^{\mathrm{Ln},\mathbf{L}k,\mathrm{hfac}}$)) for the System La(III)/**L*k***/hfac$^-$ (*k* = 2, 3, Acetonitrile, 298 K).[a]

Formation constants	**L2** (exp)	**L2** (calcd)	**L3** (exp)	**L3** (calcd)
log($\beta_{1,1,0}^{\mathrm{Ln},\mathbf{L}k,\mathrm{hfac}}$)	6.38(7)	6.20	5.62(16)	5.10
log($\beta_{1,2,0}^{\mathrm{Ln},\mathbf{L}k,\mathrm{hfac}}$)	11.33(13)	11.57	9.89(62)	11.55
log($\beta_{1,3,0}^{\mathrm{Ln},\mathbf{L}k,\mathrm{hfac}}$)	16.54(16)	16.40	17.02(20)	16.65
log($\beta_{1,0,1}^{\mathrm{Ln},\mathbf{L}k,\mathrm{hfac}}$)	7.39(6)	7.29	7.39(6)	7.28
log($\beta_{1,0,2}^{\mathrm{Ln},\mathbf{L}k,\mathrm{hfac}}$)	14.12(9)	13.68	14.12(9)	13.68
log($\beta_{1,0,3}^{\mathrm{Ln},\mathbf{L}k,\mathrm{hfac}}$)	18.50(10)	19.18	18.50(10)	19.20
log($\beta_{1,0,4}^{\mathrm{Ln},\mathbf{L}k,\mathrm{hfac}}$)	23.81(15)	23.71	23.81(15)	23.77
log($\beta_{1,1,3}^{\mathrm{Ln},\mathbf{L}k,\mathrm{hfac}}$)	23.56(7)	23.11	24.18(11)	23.59
log($\beta_{1,2,2}^{\mathrm{Ln},\mathbf{L}k,\mathrm{hfac}}$)	22.16(17)	22.49	23.15(19)	23.59
AF_{Lk} [b]	-	$4.2\cdot10^{-4}$	-	$7.7\cdot10^{-4}$

[a] Acetonitrile contains a fixed total concentration of 10^{-4} M of diglyme for stabilizing [Ln(hfac)$_3$].

[b] Willcott agreement factor $AF_{\mathrm{Lk}} = \sqrt{\dfrac{\sum_{i,j,k}\left[\log\left(\beta_{i,j,l,\mathrm{exp}}^{\mathrm{Ln},\mathbf{L}k,\mathrm{hfac}}\right)-\log\left(\beta_{i,j,l,\mathrm{calcd}}^{\mathrm{Ln},\mathbf{L}k,\mathrm{hfac}}\right)\right]^2}{\sum_{i,j,k}\left[\log\left(\beta_{i,j,l,\mathrm{exp}}^{\mathrm{Ln},\mathbf{L}k,\mathrm{hfac}}\right)\right]^2}}$.

Table S23 Ligand-centered Absorption and Emission Properties of **L2**, **L3** and of their Complexes [Ln(**L*k***)(hfac)$_3$].

Compound	$\lambda_{max,abs}$ /cm^{-1} [a]	$\lambda_{max,flu}$ /cm^{-1} [b]	$\lambda_{max,phos}$ /cm^{-1} [b]	Lifetime /ms
	$^1\pi\pi \rightarrow {}^1\pi\pi^*$	$^1\pi\pi^* \rightarrow {}^1\pi\pi$	$^3\pi\pi^* \rightarrow {}^1\pi\pi$	τ ($^3\pi\pi^*$)
[Gd(hfac)$_3$(diglyme)]	33170(30990)	27000(sh) 25970 23585	21550 20600	1.17(2)
[Eu(hfac)$_3$(diglyme)]	33110(31020)	[c]	[c]	1.04(1) [d]
L2	31200(37680)	26280 25030	19880 18850	10.2(2)
L3	31300(36940)	26280 25640(sh)	19760 18850	6.4(7)
[Gd(**L2**)(hfac)$_3$]	32890(55400) 27740(14850sh)	25670 24480 21210	21030 19200 18300	0.43(1)
[Gd(**L3**)(hfac)$_3$]	33160(57000) 27740(11500sh)	25060 24130 20700	21000(sh) 18700 17510	0.99(2)
[Eu(**L2**)(hfac)$_3$]	32890(55550) 27740(16100sh)	[c]	[c]	0.97(1) [d]
[Eu(**L3**)(hfac)$_3$]	33170(56900) 27740(13700sh)	25100 24030	[c]	0.97(1) [d]

[a] The molar absorption coefficients ε are given between parentheses in M^{-1}·cm^{-1} for 10^{-4} M solution in acetonitrile at 293 K after correcting for partial dissociation. [b] Recorded on solid state sample at 77 K. [c] Quenched by quantitative transfer onto Eu(III). [d] Eu($^5D_0$) lifetime recorded at 293 K.

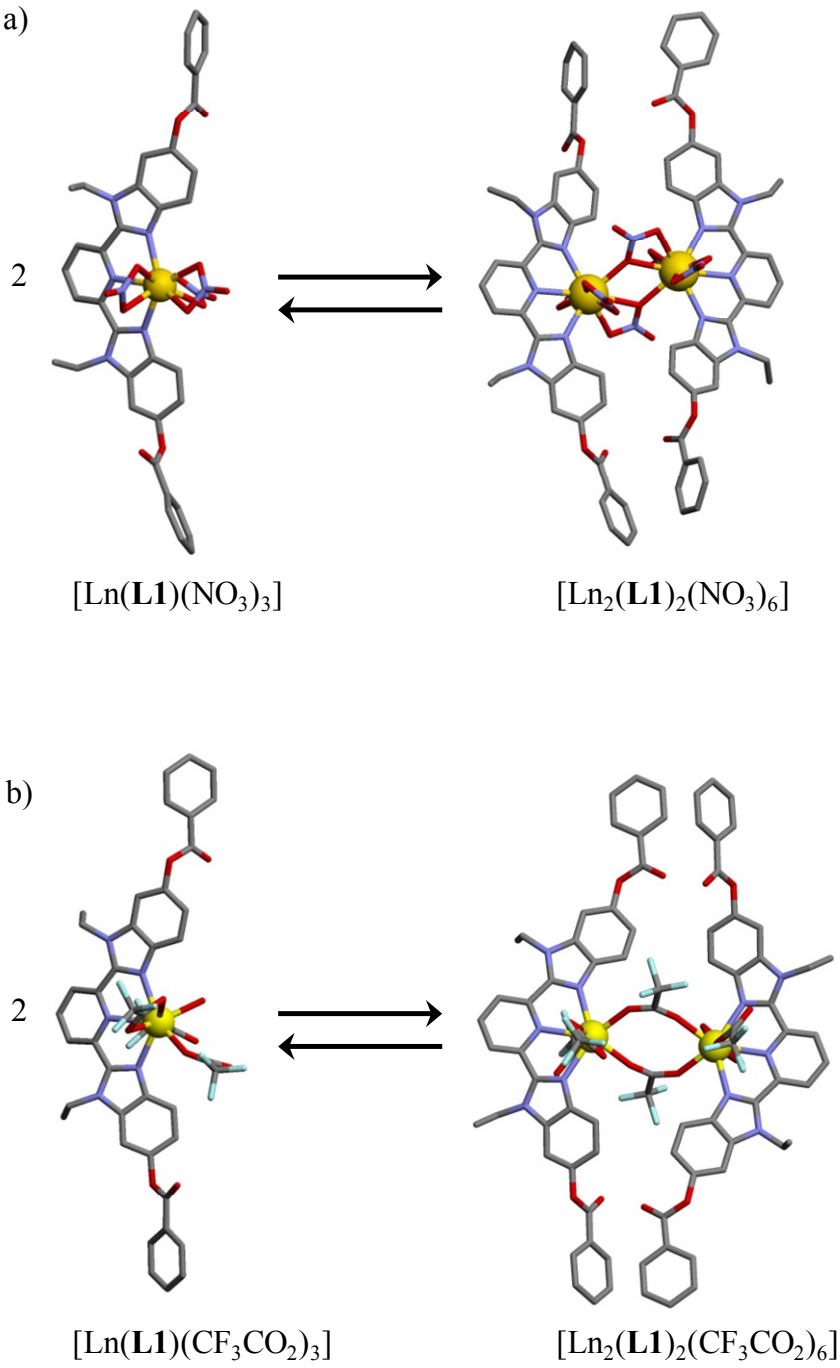

Figure S1 Dimerization of [Ln(**L1**)X_3] occurring in polar aprotic solvent with a) X = NO_3^- and b) X = $CF_3CO_2^-$.[10]

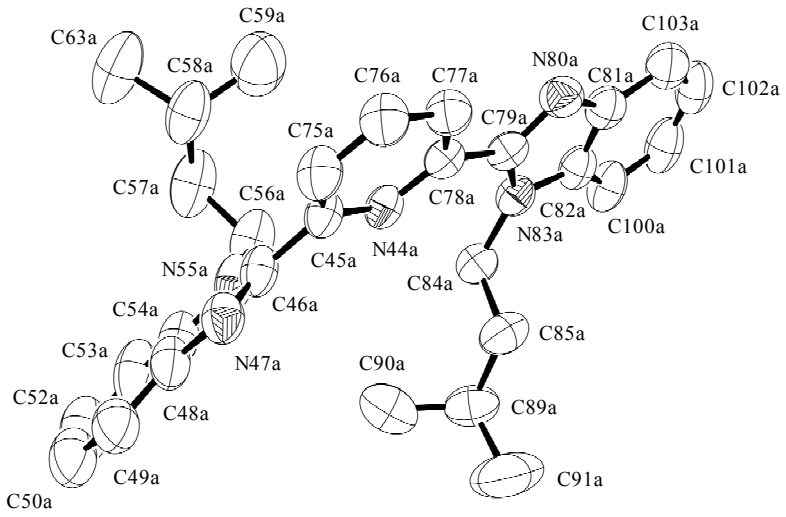

Figure S2 ORTEP view of ligand **L3** with atomic numbering scheme. Thermal ellispoids are represented at the 50% probability level.

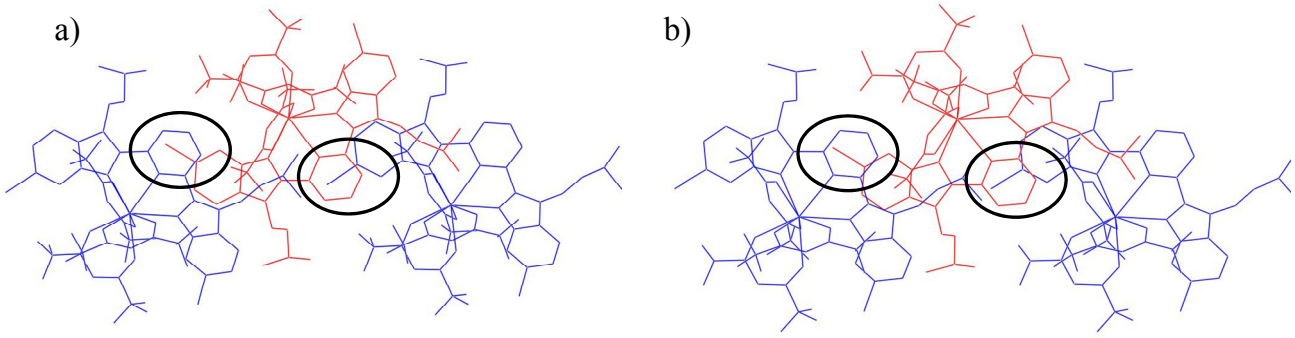

Figure S3 Views along the *a* direction in the crystal structures of a) [La(**L2**)(hfac)$_3$] and b) [Eu(**L2**)(hfac)$_3$] showing intermolecular Br-π-stacking interactions between neighboring molecules ([La(**L2**)(hfac)$_3$]: Br-pyridine distance = 3.95 Å; [Eu(**L2**)(hfac)$_3$]: Br-pyridine distance = 3.96 Å).

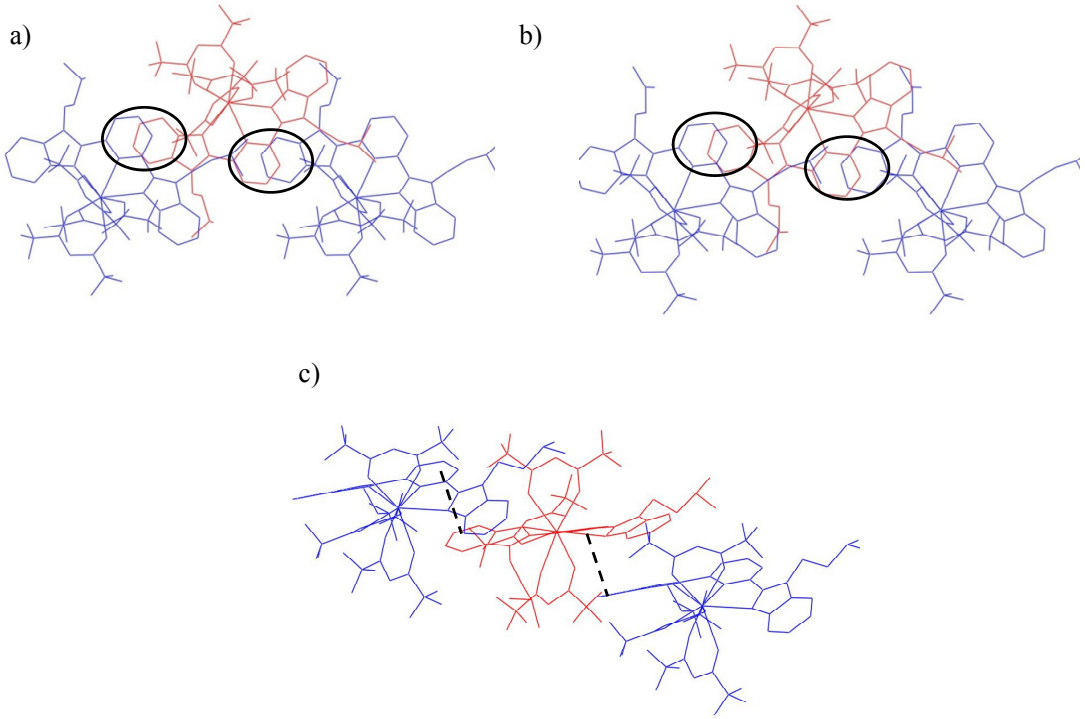

Figure S4 Views along the *a* direction in the crystal structures of a) [La(**L3**)(hfac)$_3$] and b) [Eu(**L3**)(hfac)$_3$] showing intermolecular π–π-staking interactions between neighboring molecules ([La(**L3**)(hfac)$_3$]: interplanar pyridine-benzimidazole angle = 3.5°, interplanar distance = 3.51 Å; [Eu(**L3**)(hfac)$_3$]: interplanar pyridine-benzimidazole angle = 3.8°, interplanar distance = 3.52 Å). c) View of the intermolecular ππ-staking interactions perpendicular to the *a* direction in [Eu(**L3**)(hfac)$_3$].

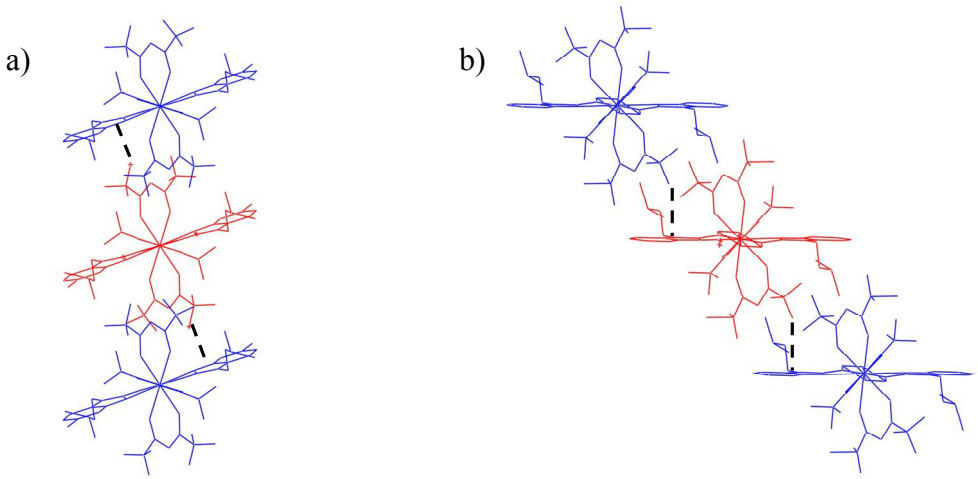

Figure S5 Views along the *b* direction in the crystal structures of a) [Lu(**L2**)(hfac)$_3$] and b) [Lu(**L3**)(hfac)$_3$] showing intermolecular short F-benzimidazole contact distances ([Lu(**L2**)(hfac)$_3$]: F16-benzimidazole = 3.36 Å; [Lu(**L3**)(hfac)$_3$]: F16-benzimidazole = 3.155 Å).

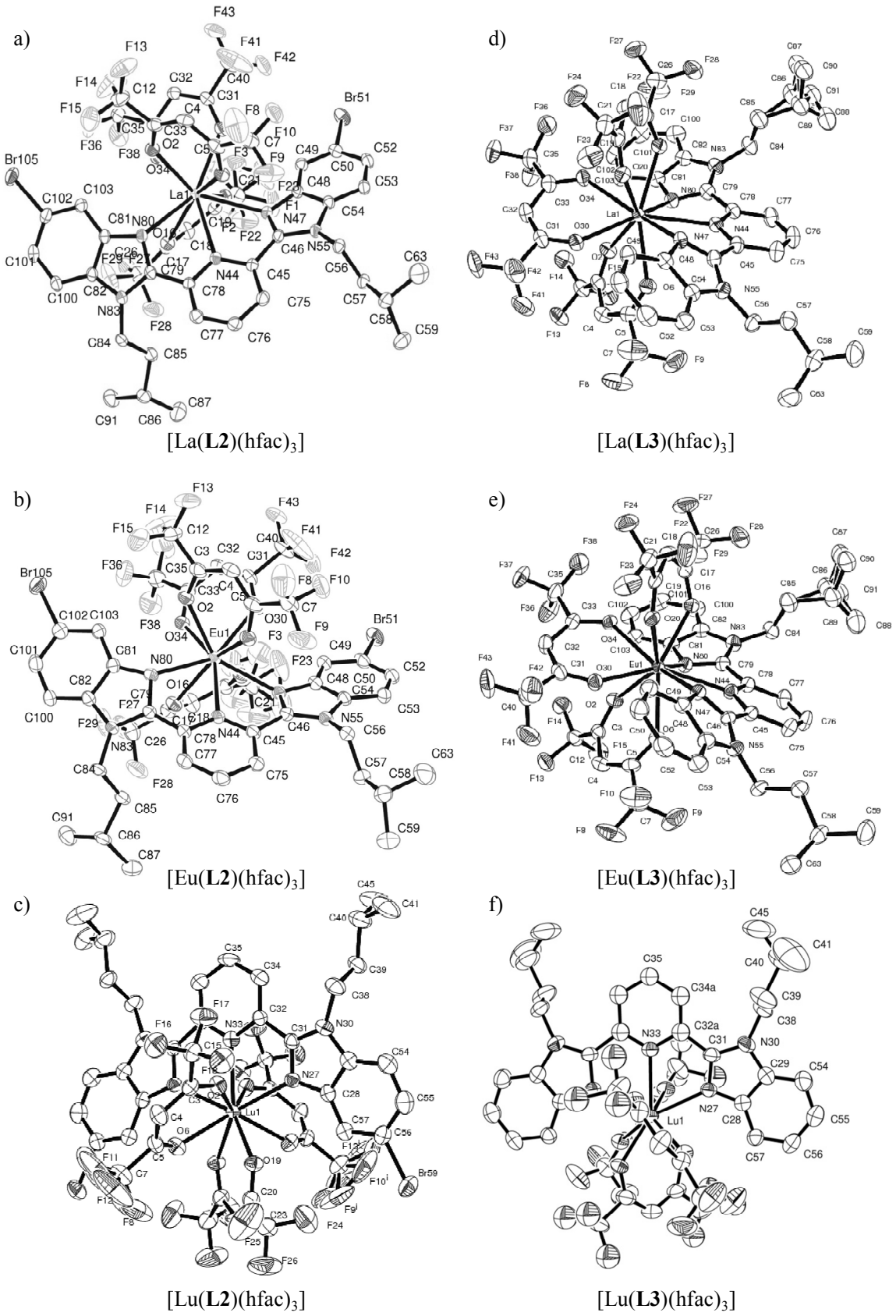

Figure S6 ORTEP views of complexes [Ln(**L2**)(hfac)$_3$] and [Ln(**L3**)(hfac)$_3$] (Ln = La, Eu, Lu) with atomic numbering scheme. Thermal ellispoids are represented at the 50% probability level.

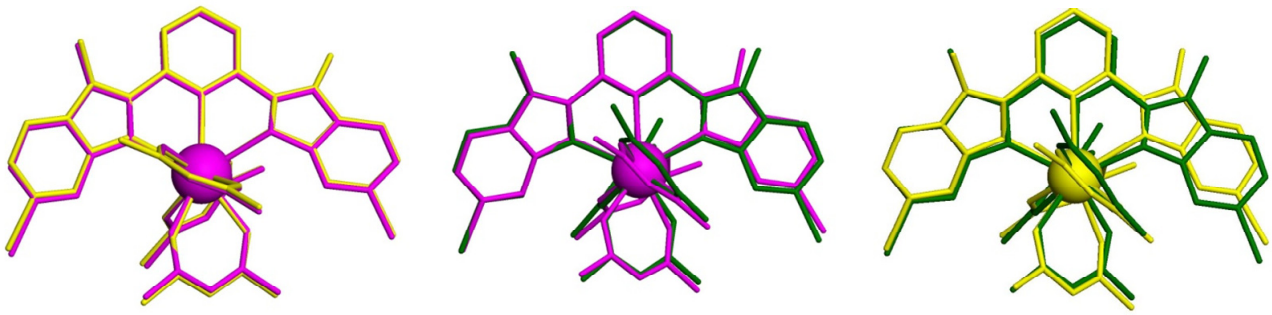

Figure S7 Pair superimpositions of the molecular structures of [La(**L2**)(hfac)$_3$] (yellow), [Eu(**L2**)(hfac)$_3$] (magenta) and [Lu(**L2**)(hfac)$_3$] (green). The terminal isobutyl residues and the fluorine atoms have been omitted for clarity.

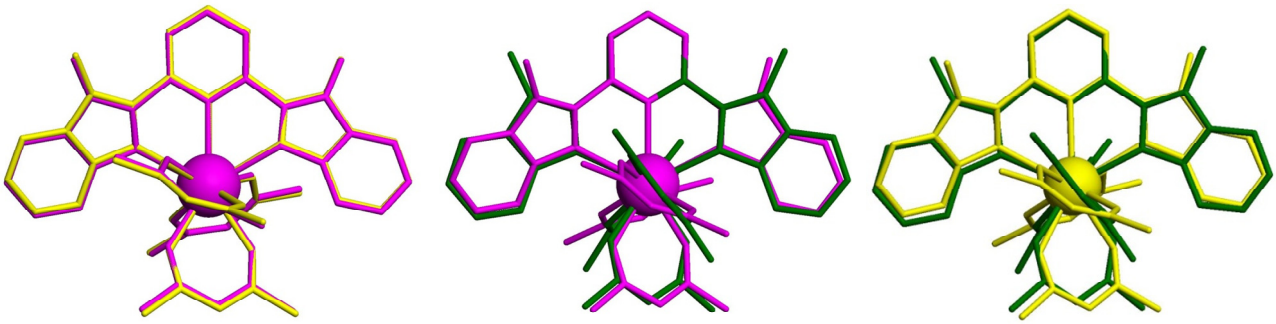

Figure S8 Pair superimpositions of the molecular structures of [La(**L3**)(hfac)$_3$] (yellow), [Eu(**L3**)(hfac)$_3$] (magenta) and [Lu(**L3**)(hfac)$_3$] (green). The terminal isobutyl residues and the fluorine atoms have been omitted for clarity.

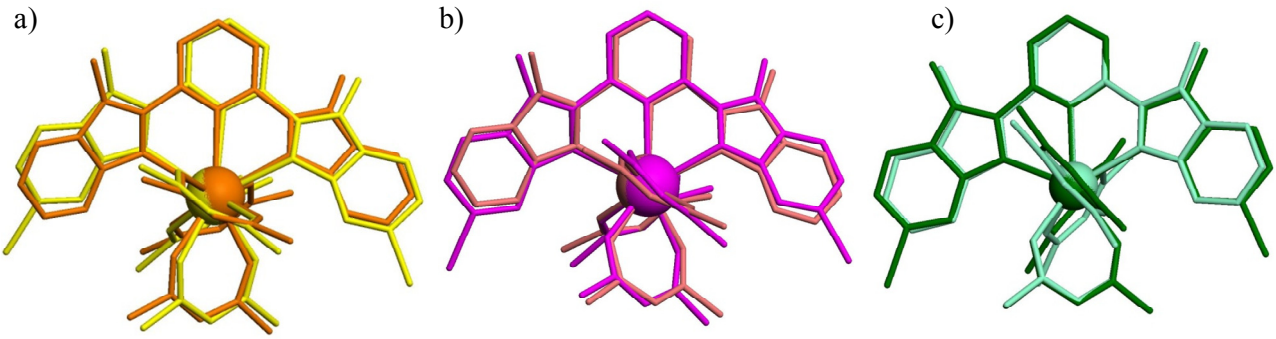

Figure S9 Pair superimpositions of the molecular structures of a) [La(**L2**)(hfac)$_3$] (yellow)/[La(**L3**)(hfac)$_3$] (orange), b) [Eu(**L2**)(hfac)$_3$] (magenta)/[Eu(**L3**)(hfac)$_3$] (pink) and c) [Lu(**L2**)(hfac)$_3$] (green)/[Lu(**L3**)(hfac)$_3$] (pale blue). The terminal isobutyl residues and the fluorine atoms have been omitted for clarity.

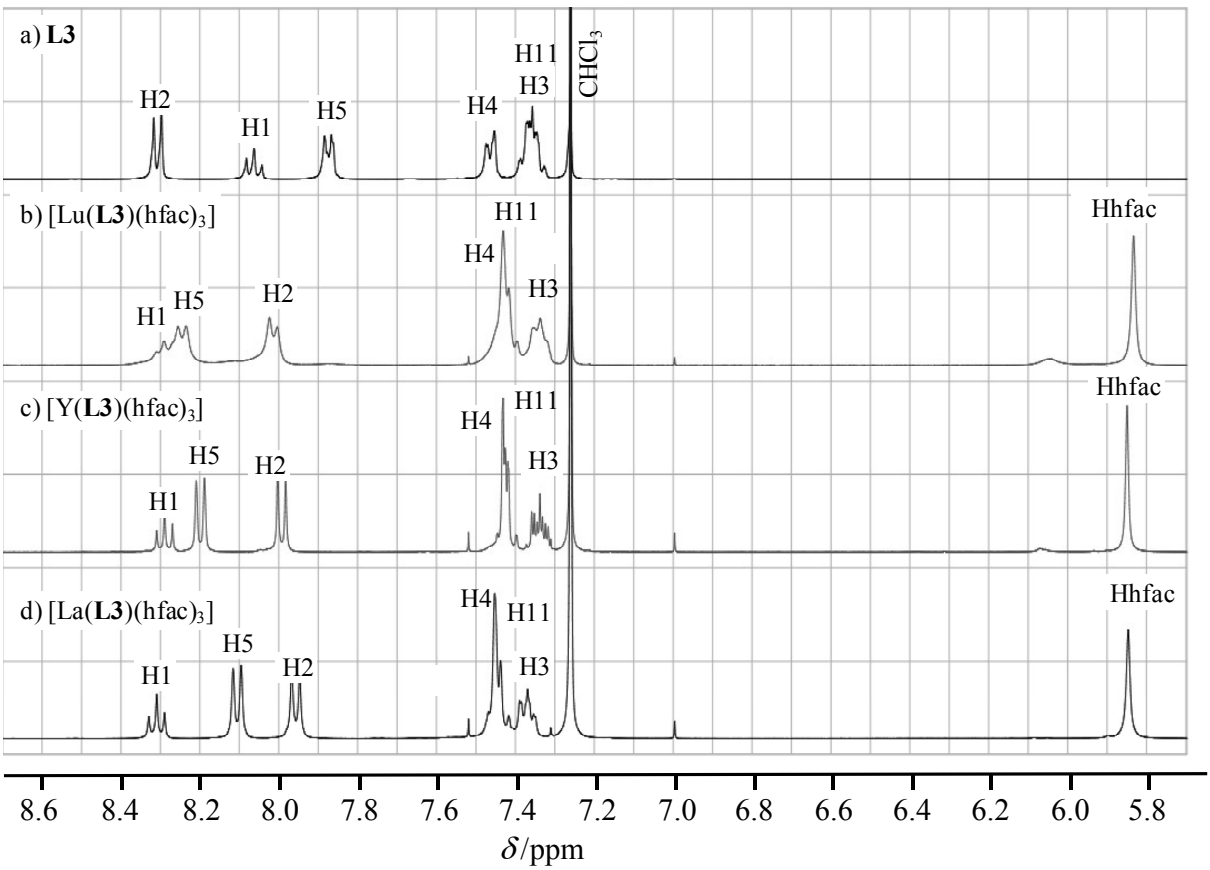

Figure S10 ^{1}H NMR spectra of a) the ligand **L3** and its diamagnetic complexes b) [Lu(**L3**)(hfac)$_3$], c) [Y(**L3**)(hfac)$_3$] and d) [La(**L3**)(hfac)$_3$] in $CDCl_3$ (total ligand concentration 5 mM, 293 K, numbering is given in Scheme 3).

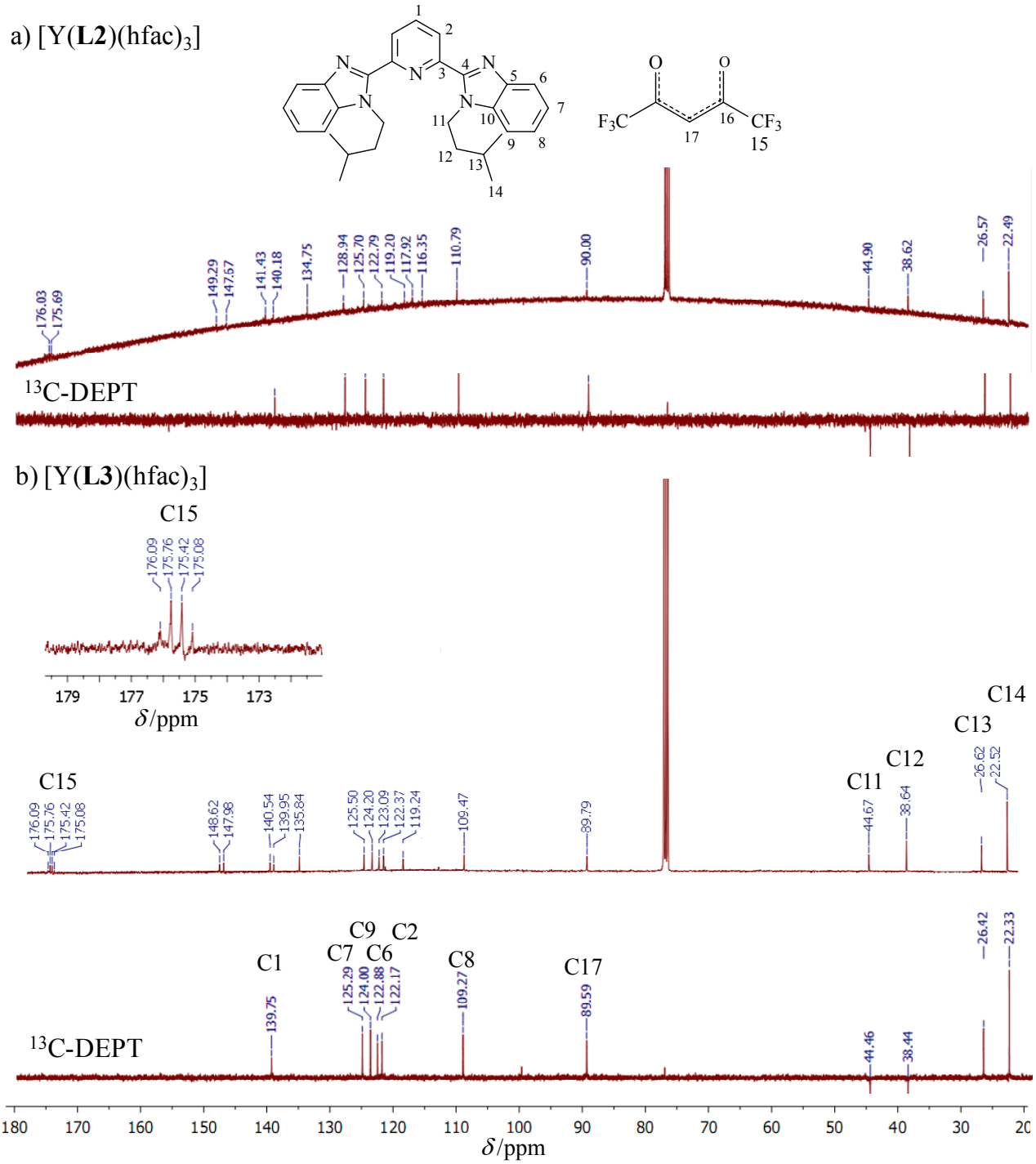

Figure S11 ^{13}C NMR spectra of a) [Y(**L2**)(hfac)$_3$] and b) [Y(**L3**)(hfac)$_3$] (total ligand concentration 10 mM, 293 K, $CDCl_3$).

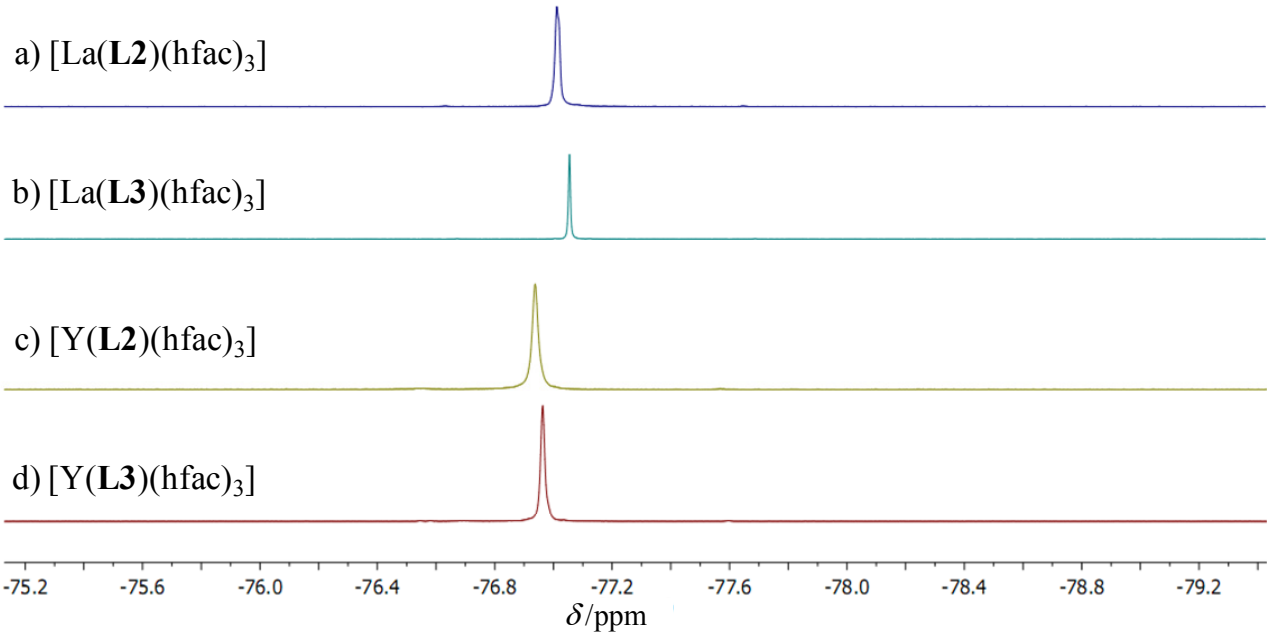

Figure S12 ^{19}F NMR spectra of a) [La(**L2**)(hfac)$_3$], b) [La(**L3**)(hfac)$_3$], c) [Y(**L2**)(hfac)$_3$] and d) [Y(**L3**)(hfac)$_3$] (total ligand concentration 10 mM, 293 K, $CDCl_3$).

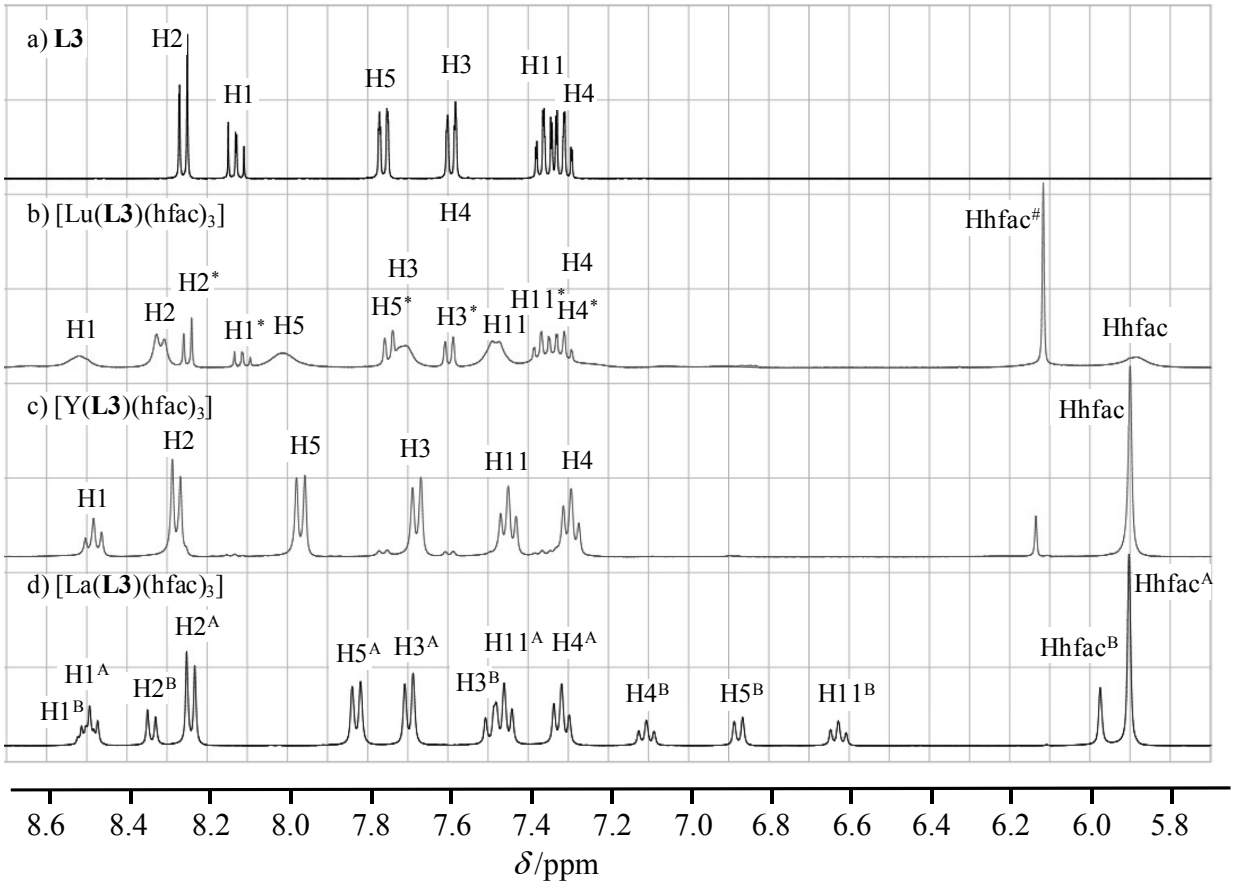

Figure S13 ^{1}H NMR spectra of a) the ligand **L3** and its diamagnetic complexes b) [Lu(**L3**)(hfac)$_3$] (* = free ligand, # = free Lu(hfac)$_3$), c) [Y(**L3**)(hfac)$_3$] and d) [La(**L3**)(hfac)$_3$] in CD_3CN (total ligand concentration 5 mM, 293 K, numbering is given in Scheme 3).

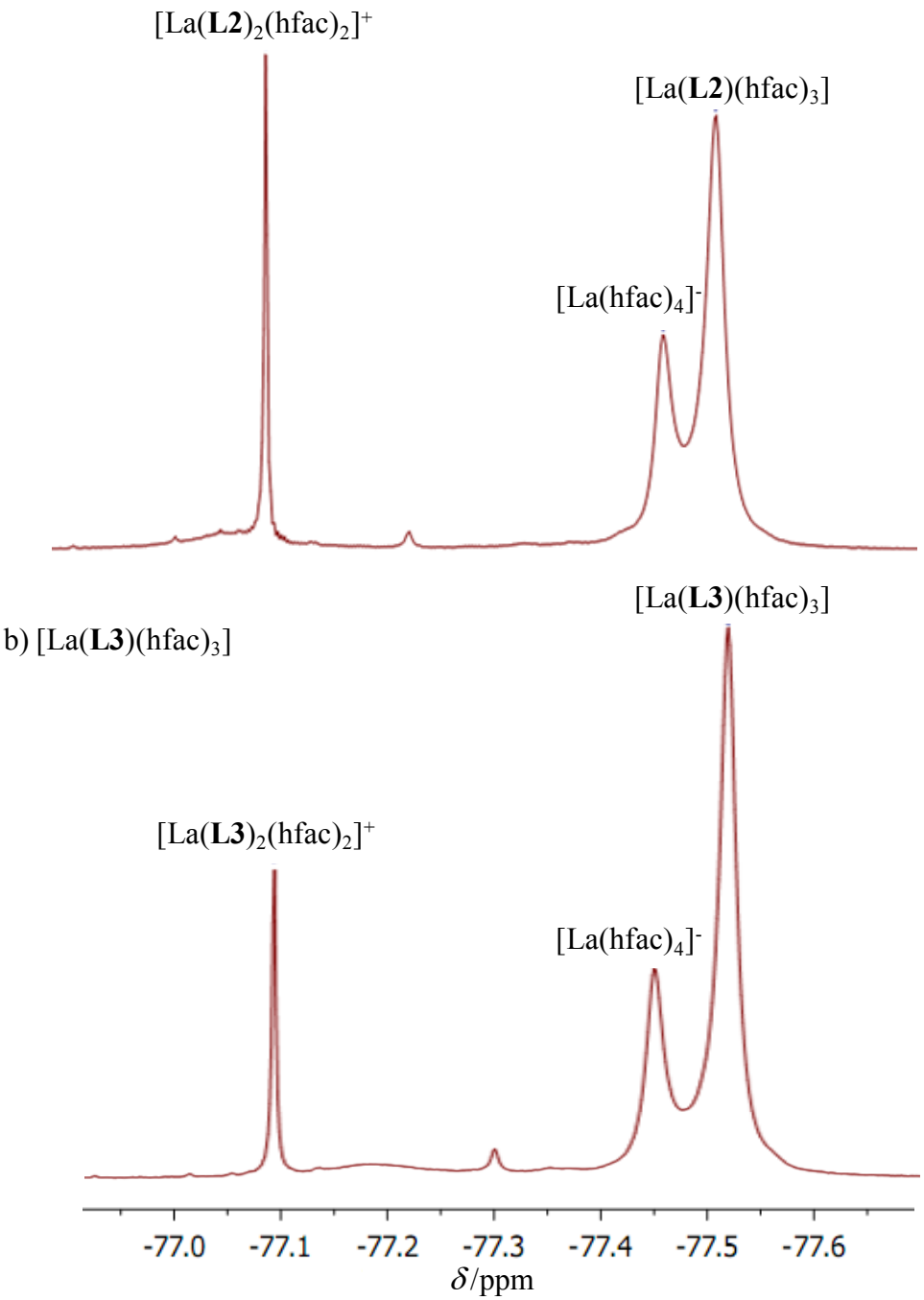

Figure S14 ^{19}F NMR spectra of a) [La(**L2**)(hfac)$_3$] and b) [La(**L3**)(hfac)$_3$] in CD_3CN (total ligand concentration 5 mM, 293 K).

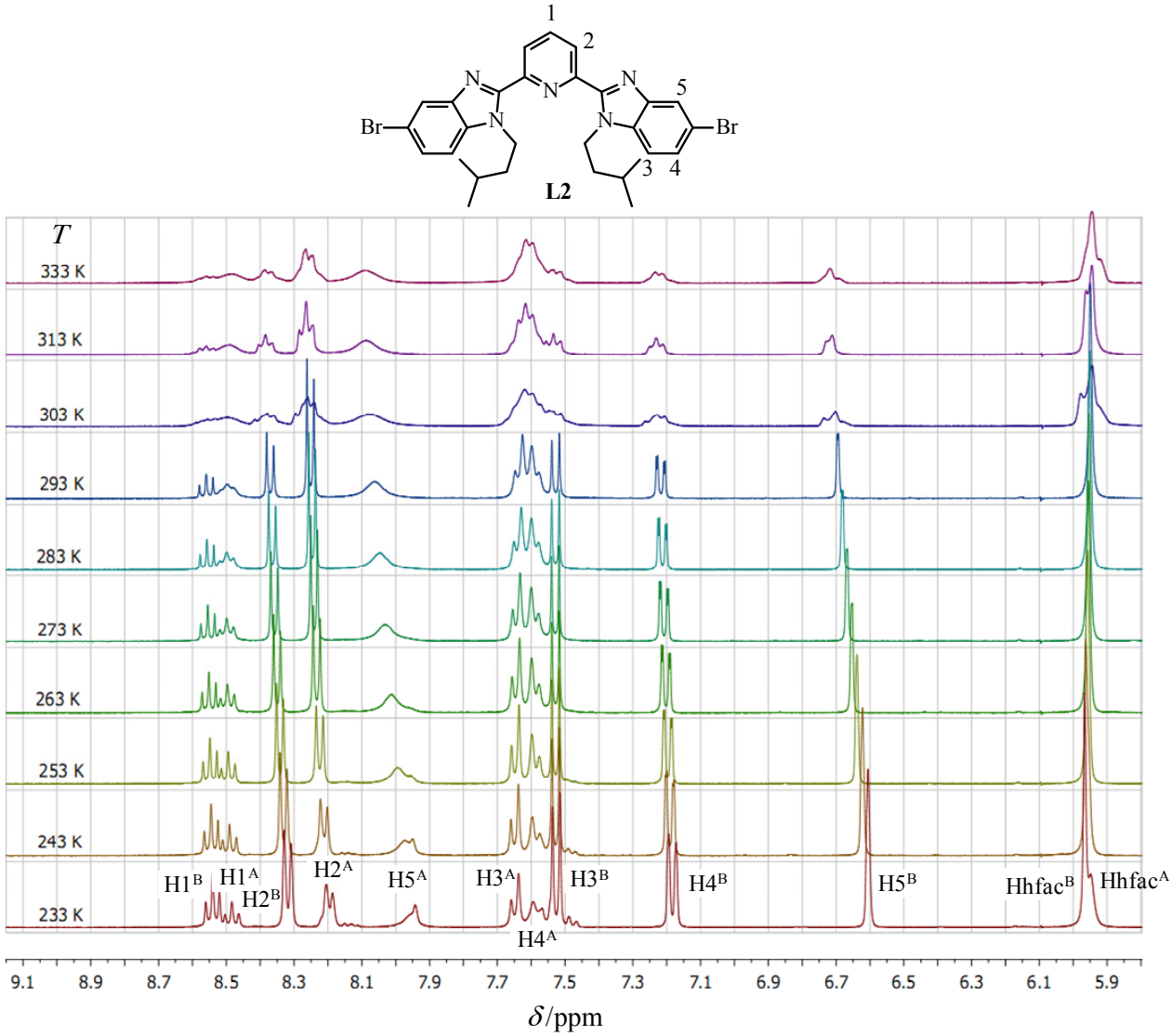

Figure S15 VT-^{1}H NMR spectra of [La(**L2**)(hfac)$_3$] in CD_3CN (total ligand concentration 5 mM).

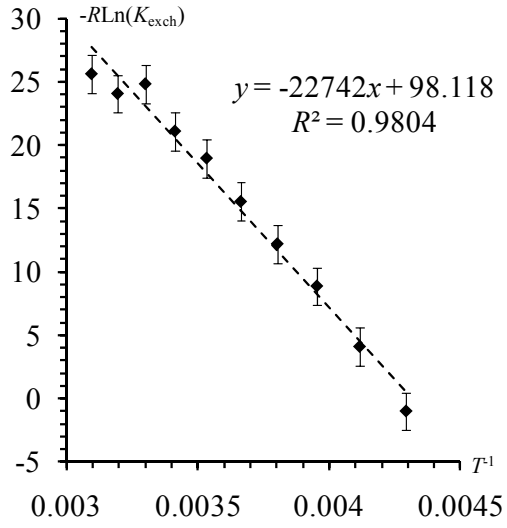

Figure S16 Van't Hoff plots for [La(**L2**)(hfac)$_3$] in CD_3CN according to equilibrium 5.

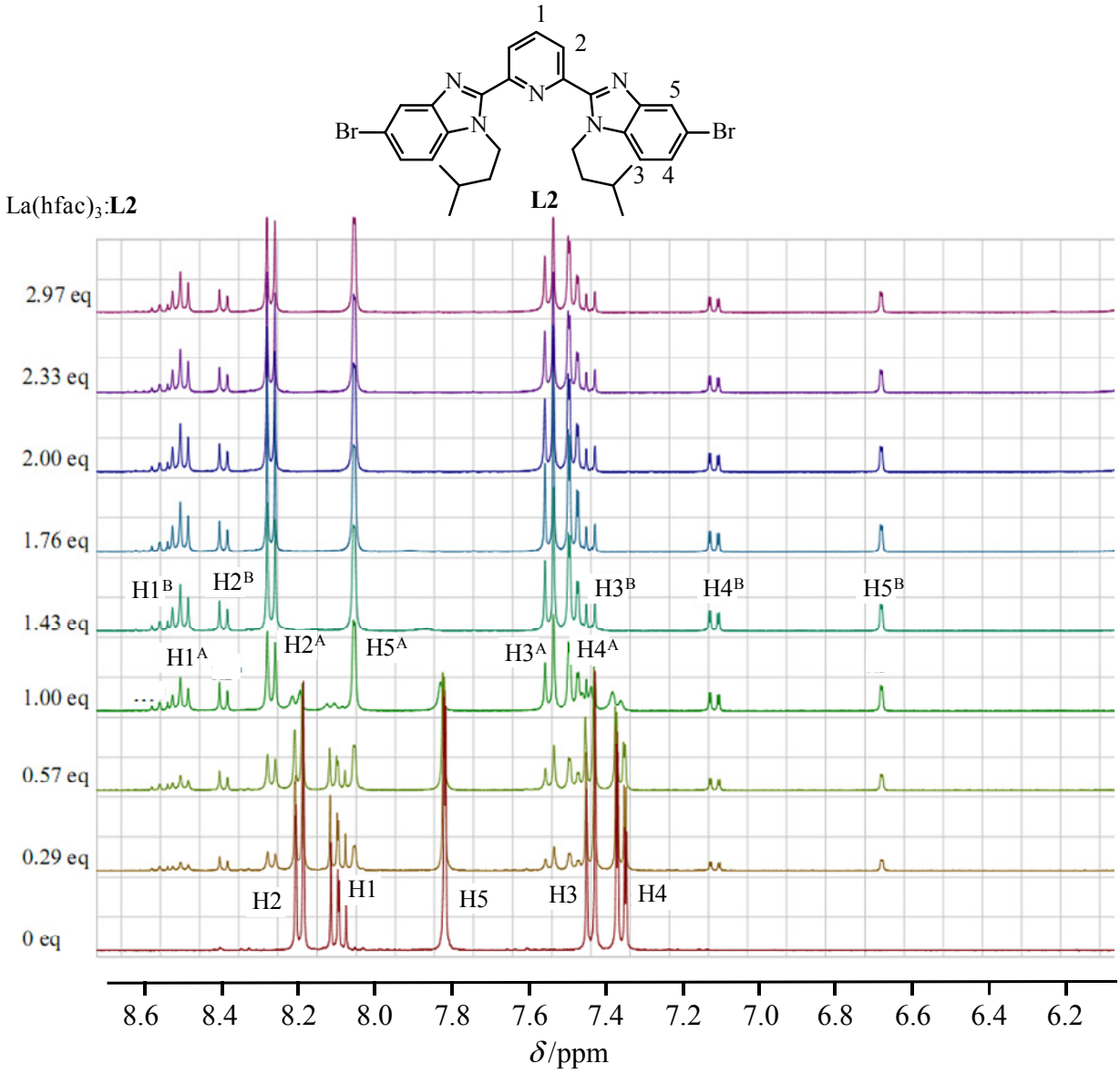

Figure S17 ^{1}H NMR titration of **L2** with [La(hfac)$_3$(diglyme)] in CD_3NO_2 (total ligand concentration 10 mM).

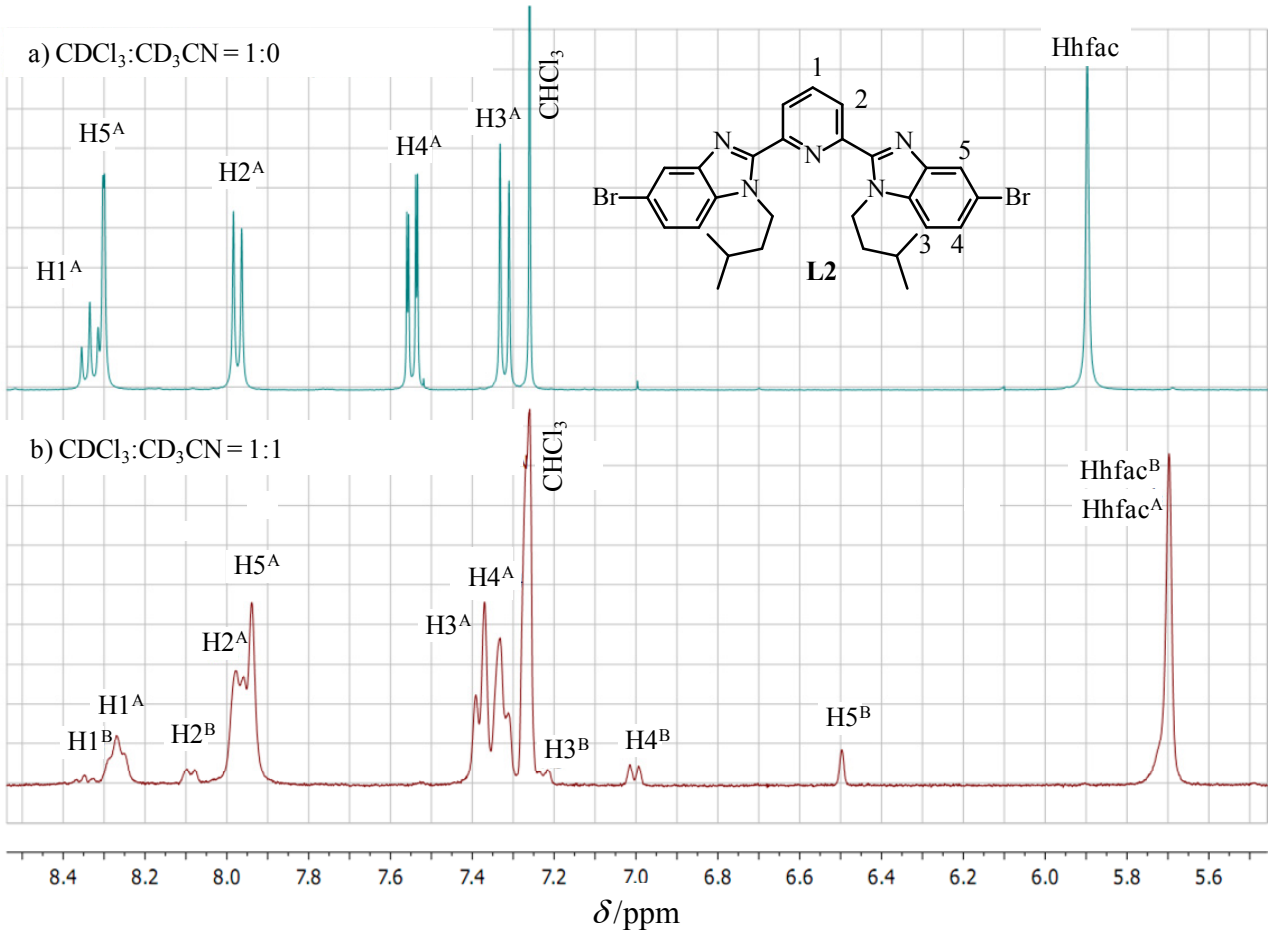

Figure S18 ^{1}H NMR spectra of [La(**L2**)(hfac)$_3$] in a) $CDCl_3$ and b) $CDCl_3$:CD_3CN = 1:1 (total ligand concentration 10 mM).

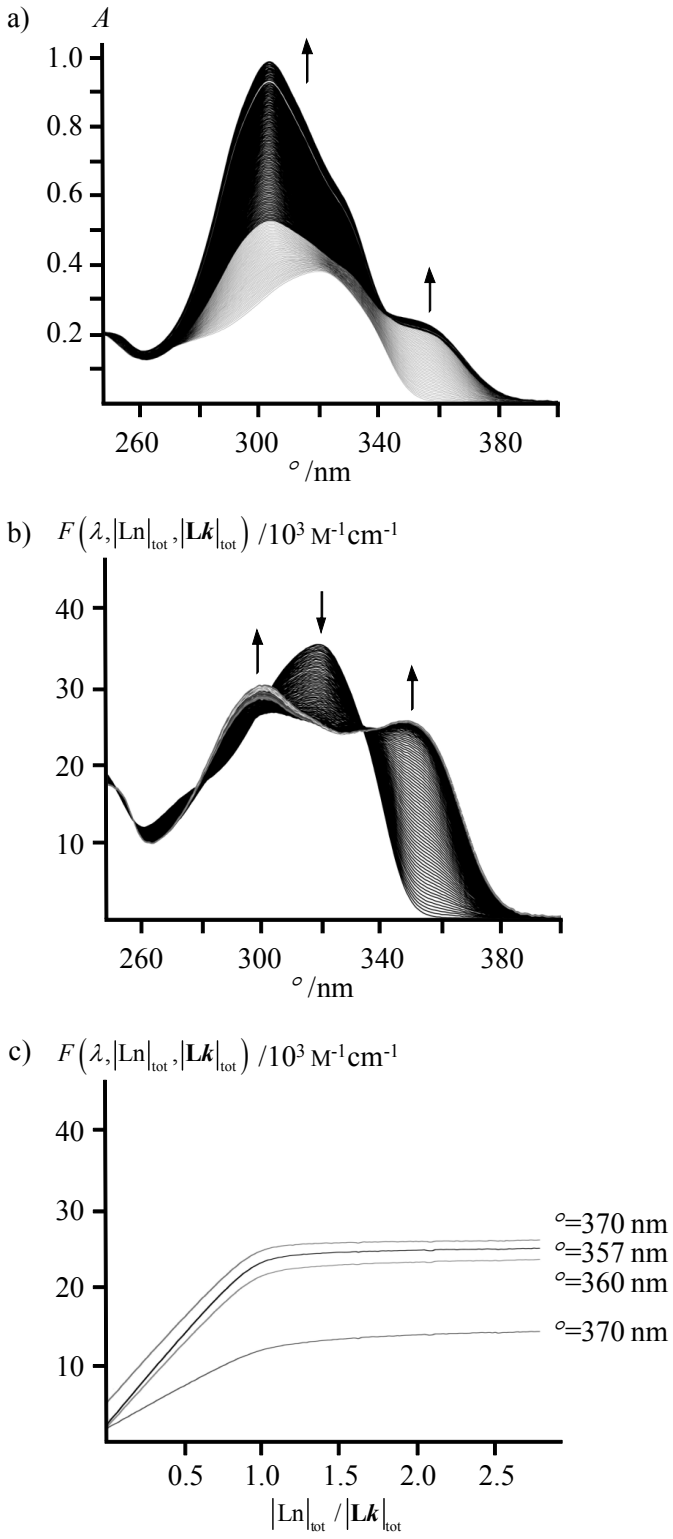

Figure S19 Variation of a) absorption spectra and b) corrected absorption spectra ($F\left(\lambda,|\mathrm{Ln}|_{\mathrm{tot}},|\mathbf{L}\boldsymbol{k}|_{\mathrm{tot}}\right)$, see eq S13 in Appendix 3), and c) corresponding variation of corrected molar extinctions at 4 different wavelengths observed for the spectrophotometric titrations of **L2** (10^{-4} M) with [Eu(hfac)$_3$(diglyme)] (acetonitrile + 10^{-4} M diglyme, 298 K).

Macroconstants	Microconstants	Point groups	$\omega_{m,n,p}^{\text{chiral}}$	$\omega_{m,n,p}^{\text{Ln,L}k\text{hfac}}$
$\beta_{1,1,3}^{\text{Ln,L}k\text{hfac}}$	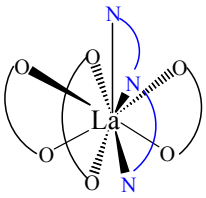	C_{2v}	1	48
$\beta_{1,2,2}^{\text{Ln,L}k\text{hfac}}$	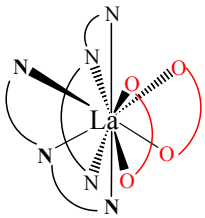	C_{2v}	1	48
	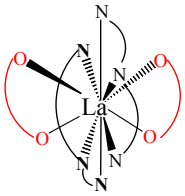	D_{2h}	1	24
$\beta_{1,0,1}^{\text{Ln,L}k\text{hfac}}$	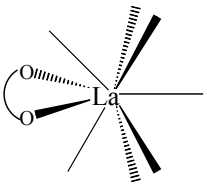	C_s	1	12
$\beta_{1,0,2}^{\text{Ln,L}k\text{hfac}}$	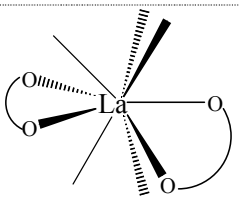	C_2	1	24
	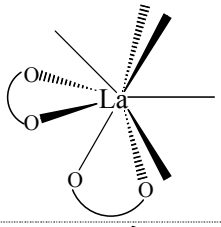	C_s	1	24
$\beta_{1,0,3}^{\text{Ln,L}k\text{hfac}}$	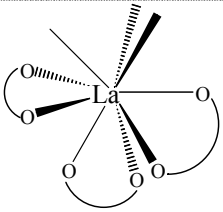	C_{3v}	1	16

Macroconstants	Microconstants	Point groups	$\omega_{m,n,p}^{\text{chiral}}$	$\omega_{m,n,p}^{\text{Ln,L}k\text{hfac}}$
$\beta_{1,0,4}^{\text{Ln,L}k\text{hfac}}$	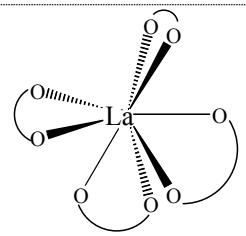	D_2	1	24
$\beta_{1,1,0}^{\text{Ln,L}k\text{hfac}}$	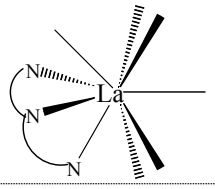	C_{2v}	1	6
$\beta_{1,2,0}^{\text{Ln,L}k\text{hfac}}$	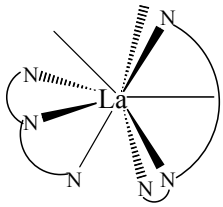	C_{2v}	1	12
$\beta_{1,3,0}^{\text{Ln,L}k\text{hfac}}$	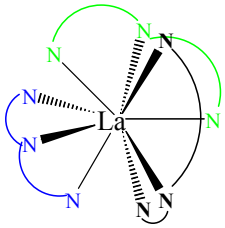	D_3	1	16

Figure S20 Determination of symmetry numbers (σ^{ext}, σ^{int}, σ^{chiral})[43] and statistical factors for equilibria (13)-(20). The symmetry point groups are those expected for idealized arrangements of the donor groups in the first coordination sphere of the lanthanide. *CN* = 9 with idealized tricapped trigonal prismatic geometries (TTP) is systematically considered except for $[La(\mathbf{L2})_2(hfac)_2]^+$ (*CN* = 10 and bicapped square antiprismatic geometry (BSA)) and for $[La(hfac)_4]^-$ (*CN* = 8 and square-antiprismatic).

a) La(III)/**L2**/hfac

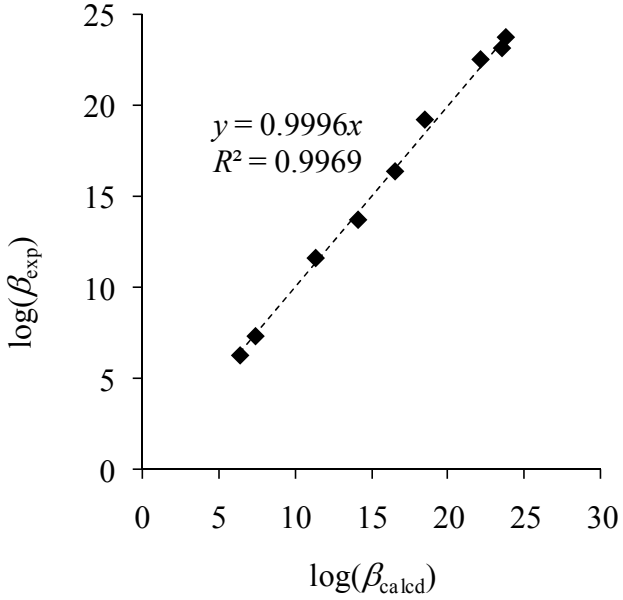

b) La(III)/**L3**/hfac

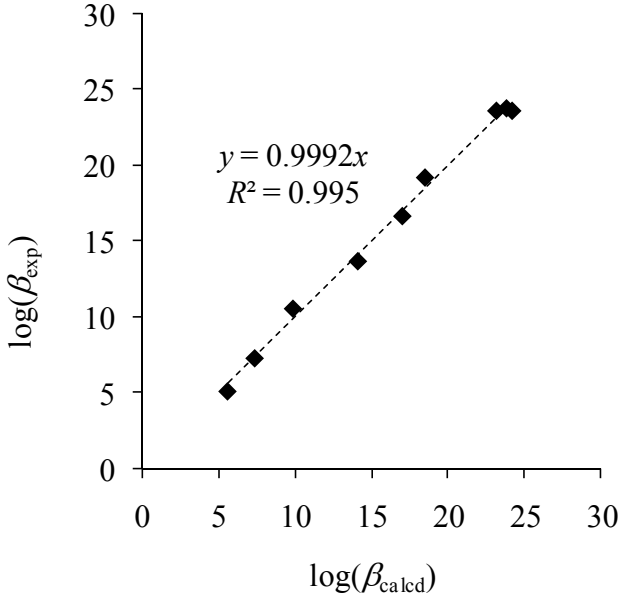

Figure S21 Correlation between experimental $\log\left(\beta_{i,j,l,\mathrm{exp}}^{\mathrm{La},\mathbf{L}k,\mathrm{hfac}}\right)$ and calculated $\log\left(\beta_{i,j,l,\mathrm{calcd}}^{\mathrm{La},\mathbf{L}k,\mathrm{hfac}}\right)$ formation constants for the a) La/**L2**/hfac and b) La/**L3**/hfac systems (CH_3CN, 293 K).

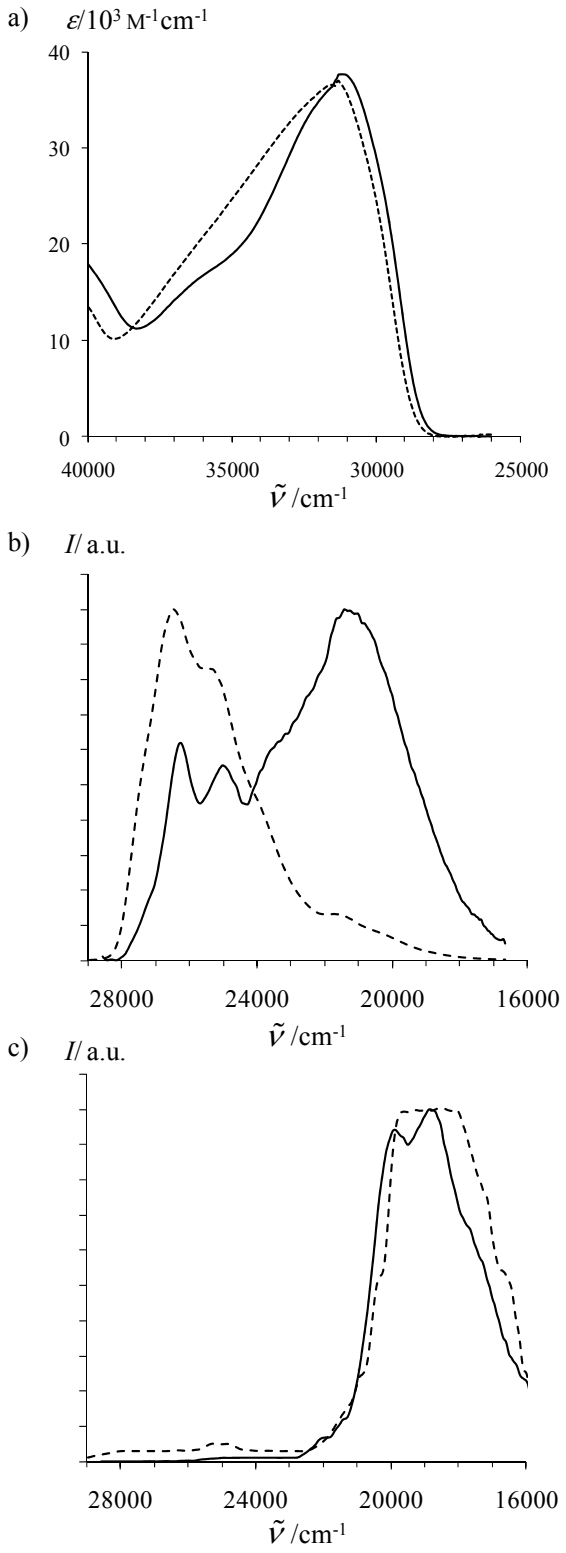

Figure S22 a) Absorption (10^{-4} M in CH_3CN, 293K), b) fluorescence (solid state, 77K) and c) phosphorescence (solid state, 77K, delay time after excitation flash = 0.05 ms) spectra recorded for **L2** (full line, $\tilde{\nu}_{exc}$ = 31250 cm^{-1}) and **L3** (dotted line, $\tilde{\nu}_{exc}$ = 31250 cm^{-1}). The emission spectra are arbitrarily normalized to 1.

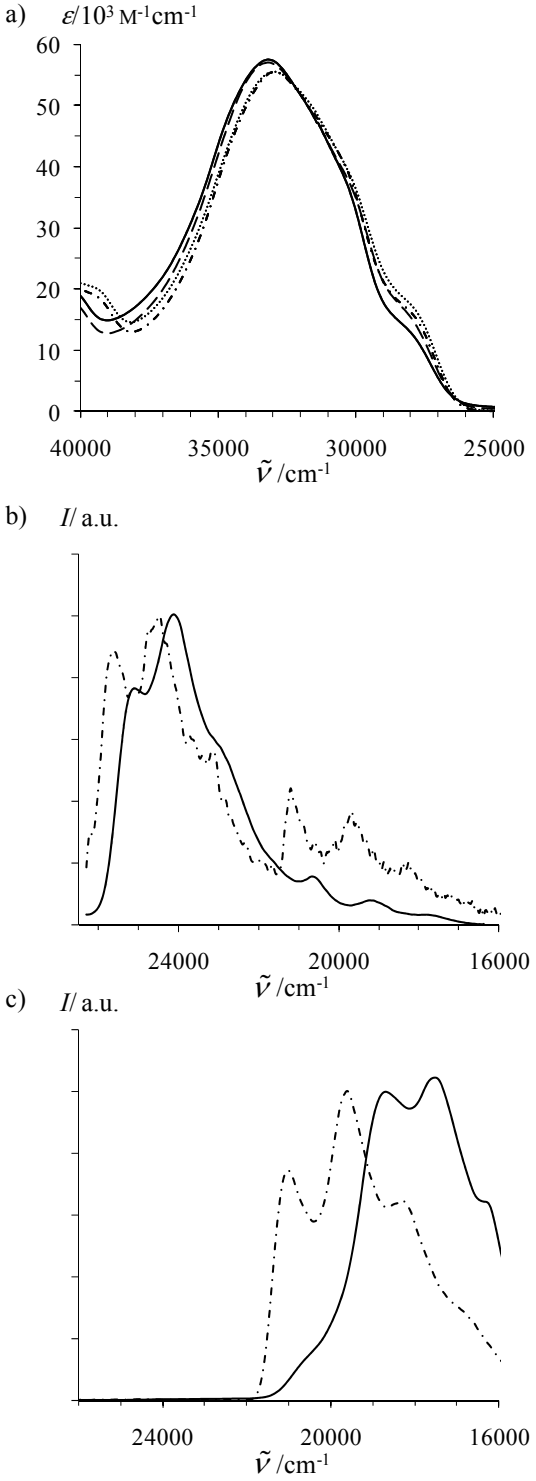

Figure S23 a) Electronic absorption spectra of [Gd(**L2**)(hfac)$_3$] (alternated line), [Gd(**L3**)(hfac)$_3$] (full line), [Eu(**L2**)(hfac)$_3$] (dotted line) and [Eu(**L3**)(hfac)$_3$] (dashed line, 10^{-4} M in CH_3CN, 293K, corrected for partial dissociation, see Appendix 3). b) Fluorescence (solid state, 77K) and c) phosphorescence (solid state, 77K, delay time after excitation flash = 0.05 ms, $\tilde{\nu}_{exc}$ = 27780 cm^{-1}) emission spectra recorded for [Gd(**L2**)(hfac)$_3$] (alternated line) and [Gd(**L3**)(hfac)$_3$] (full line). The emission spectra are arbitrarily normalized to 1.

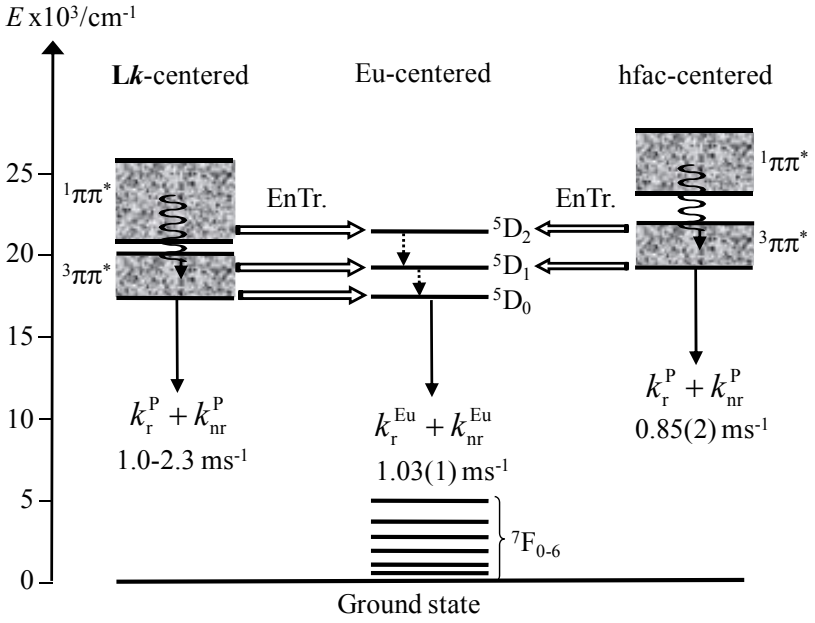

Figure S24 Simplified Jablonski diagram established for the ternary complex [Eu(**L*k***)(hfac)$_3$] (*k* = 2, 3). Ondulated downward arrows = intersystem crossing processes (including internal conversion), dashed downward arrows = internal conversions and horizontal arrows = ligand-to-metal energy transfers.